ASSESSING THE EFFECTS OF CONFINING STRESS STATE ON THE MOBILIZATION OF AXIAL COMPRESSIVE RESISTANCE FOR A SINGLE AGGREGATE PIER

A THESIS SUBMITTED TO
THE GRADUATE SCHOOL OF NATURAL AND APPLIED SCIENCES
OF
MIDDLE EAST TECHNICAL UNIVERSITY

BY

ALPARSLAN DOĞAN

IN PARTIAL FULFILLMENT OF THE REQUIREMENTS
FOR THE DEGREE OF MASTER OF SCIENCE
IN
CIVIL ENGINEERING

MAY 2014

Approval of the thesis:

ASSESSING THE EFFECTS OF CONFINING STRESS STATE ON THE MOBILIZATION OF AXIAL COMPRESSIVE RESISTANCE FOR A SINGLE AGGREGATE PIER

submitted by **ALPARSLAN DOĞAN** in partial fulfillment of the requirements for the degree of **Master of Science in Civil Engineering Department, Middle East Technical University** by,

Prof. Dr. Canan Özgen ______________________
Dean, Graduate School of **Natural and Applied Sciences**

Prof. Dr. A. Cevdet Yalçıner ______________________
Head of Department, **Civil Engineering**

Prof. Dr. K. Önder Çetin ______________________
Supervisor, **Civil Engineering Dept., METU**

Examining Committee Members:

Prof. Dr. Orhan Erol ______________________
Civil Engineering Dept., METU

Prof. Dr. K. Önder Çetin ______________________
Civil Engineering Dept., METU

Assoc. Prof. Dr. Zeynep Gülerce ______________________
Civil Engineering Dept., METU

Dr. Kartal Toker ______________________
Civil Engineering Dept., METU

Dr. H. Tolga Bilge ______________________
Geodestek Co. Ltd.

Date: *30.05.2014*

I hereby declare that all information in this document has been obtained and presented in accordance with academic rules and ethical conduct. I also declare that, as required by these rules and conduct, I have fully cited and referenced all material and results that are not original to this work.

Name, Last name :

Signature

ABSTRACT

ASSESSING THE EFFECTS OF CONFINING STRESS STATE ON THE MOBILIZATION OF AXIAL COMPRESSIVE RESISTANCE FOR A SINGLE AGGREGATE PIER

Doğan, Alparslan
M.Sc., Department of Civil Engineering
Supervisor: Prof. Dr. K. Önder Çetin

May 2014, 106 pages

Aggaregate piers are widely used to enhance the performance of cohesionless and cohesive foundations soils. It is an effective and economical solution to several geotechnical engineering problems including insufficient bearing capacity, excessive settlements, slope instability and liquefaction. The performance of stone columns is governed by a number of factors including installation procedure, area replacement ratio, column length, shear strength characteristics of the column and native soil characteristics.

Within the scope of this thesis, the effect of construction induced confining stresses on the mobilization of axial compressive resistance of a single aggregate pier is examined. For this purpose, series of finite element based numerical simulations were performed by modeling piers of different length to diameter (L/D) and cavity expansion ratios ($\Delta r/R_0$). Both components of resistance including shaft friction and end bearing were evaluated by utilizing an axisymmetric finite element model. Finally, normalized resistance vs. normalized settlement curves were developed for piers of different length to diameter and cavity expansion ratios to demonstrate mobilization of the axial resistance.

By careful invesitgation of analysis results, it was found that aggregate pier capacity increases as the confining stress increases. Also, an improvement in the settlement was observed through confining stress increase for a specified value of axial compressive stress.

Keywords: Stone column, Confining stress, Shaft resistance, Tip resistance, Numerical modelling.

ÖZ

ÇEPER BASINÇ KOŞULLARININ EKSENEL DİRENÇ GELİŞİMİNE ETKİSİNİN TEKİL BİR TAŞ KOLON İÇİN DEĞERLENDİRİLMESİ

Doğan, Alparslan
Yüksek Lisans, İnşaat Mühendisliği Bölümü
Tez Yöneticisi: Prof. Dr. K. Önder Çetin

Mayıs 2014, 106 sayfa

Taş kolonlar, kohezyonlu ve kohezyonsuz temel zeminlerini güçlendirmek için yaygın olarak kullanılmaktadır. Yetersiz taşıma gücü, aşırı oturma, şev duraysızlığı ve sıvılaşma dahil bir çok geoteknik mühendisliği probleminde taş kolanlar etkin ve ekonomik bir çözümdür. Taş kolonların davranışı, yerleştirme yöntemi, alan/yer değiştirme oranı, kolon uzunluğu, kolon ve yerel zemin malzemesinin kayma dayanım özellikleri gibi birtakım etmenler tarafından belirlenir.

Bu tez kapsamında, imalattan kaynaklanan çeper basıncının eksenel basınç altındaki tekil taş kolonda oluşan mukavemet (direnç) unsurlarına etkisi incelenmiştir. Bu amaçla, sonlu eleman tabanlı modeller ile simülasyonlar farklı uzunluk-çap ve kovuk genişletme oranlarına sahip taş kolonlar modellenerek gerçekleştirilmiştir. Çeper sürtünmesi ve uç direnci olmak üzere iki direnç bileşeni de aksisimetrik sonlu elemanlar kullanılarak değerlendirilmiştir. Sonuç olarak, farklı boy-çap ve kovuk genişletme oranlarına sahip taş kolonlardaki direnç gelişimini göstermek için normalize edilmiş direnç-oturma eğrileri hazırlanmıştır.

Sonuçların dikkatli incelenmesiyle, çeper basıncının artmasıyla kapasitenin arttığı saptanmıştır. Ayrıca, belirli bir eksenel yük altında meydana gelen oturmalarda da iyileşme gözlemlenmiştir.

Anahtar Kelimeler: Taş kolon, Çeper basıncı, Çeper sürtünmesi, uç direnci, nümerik modelleme.

To My Parents

ACKNOWLEDGEMENTS

The author would like to express his gratitude to his supervisor Prof. Dr. K. Önder ÇETİN for his guidance and criticism in completion of this study.

Specially thanks go to Assoc. Prof. Dr. Yalın ARICI, who is really the special professor of civil engineering department. I will not forget his role as “Big Brother” during my academic study.

My next gratitude goes to my dear friends Sinan ABDÜLMECİT, Gökhan ARIKAN and İsmail BELKAYA for their endless moral support and friendship during this study.

My last but not least thanks go to my dear family; to my brother M. DOĞAN, to my mother H. DOĞAN and to my father E. DOĞAN.

TABLE OF CONTENTS

ABSTRACT v

ÖZ vii

To My Parents ix

ACKNOWLEDGEMENTS x

TABLE OF CONTENTS xi

LIST OF TABLES xiv

TABLES xiv

LIST OF FIGURES xv

FIGURES xv

CHAPTER 1. 1

INTRODUCTION 1

- 1.1. Research Objectives 2

CHAPTER 2. 5

A GENERAL OVERVIEW OF STONE COLUMNS 5

- 2.1. Introduction 5
- 2.2. Stone Column Construction Techniques 6
  - 2.2.1. Vibro Replacement Stone Columns 6
  - 2.2.2. Rammed Aggregate Piers 9
- 2.3. Design of Stone Columns 11
  - 2.3.1. Principal Behavior and Ultimate Load Analysis of Single Stone Columns… 12
  - 2.3.2. Present Design Methods of Single Stone Columns 13

2.3.3. Tip Resistance 15

2.4. The Effect of Construction-Induced Lateral Stresses on Behavior of Stone Columns 16

2.4.1. Overview of Lateral Stress Influence on Behavior 16

2.4.2. Studies in Literature Associated with Lateral Stress Around Aggregate Pier 18

CHAPTER 3 21

NUMERICAL ASSESSMENT 21

3.1. An Overview of Material Modeling 21

3.1.1. Hardening Soil Model 22

3.2. Description of the Numerical Simulation 26

3.2.1. Modeling of the Installation of Stone Columns 28

3.2.2. Updated Mesh Analysis 29

3.3. Selection of Model Parameters 29

3.3.1. Selection of Friction Angle 30

3.3.2 Selection of Stiffness Parameters 33

3.3.3. Other Parameters 34

3.4. Drained or Undrained Analysis 35

3.5. Summary of Analysis Cases 36

3.5.1. Analysis Case: Single aggregate pier in clay soil 36

CHAPTER 4 39

ANALYSIS RESULTS 39

4.1. Assessment of Load Displacement Curves 40

4.2. Presentation of Results 42

4.2.2. Mobilization of Tip Resistance 53

CHAPTER 5 57

DISCUSSION OF RESULTS 57

5.1. Mobilization of Shaft Friction 57

5.2. Mobilization of Tip Resistance 66

5.3. Mobilization of Modulus of Subgrade Reaction 69

5.4 Mobilization of Lateral Stress (K*) 72

CHAPTER 6. 75

CONCLUSION AND RECOMMENDATIONS 75

6.1. Recommendations for Future Studies 78

REFERENCES 81

APPENDIX A 84

OUTPUTS OF AGGREGATE PIERS OF L/D=4, 6, 9, 12 AND 15 85

LIST OF TABLES

TABLES

Table 2.1 N_c coeficients suggested by different authors for different cases 15
Table 3.1 Design parameters used by selected organizations for stability analyses of stone column reinforced ground (adopted from Barksdale and Bachus, 1983) 31
Table 3.2 Elastic modulus values for gravels (AASHTO, 1996) 34
Table 3.3 Summary of Analysis Cases 37
Table 4. 1 Top stage load vs. top displacement curve data in tabular form for L/D=3 and $\Delta r/r_0 = 0.3$ 44
Table 4.2 Tip stress vs. tip displacement curve data in tabular form for L/D=3 and $\Delta r/r_0 = 0.3$ 45

LIST OF FIGURES

FIGURES

Figure 2.1 Construction phases of a dry bottom feed stone column (adapted from http://www.vibroflotation.com) 6
Figure 2.2 Typical view of a vibrotor to construct a dry bottom feed stone column (Keller Brochure 10-02 E) 7
Figure 2.3 Typical View of a vibrotor to construct a wet top feed stone column (Keller Brochure 10-02 E) 8
Figure 2.4 Construction phases of a wet top feed stone column (adapted from http://www.vibroflotation.com) 9
Figure 2.5 Diagrammatic Representation of a rammed stone Column Construction (taken from http://sentezinsaat.com.tr) 10
Figure 2.6 Construction steps of a rammed stone column in India region (Datye and Nagaraju, 1975) 10
Figure 2.7 Diagrammatic representation of a rammed stone column construction (taken from http://www.helicaldrilling.com/) 11
Figure 2.8 Conceptual analogy for load carrying mechanism of a single floating stone column 12
Figure 2.9 Possible failure modes for a single stone column (Kirsch, 2004) 13
Figure 2.10 Change of lateral stress state at in-situ soil after construction and foundation loading (Handy, 2001) 16
Figure 2.11 Friction reversals among soil grains to explain increased allowable vertical stress (Handy, 2001) 17
Figure 2.12 Conceptual representation of load carrying mechanisms in a single stone column 18
Figure 3.1 Comparison of real soil behavior with model predictions (adapted from Ehsan R., 2013) 21

Figure 3.2 Definition of E_0 and E_{50} for standard drained triaxial test results (Plaxis, 2002) 23
Figure 3.3 Definition of E^{ref}_{oed} in oedometer test results (Plaxis, 2002) 23
Figure 3.4 Hyperbolic stress-strain relation in primary loading (Plaxis, 2002) 24
Figure 3.5 Yield surfaces of Hardening-Soil model in p-q stress space 25
Figure 3.6 Representation of total yield contour of the Hardening-Soil model in principal stress space for cohesionless soil (Plaxis 2002) 25
Figure 3.7 Schematic illustration of the geometry of analysis case 27
Figure 3.8 a) 2D Modeling of Axisymmetric Problem b) Triangular Mesh Element (Plaxis 2002) 28
Figure 3.9 Numerical Simulation of Stone Column Construction 29
Figure 3.10 Variation of φ' with plasticity index for normally consolidated remolded clays (Gibson, 1953). 30
Figure 3.11 Summary of peak friction angle results (FHWA, 2013) 31
Figure 3.12 Angle of friction of rockfill obtained from large diameter triaxial tests (Barksdale and Bachus, 1983) 32
Figure 3.13 Illustration of the analysis case 37
Figure 4.1 Normalized Load Transfer in side-shear and end-bearing capacity vs. Settlement in cohesive soils(After Reese and O'Neill, 1988) 40
Figure 4. 2 Deformed shape after application of lateral displacement of $\Delta r/r_0=0.3$ .. 42
Figure 4.3 Lateral stresses around the pier of L/D=3 after $\Delta r/r_0=0.3$. (Note: Color scale on the right gives mean lateral stress with depth) 43
Figure 4. 4 Top stage load ratio vs. top displacement curve of pier L/D=3 for $\Delta r/r_0 = 0.3$ (output of Plaxis 8.2) 46
Figure 4. 5 Tip stress vs. tip displacement curve for pier of L/D=3 and $\Delta r/r_0 = 0.3$ (output of Plaxis 8.2) 46
Figure 4. 6 a) & b) Hyperbolic regression curves with shaft friction vs. settlement curves for cavity expansion ratio of 0 and 0.1. 47
Figure 4. 7 a) & b) Hyperbolic regression curves with shaft friction vs. settlement curves for cavity expansion ratio of 0.3 and 0.7. 47
Figure 4. 8 Shaft friction vs. settlement curves for cavity expansion ratio of 1. 48

Figure 4. 9 Average shaft friction values for aggregate pier with L/D=3 and various cavity expansion ratios. 48
Figure 4.10 Normalized average shaft resistances of pier for L/D=3 49
Figure 4.11 Normalized average shaft resistances after simplifying the overlapped curves 50
Figure 4.12 Normalized mean curve with upper and lower threshold curves for L/D=3 51
Figure 4.13 a) and b) Deformed mesh of aggregate pier of L/D=3 for $\Delta r/r_0$ =0.3 (Scale factor=1) 52
Figure 4.14 Total vertical displacement shading of aggregate pier of L/D = 3 for $\Delta r/r_0$=0.3 52
Figure 4.15 Vertical effective stress at state of failure for L/D = 3 and $\Delta r/r_0$=0.3 53
Figure 4.16 Tip Resistances mobilized in different confining state of stresses for L/D=3 55
Figure 4.17 Linear regression to normalized tip resistances 55
Figure 5.1 Mobilized shaft friction of pier L/D=3 58
Figure 5.2 Mobilized shaft friction of pier L/D=6 59
Figure 5.3 Normalized mobilized shaft friction of pier L/D=6 60
Figure 5.4 Normalized mobilized shaft friction of pier L/D=3 60
Figure 5.5 Normalized mobilized shaft friction of pier L/D=9 61
Figure 5.6 Normalized mean curves for different L/D ratios 62
Figure 5.7 Normalized mean curves for different L/D ratios 63
Figure 5.8 Mean of normalized mean curves 64
Figure 5.9 Mean of normalized mean curves with standard deviation 65
Figure 5.10 Mobilization of shaft friction with cavity expansion for the pier of L/D=3 66
Figure 5.11 Mobilization of tip resistance in different state of confining stresses for pier of L/D=3 67
Figure 5. 12 Mobilization of tip resistance in different state of confining stresses for pier of L/D=6 67
Figure 5.13 Mobilization of tip resistance in different state of confining stresses for pier of L/D=9 68

Figure 5.14 Mean mobilized tip resistance with standard deviation 69
Figure 5. 15 Change in modulus of subgrade reaction vs. cavity expansion for L/D=3 70
Figure 5.16 Change in modulus of subgrade reaction vs. cavity expansion ratio for pier of L/D=3, 4, 6, 9, 12 and 15 71
Figure 5.17 Change in modulus of subgrade reaction for pier of different L/D ratios 71
Figure 5.18 Change in lateral stress state with cavity expansion for L/D=3 73
Figure 6.1 Median normalized mobilized shaft resistance with one standard deviation range 76
Figure 6.2 Mean mobilized tip resistance with one standard deviation range 77
Figure 6.3 Mobilized shaft resistance as a function of expansion ratio 78
Figure a. 1 Average shaft resistance for aggregate pier for L/D=4 85
Figure a.2 Normalized average shaft resistances for L/D=4 86
Figure a.3 Average normalized curve with upper and lower threshold curves for L/D=4 86
Figure a.4 Normalized tip resistances of aggregate pier of L/D=4 87
Figure a.5 Deformed shape after application of lateral displacement ($\Delta r/r_0$ =1) to pier of L/D=4 87
Figure a.6 Confining stresses around the pier of L/D=4 for $\Delta r/r_0$ =1 88
Figure a.7 Deformed mesh of aggregate pier of L/D=4 for $\Delta r/r_0$ =1 (Scale factor=1) 88
Figure a.8 Deformed mesh of aggregate pier of L/D=4 for $\Delta r/r_0$ =1 (Scale factor=1) 89
Figure a.9 Total displacement shading of aggregate pier of L/D=4 for $\Delta r/r_0$ =1 89
Figure a.10 Maximum average shaft resistance vs. cavity expansion ratio for L/D=4 90
Figure a.11 Modulus of subgrade reaction vs. cavity expansion ratio for L/D=4 90
Figure a.12 Average shaft resistance for aggregate pier for L/D=6 91
Figure a.13 Normalized average shaft resistances of pier for L/D=6 91
Figure a.14 Normalized mean curve with upper and lower threshold curves for L/D=6 92

Figure a.15 Normalized tip resistances of aggregate pier of L/D=6 92
Figure a.16 Deformed shape after application of lateral displacement of $\Delta r/r_0$ =0.3 93
Figure a.17 Confining stresses around the pier of L/D=6 after installation............... 93
Figure a. 18 a) and b) Deformed mesh of aggregate pier of L/D=6 for $\Delta r/r_0$ =0.3 (Scale factor=3)... 94
Figure a.19 Total displacement shading of aggregate pier of L/D=6 95
Figure a.20 Maximum average shaft resistance vs. cavity expansion ratio for L/D=6 95
Figure a. 21 Modulus of subgrade reaction vs. cavity expansion ratio for L/D=6 96
Figure a. 22 Average shaft resistance for aggregate pier for L/D=9.......................... 96
Figure a.23 Normalized average shaft resistances for L/D=9.................................... 97
Figure a.24 Average normalized curve with upper and lower threshold curves for L/D=9 97
Figure a.25 Normalized tip resistances of aggregate pier of L/D=9.......................... 98
Figure a.26 Deformed shape after application of lateral displacement ($\Delta r/r_0$ =1) to pier of L/D=9 98
Figure a.27 Confining stresses around the pier of L/D=9 for $\Delta r/r_0$ =1 99
Figure a.28 a) and b) Deformed mesh of aggregate pier of L/D=9 for $\Delta r/r_0$ =1 (Scale factor=1)... 100
Figure a.29 Total displacement shading of aggregate pier of L/D=9 for $\Delta r/r_0$ =1... 100
Figure a.30 Maximum average shaft resistance vs. cavity expansion ratio for L/D=9 101
Figure a.31 Modulus of subgrade reaction vs. cavity expansion ratio for L/D=9 ... 101
Figure a.32 Average shaft resistance for aggregate pier for L/D=12....................... 102
Figure a.33 Normalized average shaft resistances for L/D=12................................ 102
Figure a.34 Average normalized curve with upper and lower threshold curves for L/D=12 103
Figure a.35 Maximum average shaft resistance vs. cavity expansion ratio for L/D=12 103
Figure a.36 Modulus of subgrade reaction vs. cavity expansion ratio for L/D=12 . 104
Figure a.37 Average shaft resistance for aggregate pier for L/D=15....................... 104
Figure a.38 Normalized average shaft resistances for L/D=15................................ 105

Figure a.39 Average Shear Stresses Along Pier Shaft for L/D=15 105

Figure a. 40 Maximum average shaft resistance vs. cavity expansion ratio for L/D=15 106

Figure a. 41 Modulus of subgrade reaction vs. cavity expansion ratio for L/D=15. 106

CHAPTER 1.

INTRODUCTION

When natural soils are insufficient to carry the applied structural loads, columnar replacement or inclusion into weak soil by using a stiffer and stronger material is a commonly used engineering solution. The main purpose of using such columnar reinforcing element is to increase the bearing capacity, reduce total and differential settlements and improve slope stability. The columns may be either in the form of concrete-steel (conventional piles) or granular/cemented material (stone/gravel – lime/cement columns).

Several methods have been developed for the improvement of soft soils with stone column for decades. The technique utilized in construction of stone column depends mostly on site conditions and the contractor. The techniques are separated from each other in terms of drilling of soft ground and compaction of backfill material.

However, among all columnar reinforcement techniques, stone columns are the most cost-effective solution especially when traditional deep foundation methods are not strongly necessary due to the nature of the problem. In some engineering problems, performance requirements cannot be met simply by shallow footings and there is no need to bypass a thick zone of weak ground. Therefore, the use of the stone columns, which can be seen as an intermediate foundation solution, eliminates the need for massive over-excavation or expensive deep foundation system.

In order to construct stone columns, 10 to 35 percent of the weak soil is replaced with gravel. First, a hole is created in the ground by drilling or jetting. Then, the hole is filled and usually further expanded with compaction of gravel by vibration or ramming (impact) action. Final product is a form of stiffer composite mass of granular cylinders with local soil around them. This procedure provides stronger elements and stiffens the composite soil with higher shear strength and lower compressibility than its native form.

There are some feasibility requirements to use aggregate piers in engineering problems. The applicable design load on the stone column is between 5 and 50 tons per column. The loading is suggested to be relatively uniform. Also, experience showed that the method is not suitable for soils, which have shear strength less than 7 kN/m^2 and sensivities greater than 5.

1.1. Research Objectives

Different methods of aggregate pier construction inevitably introduce different lateral confining stress state on soils around piers. Well-documented research on piles shows that lateral confining stress play a major role on both bearing capacity and settlement. However, until recently very few researchers have focused on these construction-induced lateral stresses, and their significant effect on load deformation behavior of aggregate piers.

In this study, a sofware (Plaxis) including a 2D finite element based solution is utilized in order to evaluate load transfer mechanisms of a floating single aggregate pier with varying length in soft clay. Also, the effect of confining stresses produced by lateral displacement, which results from different construction techniques on the performance of the column are assessed. Furthermore, design charts showing which of the two resistances (shaft friction or tip) contributes to bearing capacity more and degree of mobilization under certain settlement requirement are clearly presented.

1.2 Scope of the Thesis

In this study, series of numerical simulations are performed by applying lateral displacements to the soil around a floating stone column to show effects of construction induced lateral stress on capacity mobilization . The simulations are also done by changing the length to diameter ratio of the stone columns. In short, Six floating columns havig length to diameter ratio (L/D) of 3, 4, 6, 9, 12 and 15 are analysed for a set of cavity expansion ratios ($\Delta r/r_0$= 0, 0.1, 0.3, 0.7 and 1)

In Chapter 2, a general overview of stone columns is presented. Assesment and details of the finite element analyses are described in Chapter 3. After giving the results of the numerical study in Chapter 4, discussions of the results are presented in Chapter 5. Finally, the summary and conclusion are given in Chapter 6.

CHAPTER 2.

A GENERAL OVERVIEW OF STONE COLUMNS

2.1. Introduction

First use of stone columns goes back to 17th century for Taj Mahal in India. "The historic structure has been successfully supported for over three centuries by hand dug pits backfilled with stone" (Townsend and Anderson, 2004). This early use of the system is a primitive form of stone column."In Europe, the concept was first applied in France in 1830 to improve a native soil" (Barksdale and Bachus, 1983).

However, a special probe which is called "vibroflot" was first developed and patented in Germany to use compaction of granular soil. Then, a variant of vibroflotation, which utilized aggregate as backfill material was developed in Germany in the 1950's. This method can be seen as the first modern (engineered) practice in which aggregate columnar inclusions (stone columns) were used. Installed columns with this method may serve as reinforcement, densification and drainage elements.

In this chapter, some essential information regarding to aggregate pier construction, design and factors which seriously influences the pier behavior will be given to clarify the basic idea behind this thesis. It is also important to note that stone column and aggregate pier terms are used interchangeably in following chapters to describe the same ground reinforcement technique as same in the literature.

2.2. Stone Column Construction Techniques

Several machinery, equipments and methods have been developed by different contractors to construct aggregate piers. The only differences in these methods are the way of installation and the compaction action exerted in the formation of the column.

In the following sections, some of the most commonly used construction methods are briefly introduced, since these methods assist to comprehend the construction-induced lateral confining pressure and its subsequent action.

2.2.1. Vibro Replacement Stone Columns

2.2.1.1. Dry Bottom Feed:

"In more stable insensitive cohesive soils with undrained shear strength values c_u=30-50 kN/m^2 the dry displacement method is applied, whereby the depth vibrator (Figure 2.2) penetrates by vibratory impact and by its own weight, sometimes increased by that of the heavy extension tubes, and always helped compressed air emanating through the bottom jets of the machine" (Kirsh K. and Kirsh F. , 2010).

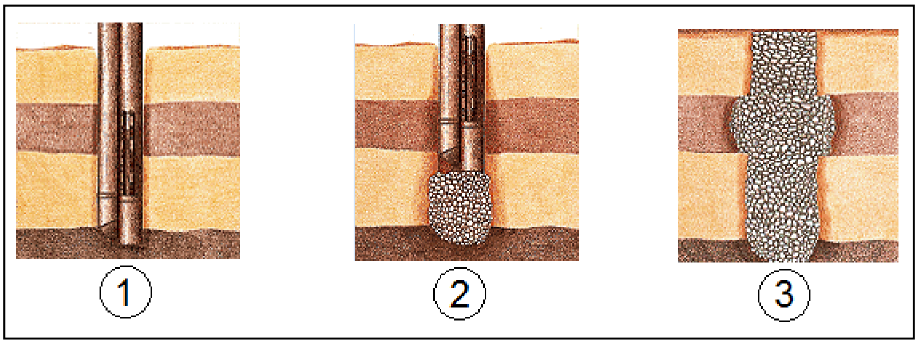

Figure 2.1 Construction phases of a dry bottom feed stone column (adopted from http://www.vibroflotation.com)

Simple description of the construction phases of dry bottom feed stone column is summarized as follows:

1. Penetration: By vibration and jetting action of air, the vibroprobe/vibroflot penetrates to the required depth. (Figure 2.1, no: 1).

2. Installation: After required treatment depth is reached, the vibroprobe is withdrawn, allowing gravel or crushed stone to immediately flow out at the tip. The stone column is created by re-lowering the vibroprobe, which compacts previously placed stone column material. (Figure 2.1, no: 2).

3. Completion: Final product is a dense, clean and uncontaminated stone column, which interlocks with the native soil. In addition, column diameter may change depending on surrounding soil stiffness. (Figure 2.1, no: 3).

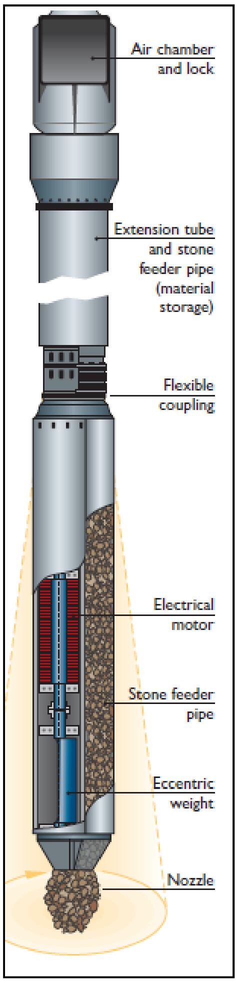
Air chamber and lock
Extension tube and stone feeder pipe (material storage)
Flexible coupling
Electrical motor
Stone feeder pipe
Eccentric weight
Nozzle

Figure 2.2 Typical view of a vibrotor to construct a dry bottom feed stone column (Keller Brochure 10-02 E)

2.2.1.2. Wet Top Feed:

"The vibro replacement wet method is employed only in water-bearing soft soils within a strength range of around c_u=10-30 kN/m^2 " (Kirsh K. and Kirsh F. , 2010). A special equipment called "vibrotor" (Figure 2.3) is employed in construction. A brief explanation of the application phases of wet top feed stone column is given below:

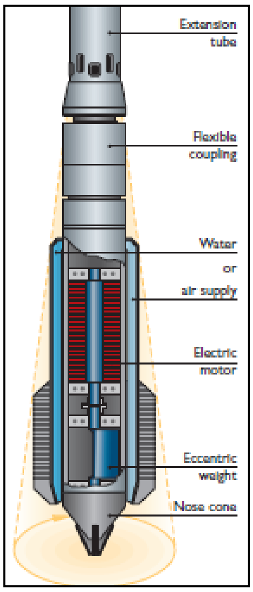

Figure 2.3 Typical View of a vibrotor to construct a wet top feed stone column (Keller Brochure 10-02 E)

1. Penetration: By the combined effect of vibration and jetting action of water, the vibrotor penetrates to the required depth. Water helps flushing of disturbed material from the hole.(Figure 2.4, no:1)

2. Installation: The vibrotor is lifted up. Coarse gravel or crushed aggregate is added into the hole and compacted by re-inserting vibrotor. The vibrator produces radial forces, which assist to force the column material horizontally out against the in-situ soil. (Figure 2.4, no:2)

3. Completion: The filling and compaction cycle is repeated to the surface. Finally, the surface is leveled and roller compacted. (Figure 2.4, no:3)

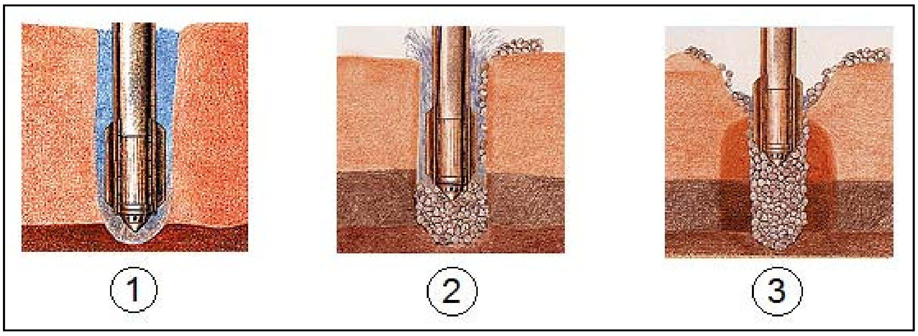

Figure 2.4 Construction phases of a wet top feed stone column (adopted from http://www.vibroflotation.com)

2.2.2. Rammed Aggregate Piers

Instead of horizontal vibration action exerted by vibrator, a vertical vibration (vibratory hammer) or a direct vertical ramming action is applied to compact the column material. Most commonly used construction procedure for rammed stone column can be specified as: i) drilling with conventional auger-filling-compaction or ii) driving a hollow steel tube-filling-compaction.

2.2.2.1 Drilling – Filling – Compaction

1. Drilling: A cavity is formed to the required depth with a conventional auger (Figure 2.5, no: 1).
2. Base formation: A firm and stable aggregate bulb is formed at the base with compaction energy produced by ramming. (Figure 2.5, no:2)
3. Installation: Layers of aggregate are filled into the hole compacted with the same ramming tamper. During construction process, the force applied by the tamper results in pushing out of aggregate material laterally to the sidewall of the cavity. (Figure 2.5, no:3)
4. Completion: Finally, a dense, very stiff and undulating-sided pier is constructed. (Figure 2.5, no:4)

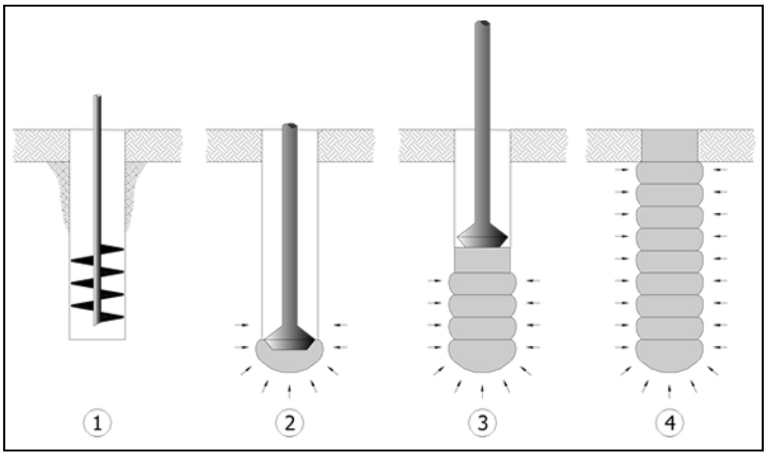

Figure 2.5 Diagrammatic Representation of a rammed stone Column Construction (taken from http://sentezinsaat.com.tr)

A very similar method has been used in India and surrounding area, with less sophisticated equipment. A heavy falling weight is utilized instead of specially design tamper. Construction steps of the method are depicted in Figure 2.6.

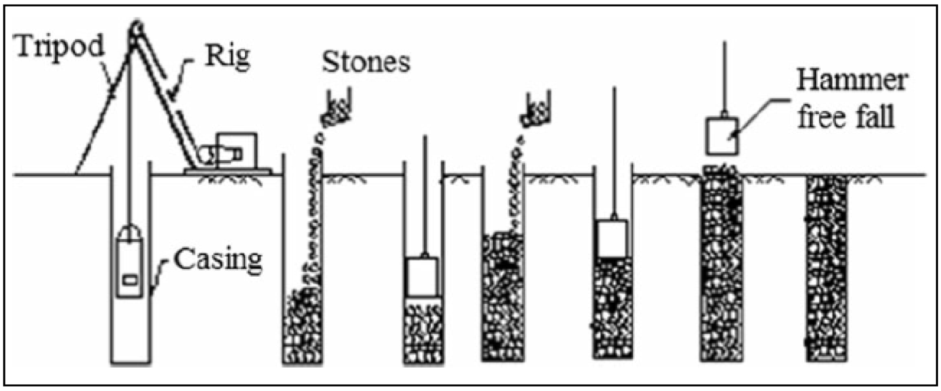

Figure 2.6 Construction steps of a rammed stone column in India region (Datye and Nagaraju, 1975)

2.2.2.2. Driving – Filling – Compaction

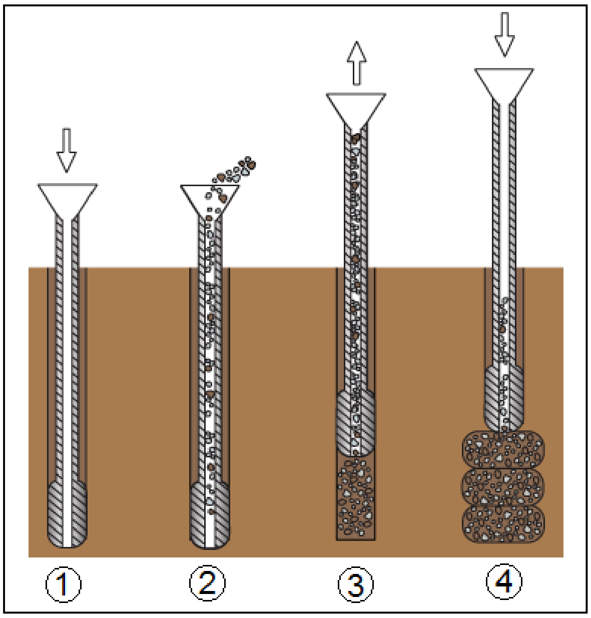

Figure 2.7 Diagrammatic representation of a rammed stone column construction (taken from http://www.helicaldrilling.com/)

1. Penetration: A closed end steel tube (mandrel) is driven into the soil to the planned depth using a static force. (Figure 2.7, no:1)

2. Installation: Inside of the tube (mandrel) is filled with aggregate and then, the mandrel is lifted up. (Figure 2.7, no: 2 and no: 3). In order to form the stone column, steel tube is pushed down and column material is compacted and laterally displaced. (Figure 2.7, no:4)

3. Completion: Filling and compacting steps are pursued until the planned elevation is reached. Final element is a very densely packed granular column.

2.3. Design of Stone Columns

Since stone column is an soil reinforcement technique integrated with native soil, the behavior of stone columns depend on many factors. First of all, after installation, the resulting column diameter depends on the properties of native soil itself and method of installation. The softer the soil and the greater the applied compaction energy as well as lateral displacement action, the larger the diameter. Secondly, for performance of groups of stone columns; application pattern, spacing, replacement ratio and stress concentration ratio are significant. Finally, mechanical properties of column backfill material after production play an important role in load settlement behavior. In the following section, some aspects of design of single isolated stone column is discussed briefly.

2.3.1. Principal Behavior and Ultimate Load Analysis of Single Stone Columns

The resistance of the floating stone column to the vertical axial load is based on shaft and less importantly on end resistance. In the literature, in order to find ultimate load capacity of a stone column, cavity expansion theories are usually utilized to find ultimate lateral support that can be achieved. However, lateral support does not directly resist on vertical load. Rather, it allows a stone column to safely transfer the vertical load through shaft shear stresses. Of course, without sufficient lateral support vertical loads cannot be transferred to skin friction and column fails due to bulging.

This phenomenon can be explained by two-chain ring system analogy (Figure 2.8). In order to carry the vertical load safely, either of the two links must not fail. Which of the two mechanisms are predominant depends on many factors (stiffness and strength of matrix soil etc.); however; usually in ultimate state, bulging failure (excessive lateral deformation) controls the bearing capacity. It means that stone column capacity can be simply improved by adding more lateral resistance (support) or retarding lateral failure of the composite soil system.

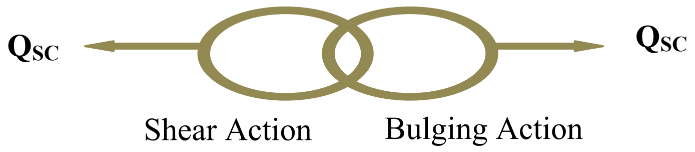

Figure 2.8 Conceptual analogy for load carrying mechanism of a single floating stone column

Van Impe and Madhav (1997) emphasized that while the tendency for bulging predominates in a stone column, it takes place together with the pile action because the only way to transfer applied loads to surrounding soil are shaft and base resistances. For a stone column in the course of bulging, not only lateral confining stress but also shear stress acts along the surface of the column.

Possible failure mechanisms of a single stone column are shown below in Figure 2.9. The failure mechanisms are for the axial compressive loading scenario, which comprises direct vertical load acting on column cross-section since type of loading also alters the failure mode. Besides, native soil parameters, column length to diameter ratio and relative ratio of column to in-situ soil stiffness play important role in failure mechanism.

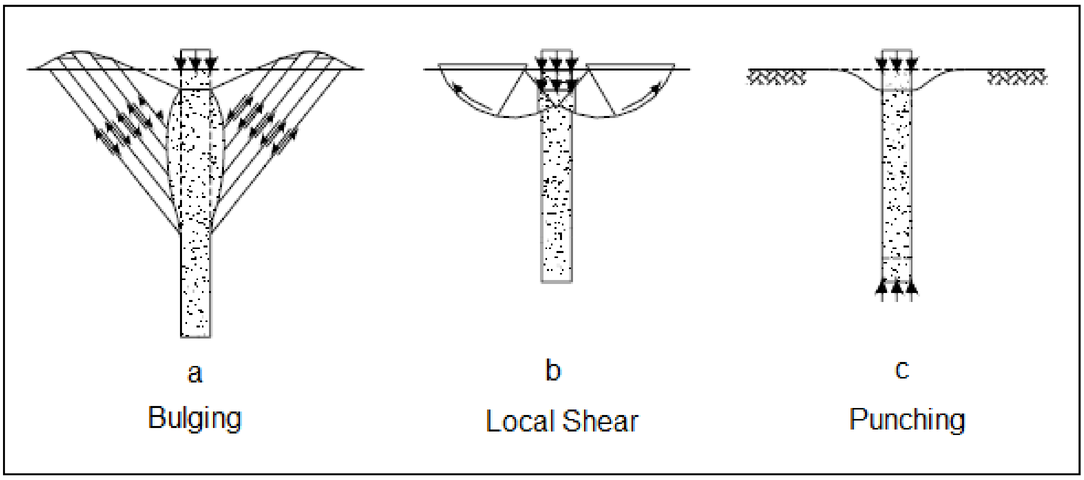

Figure 2.9 Possible failure modes for a single stone column (Kirsch, 2004)

2.3.2. Present Design Methods of Single Stone Columns

All present design methods focus on checking the lateral capacity of single stone column and do not give much information about mobilized component of resistance, (i.e. shaft friction under a permissible settlement). Some commonly utilized equations to estimate ultimate capacity of a single stone column will be presented in this section.

Bulging type behavior is idealized as an expanding infinitely long cavity to find ultimate undrained lateral capacity of surrounding soil by Hughes and Withers (1974). Ultimate lateral stress is given by the equation, which is produced for a frictionless material :

$$(\sigma_r)_{ult} = (\sigma_r)_0 + c(1+\ln (\frac{E}{2c(1+\mu)})) \tag{2.1}$$

where $(\sigma_r)_0$, c, μ and E are initial total radial lateral stress on cavity wall, undrained shear strength of the soil, Poisson's ratio and the elastic modulus of matrix soil, respectively. The equation is further simplified as:

$$(\sigma_r)_{ult} = (\sigma'_r)_0 + 4c + u_0 \tag{2.2}$$

where u_0 is initial pore water pressure in soil surrounding the stone column. For limiting vertical stress, equation can be given as:

$$(\sigma_v)_{limit} = ((\sigma'_r)_0 + 4c)*(K_p)_{stone} \tag{2.3}$$

where $(K_p)_{stone}$ is assumed by Hughes and Withers (1974) as Rankine's passive state lateral earth pressure coefficient, that is :

$$(K_p)_{stone} = \frac{1+sin\Phi}{1-sin\Phi} \tag{2.4}$$

where Φ is drained friction angle of the stone column material.

Another cavity expansion solution is suggested by Vesic (1972). The equation includes cohesion and friction terms to analyze both cohesive and cohesionless soils. Ultimate total lateral stress is given by:

$$\sigma_3 = c*F'_c + q*F'_q \tag{2.5}$$

where c, q and F'_c, F'_q are cohesion, mean (isotropic) stress $((\sigma_1+\sigma_2+\sigma_3)/3)$ at the equivalent failure depth and cavity expansion factors, respectively. In order to find ultimate vertical stress, lateral stress is multiplied by $(K_p)_{stone}$.

Another commonly used method based on bulging failure to find ultimate vertical capacity in clayey soil is a very simple formula given in Equation 2.6:

$$q_{ult} = N_c * c_u \qquad (2.6)$$

where N_c is bearing capacity factor and c_u is undrained shear strength. The bearing capacity factor can be determined theoretically by using Vesic's cavity expansion solution or by semi-empirically based field observations. The N_c values suggested in the literature are given in Table 2.1.

Table 2.1 N_c coeficients suggested by different authors for different cases

N_c	Author	Explanations
18 to 22	Barksdale and Bachus (1984)	- 22 for soil having high initial stiffness. - 18 for soils having low stiffness.
25	Mitchell (1981)	- For vibro replacement stone columns
25 to 30	Datye et al (1982	- Vibro replacement columns.
40; 45 to 50	Datye et al (1982)	- 40 for uncased, rammed stone columns. - 45-50 for cased, rammed stone columns

2.3.3. Tip Resistance

Some researchers in the literature discussed the contribution of end bearing to overall resistance. It was denoted that the contribution is insignificant, especially in long columns. Rao and Reddy (1996) reported that just 13 % of applied load is resisted by end bearing for a very short aggregate pier whose L/D ratio is 2.5.

2.4. The Effect of Construction-Induced Lateral Stresses on Behavior of Stone Columns

2.4.1. Overview of Lateral Stress Influence on Behavior

As part of the construction of stone columns, a cavity is opened by any available methods; which depends on the contractor; and column material is compacted in that open hole. The compaction energy exerted by the equipment inevitably results in lateral displacement of soil around the cavity and an increase in lateral confining stress. The phenomenon and its subsequent results are presented in figure 2.10 by Handy (2001). In Mohr diagram given below, circle “A” represents existing state of stress in soil body. After the installation of stone column, horizontal stress increases and sometimes exceeds the vertical stress by bringing soil to passive state. That alteration in stress state is denoted by circle “B”. Meanwhile, vertical increase during foundation loading is presented by circle “C”.

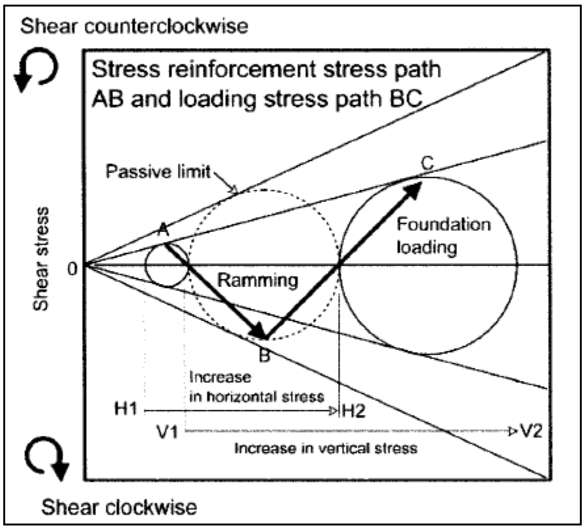
Shear counterclockwise
Stress reinforcement stress path AB and loading stress path BC
Passive limit
C
A
Foundation loading
0
Shear stress
Ramming
B
Increase in horizontal stress
H1
H2
V1
V2
Increase in vertical stress
Shear clockwise

Figure 2.10 Change of lateral stress state at in-situ soil after construction and foundation loading (Handy, 2001)

As shown in Figure 2.10, increase in lateral stress due to expansion of the cavity in the matrix soil causes increase in the bearing capacity of the column. Besides, the contact friction (shear) locked as a result of natural consolidation process is reversed by applying lateral stresses. Figure 2.11 shows the simple model suggested by Handy (2001) for normally consolidated soils. The figure shows how application of lateral stress during installation of stone column can alter the direction of shear stress among the soil grains.

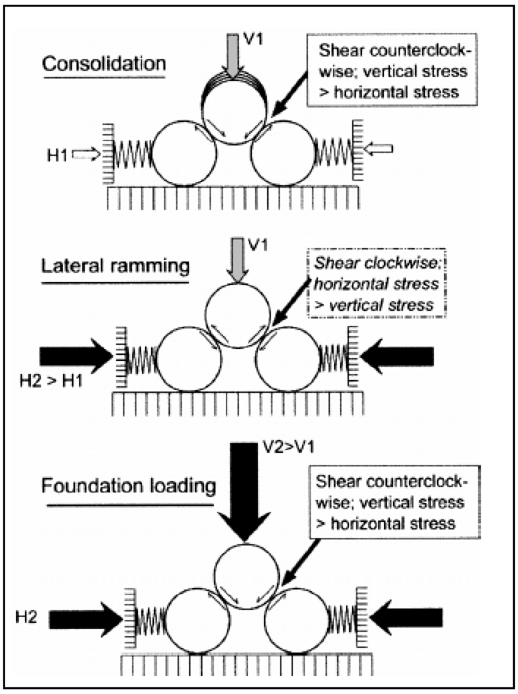
Consolidation
V1
Shear counterclockwise; vertical stress > horizontal stress
H1
Lateral ramming
V1
Shear clockwise; horizontal stress > vertical stress
H2 > H1
V2>V1
Foundation loading
Shear counterclockwise; vertical stress > horizontal stress
H2

Figure 2.11 Friction reversals among soil grains to explain increased allowable vertical stress (Handy, 2001)

Moreover, pre-mobilization of the lateral effective stresses in the construction stage results in more lateral support, and it gives rise to little radial strains in first stage of loading. Therefore, adding increased lateral support improves the load settlement behavior (i.e.: improves the stiffness) since in service loads bulging deformation of stone column is further decreased. This allows the column to carry additional axial load with shaft friction.

Figure 2.12 shows dominant load transfer mechanism of a single isolated aggregate pier. The fundamental resistance to axial load is shaft friction. However, the failure generally results from insufficient lateral resistance. Considering all these stated above, lateral confining stress is important in terms of either shaft resistance or lateral support mechanisms.

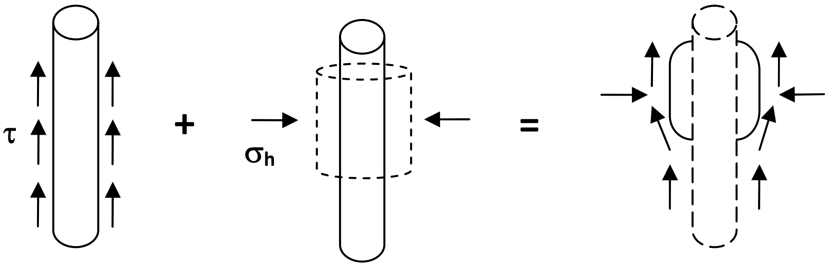

Shear Action:
Main mechansim which carries vertical load

Bulging Action:
Dominant mechanism of failure in ultimate state.

Combined Stone Column Action

***Note:** Some tip resistance is mobilized but it is significant amount in very short columns and less important under allowable settlement criteria. Therefore, tip action is not shown on the figure.

Figure 2.12 Conceptual representation of load carrying mechanisms in a single stone column

2.4.2. Studies in Literature Associated with Lateral Stress Around Aggregate Pier

Stone column insertion into weak soils as a pure replacement element creates false perceptions. It should be noted that installation is accompanied by vibration and more importantly horizontal displacement of the soil. Hence, installation of the pier produce positive changes in stress state, both in the pier and in the treated soil mass. For the optimal design of aggregate piers, lateral stress action of pier installation should be considered.

Kirsch and Sondermann (2001) presented that "vibro" process has a great influence on the state of stresses of soil surrounding the pier. Also, Elshazly et al. (2006) showed that the vibro-installation increases state of lateral stress in soil by back-calculating the ratio of horizontal to vertical soil stress (K*) in finite element based analysis. They demonstrated that post installation lateral earth pressure ratio (K*) values change between 1.1 and 2.5. Moreover, studies by Kirsch (2008) presented the individual and the global installation effects for a group of stone columns. The installation action was modeled as cavity expansion, and an increase in the confining stress was clearly stated. Finally, disregarding the lateral stress changes was shown to cause underestimation of real ultimate bearing capacity and overestimation of true field settlement.

CHAPTER 3.

NUMERICAL ASSESSMENT

3.1. An Overview of Material Modeling

In order to simulate construction induced confining stresses around stone columns and overall behavior under compressive loading, an advanced soil constitutive model widely known as “Hardening Soil Model” will be utilized. The main idea of using such a sophisticated model, instead of simpler Elasto-Plastic (linear elastic perfectly plastic, Mohr-Coulomb) model is to simulate stiffness increase due to confining stress as well as non-linear and dilational behavior of soils.

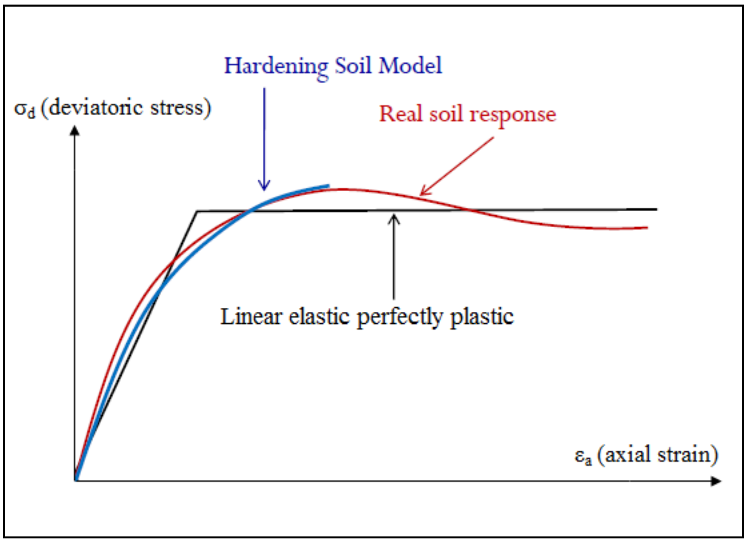

Figure 3.1 Comparison of real soil behavior with model predictions (adopted from Ehsan R., 2013)

The Figure 3.1 shows the simple representation of general stress-strain curve of a soil sample and how two models estimate this true response. The software which will be utilized in this study is Plaxis 2D version 8.2. Here, some of the basic properties and superior aspects of “Hardening Soil” model will be summarized by mostly benefiting from Plaxis manuals.

3.1.1. Hardening Soil Model

The hardening soil model is an elasto-plastic model, which takes into account elastic modulus degradation through straining and hardening that a soil undergoes during plastic state. In order to simulate decreasing stiffness, the model uses a hyperbolic stress-strain relationship. The relationship between the vertical strain, ε_1, and the deviator stress, q, in primary drained triaxial loading is defined as:

$$\varepsilon_1 = \frac{1}{E_{50}} * \frac{q}{1-q/q_a} \qquad (3.1)$$

where q_a is the asymptotic value of the shear strength.

Hardening Soil model separates the stiffness into two component, i.e.: triaxial stiffness (E_{50}, drained) and oedometer stiffness (E_{oed}). The model also has capability of defining these two stress components as stress dependent. In order to describe confining stress dependency of both Young’s Modulus and oedometer stiffness, following equations known as power law is used:

$$E_{50} = E_{50}^{ref} * \left(\frac{c*cos\varphi - \sigma_3' * sin\varphi}{c*cos\varphi + p_{ref} * sin\varphi}\right)^m \qquad (3.2)$$

$$E_{oed} = E_{oed}^{ref} * \left(\frac{c*cos\varphi - \sigma_3' * sin\varphi}{c*cos\varphi + p_{ref} * sin\varphi}\right)^m \qquad (3.3)$$

where c, φ, σ_3, p_{ref} and m are respectively; cohesion intercept, angle of friction, effective confining pressure in a triaxial test, reference pressure and power exponent m. m is an indicator of stress dependency.

E^{ref}_{50} is secant stiffness modulus corresponding to the reference confining pressure p_{ref}, which is usually taken as default 100 units. However, E^{ref}_{oed} is tangent stiffness defined in the reference confining pressure. The figures given below show the definition of both of the elastic moduli. (Figure 3.2 and 3.3).

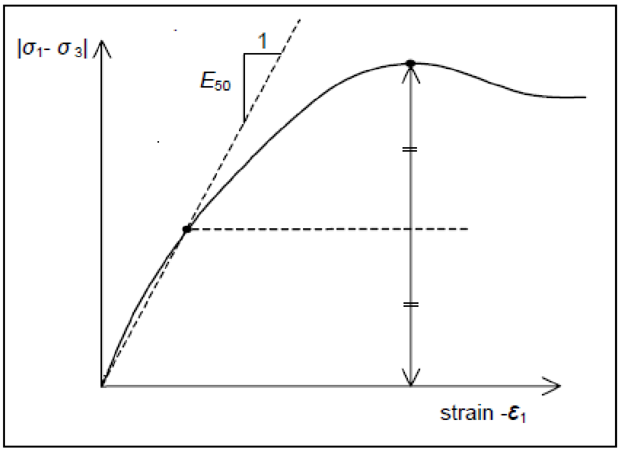

Figure 3.2 Definition of E_{50} for standard drained triaxial test results (Plaxis, 2002)

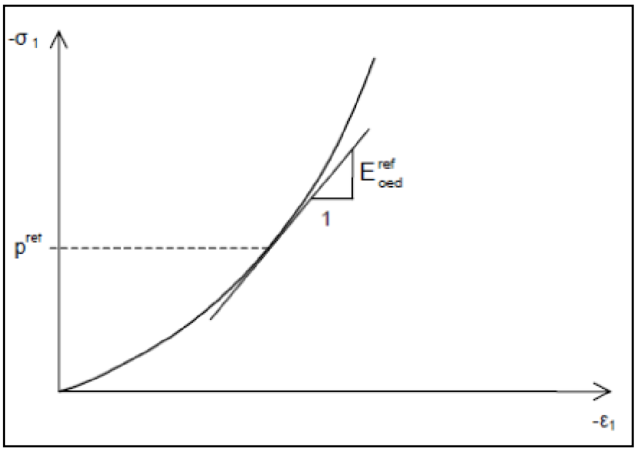

Figure 3.3 Definition of E^{ref}_{oed} in oedometer test results (Plaxis, 2002)

Besides, stress dependency of stiffness modulus is also valid for unloading and reloading phase. The unloading stifness (E_{ur}) is defined in the same manner:

$$E_{ur} = E_{ur}^{ref} * \left(\frac{c*cos\varphi - \sigma_3'**sin\varphi}{c*cos\varphi + p_{ref}*sin\varphi}\right)^m \qquad (3.4)$$

The Figure 3.4 given below is a graphical illustration showing how the model describes soil behavior. Here, q_f is asymptote of hyperbolic curve and usually a ratio of $R_f = q_a/q_f = 0.9$ is assumed. When ultimate state is reached, the failure criterion described by the Mohr-Coulomb is satisfied and perfectly plastic yielding occurs.

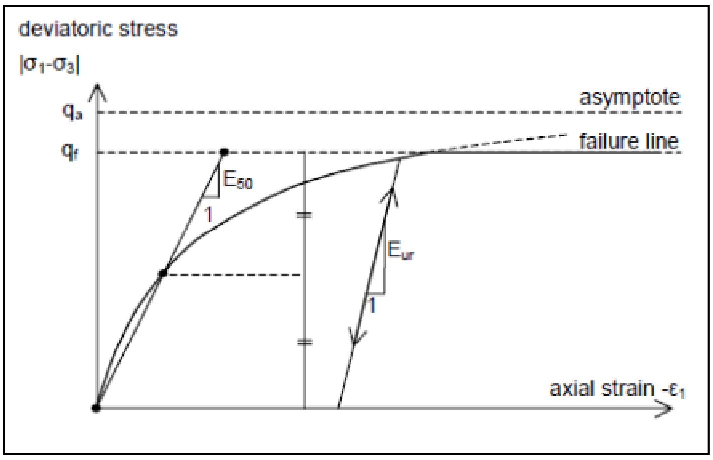

Figure 3.4 Hyperbolic stress-strain relation in primary loading (Plaxis, 2002)

Moreover, the “Hardening Soil” model addresses the hardening phenomenon in two parts; shear hardening and volumetric hardening. The shear hardening part defines the plastic shear strains in deviatoric loading, whereas volumetric hardening accounts for the volumetric strain in primary compression. Figure 3.5 shows the two yield surfaces in principal p-q space.

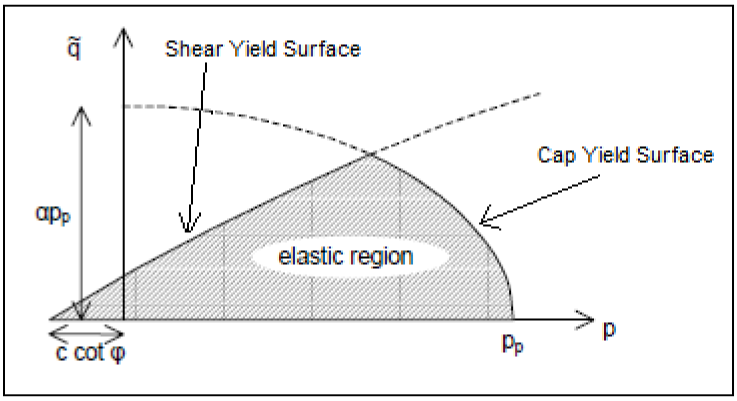

Figure 3.5 Yield surfaces of Hardening-Soil model in p-q stress space

Total yield contour of the "Hardening Soil" model in principal stress space for a cohesionless soil is given in Figure 3.6. In plastic straining phase, the yield surfaces can expand homothetically.

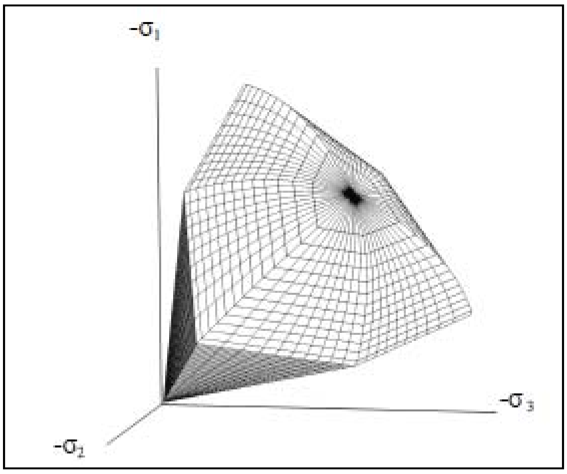

Figure 3.6 Representation of total yield contour of the Hardening-Soil model in principal stress space for cohesionless soil (Plaxis 2002)

In summary, "Hardening Soil" model has advantages compared to "Elasto-Plastic" (better to refer it as linear elastic-perfectly plastic Mohr-Coulomb) model. In the literature, it is recommended to use "Elasto-Plastic" model for preliminary assessments and for safety factor (stability) calculations. Whereas, "Hardening Soil" model should be utilized to obtain more accurate deformation predictions. Advanced capabilities of the "Hardening Soil" model are:

- Hyperbolic stress-strain relationship in axial compression
- Plastic strain in mobilizing friction (shear hardening)
- Plastic strain in primary compression (volumetric hardening)
- Stress-dependent stiffness according to a power law.
- Elastic unloading/ reloading compared to virgin loading
- Memory of pre-consolidation stress
- Dilatancy below Mohr- Coulomb line

However, beside these complexities of the real soil behavior that the model describes, the Mohr-Coulomb failure (yield) criteria is still employed to define the failure because Mohr-Coulomb failure criteria is sufficiently accurate and numerically efficient.

3.2. Description of the Numerical Simulation

Schematic view of finite element model used in this study is shown in Figure 3.7. A pier element installed in a single matrix soil is modeled for analysis. The physical boundary of the model was extended radially from the center of the pier to minimum 15D; where D is the diameter of the stone column. The bottom of the model is extended to 2L; L is length of the column; and full fixity boundary conditions were defined. The compressive load on the stone column was applied directly at the column head by a loading plate. The loading plate was selected as a circular concrete footing, which is modeled as a linear elastic, nonporous material and same diameter with the pier.

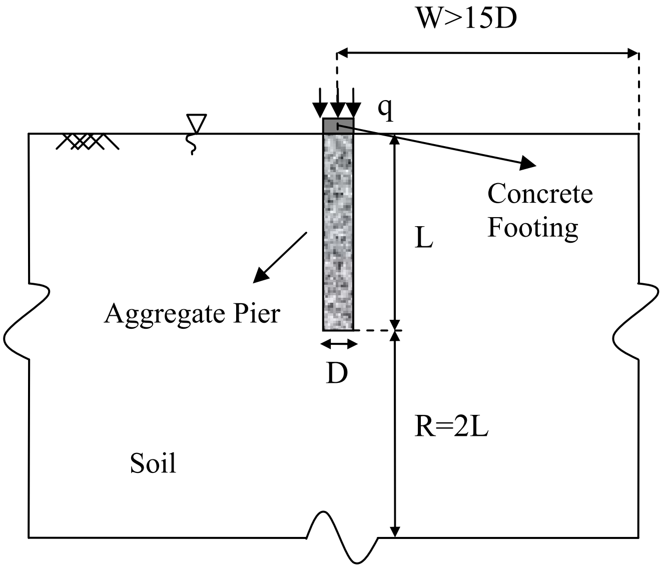

Figure 3.7 Schematic illustration of the geometry of analysis case

Moreover, a fully drained condition was assumed for all phases including installation of the pier and pier loading processes. A static pore water pressure profile was generated by assuming water table at the ground surface.

Finally, axi-symmetric finite element (FE) model with unstructured mesh including 15-node, triangular elements was utilized. Figure 3.8 (a and b) shows the idea behind an axi-symmetric model and 15-node triangular element. The axi-symmetric model executes deformation and stress as identical in any radial direction for structures, which have a symmetric cross-section and a loading scheme around their central axis.

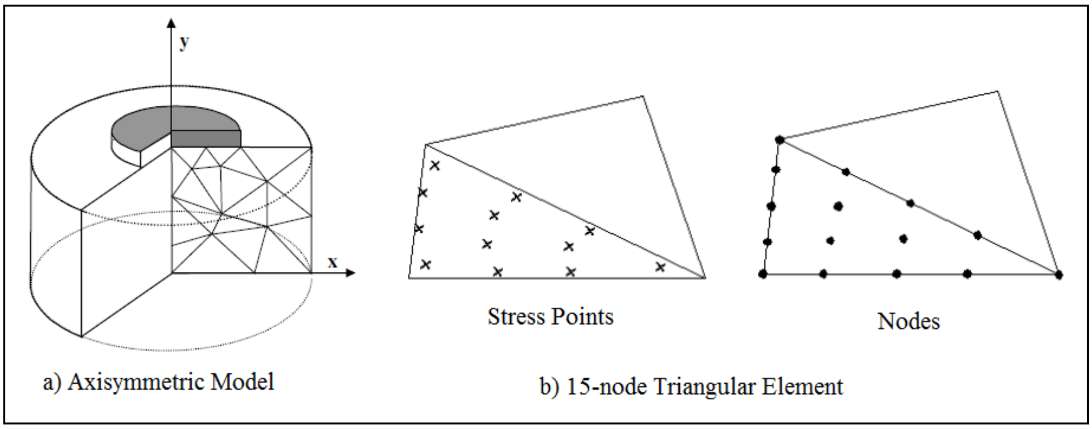

Figure 3.8 a) 2D Modeling of Axisymmetric Problem b) Triangular Mesh Element (Plaxis 2002)

3.2.1. Modeling of the Installation of Stone Columns

During the installation of the stone column, lateral displacement is exerted by the machinery equipment. The lateral displacement causes several effects in matrix soil that were discussed in literature review section of this thesis. As specified previously, the main result of this lateral displacement is the increase in stress confining the column.

In order to imitate the construction-induced lateral displacement to a certain degree, the predrilled hole is expanded. Schematic view of the procedure is given in the Figure 3.9 below. A cavity is formed and then previously designated lateral displacement is applied to expose stone column to compressive stresses.

It is important to note that in simulating cavity expansion process, *drained* analysis was adopted since the field of interest is the behavior of aggregate pier under certain effective confining pressure induced by lateral expansion.

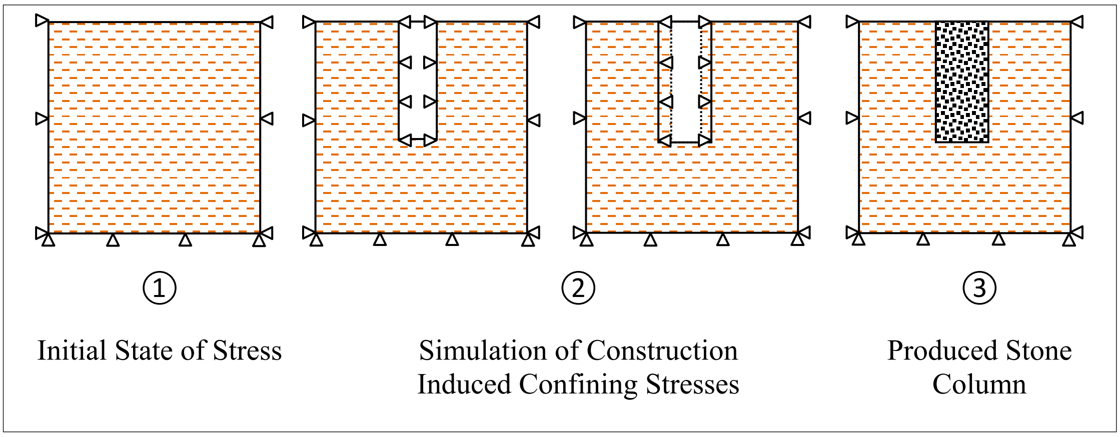

Figure 3.9 Numerical simulation of stone column construction

3.2.2. Updated Mesh Analysis

In original finite element formulation, the effect of the geometry change of the mesh on the equilibrium conditions is neglected. It is generally a good approximation in case of relatively small deformations. However; several trial analyses performed within the scope of this thesis revealed that large strains were observed especially after confining stress around the pier was considerably increased. Therefore, the “updated mesh” analysis option integrated in Plaxis (8.2) was adopted to take this effect into account.

Since the updated mesh option was selected, the calculation is not performed according to the small deformation theory. Now, the stiffness matrix in the updated mesh analysis is based on the deformed geometry. It was experienced by the author that the load displacement curve is different when large strains are of concern. An increase in ultimate stress and decrease in strain was observed in updated mesh calculation compared to normal calculation.

3.3. Selection of Model Parameters

A medium soft clay of intermediate plasticity is selected as the surrounding soil material (PI=20 % - 30 %). Mostly crushed stone or gravel is used as a backfill material for stone columns, therefore, a well graded coarse granular material is assumed. Based on these assumptions, “Hardening Soil” model parameters will be selected by using documented correlations in literature.

3.3.1. Selection of Friction Angle

Clay Material:

Drained friction angle of normally consolidated clays is given by Gibson (1953) as shown in Figure 3.10. From the figure, friction angle of clay with a PI value of 20-30 is determined as 27°.

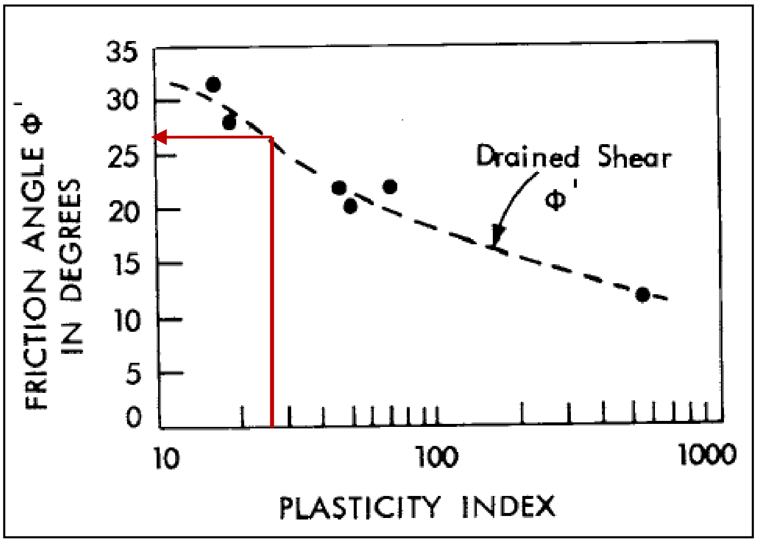

Figure 3.10 Variation of φ' with plasticity index for normally consolidated remolded clays (Gibson, 1953).

Column material:

Friction angle of coarse backfill material is determined by comparing values from different sources. The most typically used design parameters are summarized in Table 3.1 below by Barksdale and Bachus (1983):

Table 3.1 Design parameters used by selected organizations for stability analyses of stone column reinforced ground (adopted from Barksdale and Bachus, 1983)

Organization	Stress Concentration (n)	φ (°)	S.F.
Vibroflotation Foundation Company	2	42	1.25-1.5
GKN Keller	2	45 40	1.3-1.4
PBQD	1-2	42	1.3
Japanese (Sand compaciton piles)	3-5	30--35	1.2-1.3

Figure 3.11 given below shows the friction angle of aggregates having different gradations specified by AASHTO.

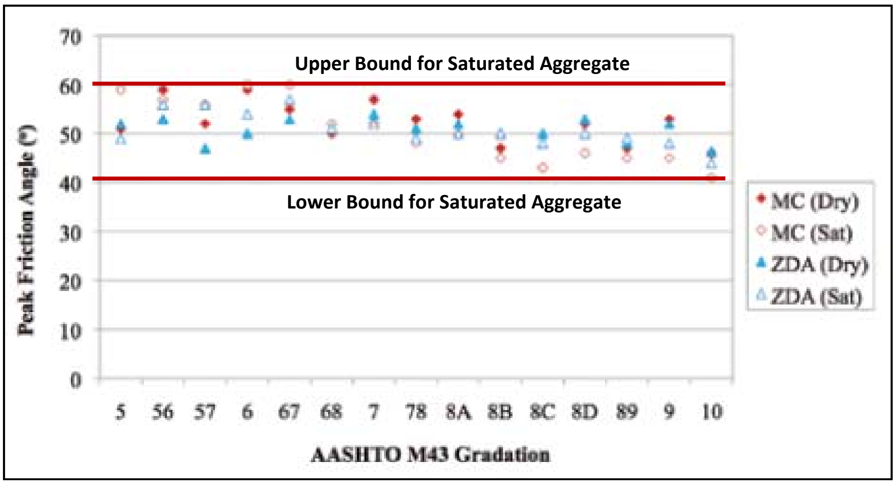

Figure 3.11 Summary of peak friction angle results (FHWA, 2013)

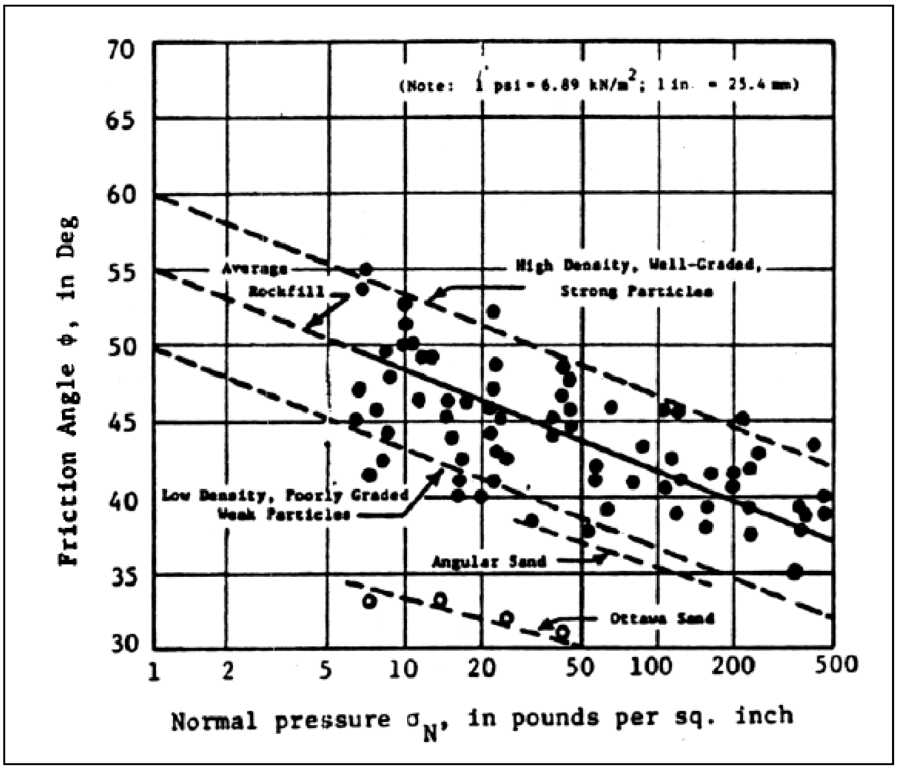

Figure 3.12 Angle of friction of rockfill obtained from large diameter triaxial tests (Barksdale and Bachus, 1983)

Barksdale and Bachus (1983) reported that friction angle of stone column material varies between 40 and 45 degrees. Fox and Cowell (1998) stated angle of friction of aggregate material as 48 to 52 degrees. In the light of proposals from different researchers and using the charts and the table above (Table 3.1, Figure 3.10, 3.11 and Figure 3.12) as a guideline, friction angle of the pier material is assumed as 45^{o}. Angle of dilation of the material is determined as 12^{o} by using the equation 3.5 as recommended by Bolton (1986):

$$\psi = \varphi_c - 33^{o} \qquad (3.5)$$

3.3.2 Selection of Stiffness Parameters

Stiffness parameters of a normally consolidated clay can be determined by utilizing the following correlation in literature based on vertical effective stress and plasticity index (Brinkgreve, 2005):

$$E_{oed} \approx \frac{500}{I_p} \sigma'_1 \tag{3.6}$$

Average value of I_p is between 20 to 30. For reference stress of $\sigma'_1 = 100$ kPa and $I_p = 25$, stiffness modulus :

$$E_{oed}^{ref} \approx 500/25*100 \approx \mathbf{2\ Mpa}$$

For normally consolidated clays, the oedometer stiffness may be approximated by simply taking the half of the reference triaxial stiffness (Brinkgreve, 2005):

$$E_{oed}^{ref} \approx \tfrac{1}{2} E_{50}^{ref} \tag{3.7}$$

$$E_{50}^{ref} \approx \mathbf{4\ Mpa}$$

Stiffness parameters for aggregate / stone material:

The relation suggested for sands by Janbu (1963) may be used as a guide to determine stiffness properties of stone column material:

$$E_{oed} \approx E_{oed}^{ref} \sqrt{\frac{\sigma'_1}{p^{ref}}} \tag{3.8}$$

where the reference stifnesss E_{oed}^{ref} at reference stress of 100 kPa is suggested by Janbu (1963) as 50 Mpa.

$$E_{oed}^{ref} \approx 50 \text{ Mpa}$$

The triaxial reference stiffness is about equal to reference oedometer stiffness. As a result;

$$E_{oed}^{ref} \approx E_{50}^{ref} \approx 50 \text{ Mpa}$$

may be used for practical purposes.

However, elastic constants of gravels based on soil type (modified after AASHTO, 1996) is give as:

Table 3.2 Elastic modulus values for gravels (AASHTO, 1996)

E_{50} of Gravels (Mpa)	
Loose	30 to 80
Medium dense	80 to 100
Dense	100 to 200

The table above gives clue about possible range of values of triaxial modulus of elasticity but the reference pressure is not specified. In the light of that information triaxial elastic modulus of aggreate material is selected as **75 Mpa** conservatively. Also, the elastic modulus values studied in literature correspond to stiffness ratio between the aggregate pier and surrounding soil varying from 5 to 60. As a result, the suggested value of $(E^{ref}{}_{50})_{column}/(E^{ref}{}_{50})_{soil} = 75/4 \approx 19$ seems like a reasonable average value.

3.3.3. Other Parameters

Power law (m):

The power m determines how elastic modulus changes with change in effective stress. The effective stress dependency of stiffness can simply be modeled by the following equation:

$$E = E^{ref}\left(\frac{\sigma'_1}{p^{ref}}\right)^m \tag{3.9}$$

Here, m represents the nonlinear increase in stiffness as a function of the confining stress. It is suggested as 1 for normally consolidated clays and 0.5 for sands or gravels (Brinkgreve, 2005).

Cohession intercept (c):

For numerical efficiency, values of 1 and 5 kPa are assumed for normally consolidated clay and aggregate; respectively.

3.4. Drained or Undrained Analysis

The factors which determine whether a soil is in drained or undrained condition are rate of loading and permeability of the soil. It is a well-known fact that even if a soil is a highly permeable one, if the rate of loading is sufficiently fast to cause excess pore pressure to be developed, the soil is under undrained conditions.Conversely, a case of loading on a less permeable soil may be treated as drained if long term behavior is to be assessed.

In case of analysis of stone column construction and vertical loading, a drained condition is likely to occur by considering the associated loading time and drainage facility of stone column. In order to assist to consider a loading case as drained or undrained following suggestion was made by Vermeer and Meier (1998):

For $T_v < 0.01$ $U < 10\%$ → undrained analysis
For $T_v > 0.40$ $U > 70\%$ → drained analysis

$$T_v = c_v.t/d^2 \tag{3.10}$$

where U, T_v, c_v, t and d are average degree of consolidation, dimensionless consolidation time, coefficient of consolidation, consolidation duration and length of the drainage path, respectively. The suggestion was made using 1D consolidation theory and associated equations.

“Values of c_v for clays vary from about 1.0 cm^2/h (10 ft_2 /yr) to about 100 times this value. Values of c_v for silts are on the order of 100 times the values for clays, and values of cv for sands are on the order of 100 times the values for silts, and higher. These typical values can be used to develop some rough ideas of the lengths of time required to achieve drained conditions in soils in the field”. (Duncan and Wright, 2005). By assuming average values of the necessary parameters:

For undrained case → $U= 70\ \%$ and $T_v \approx 0.4$, Vermeer and Meier (1998).

Assume a coefficient of consolidation (c_v) as 50 cm^2/h and a length of drainage path of 50 cm:

$$T_v = c_v.t/d^2 , \quad 0.4 = 50*t/50^2 \quad \rightarrow \quad t = 20 \text{ hours.}$$

Since average loading time for any type of construction is much more than the calculated average drainage duration (20 hours), it is reasonable to perform analysis as drained unless short term capacity is strictly critical.

3.5. Summary of Analysis Cases

3.5.1. Analysis Case: Single aggregate pier in clay soil

The Figure 3.13 shown below, illustrates the analysis cases with material property inputs. In the same way Table 3.3 summarizes expansion ratios. Expansion ratio is defined as the ratio of lateral expansion of stone column's radius, **Δr,** to its initial radius **r_0.**

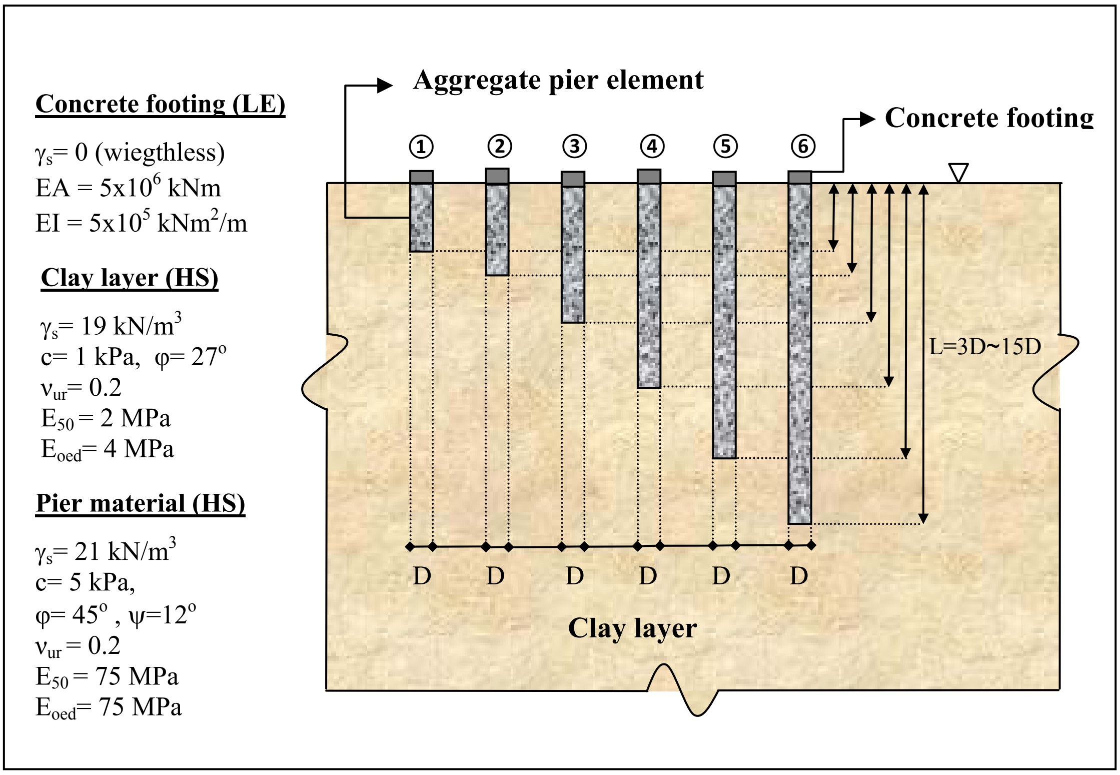
Concrete footing (LE)
γ_s= 0 (wiegthless)
EA = 5x10^6 kNm
EI = 5x10^5 kNm^2/m
Clay layer (HS)
γ_s= 19 kN/m^3
c= 1 kPa, φ= 27°
ν_{ur}= 0.2
E_{50} = 2 MPa
E_{oed}= 4 MPa
Pier material (HS)
γ_s= 21 kN/m^3
c= 5 kPa,
φ= 45° , ψ=12°
ν_{ur} = 0.2
E_{50} = 75 MPa
E_{oed}= 75 MPa
Aggregate pier element
Concrete footing
① ② ③ ④ ⑤ ⑥
L=3D~15D
D D D D D D
Clay layer

Figure 3.13 Illustration of the analysis case

Table 3.3 Summary of Analysis Cases

CASE NO	L/D	Cavity Expansion Ratios ($\Delta r/R_0$)
1	3	0, 0.1, 0.3, 0.7, 1
2	4	0, 0.1, 0.3, 0.7, 1
3	6	0, 0.1, 0.3, 0.7, 1
4	9	0, 0.1, 0.3, 0.7, 1
5	12	0, 0.1, 0.3, 0.7, 1
6	15	0, 0.1, 0.3, 0.7, 1

CHAPTER 4.

ANALYSIS RESULTS

As a reminder, the study focuses on the mobilization of resistance components of a granular inclusion system (aggreagate piers) under increasing monotonic vertical loading condition and under different confining stress state. Similarly, Reese and O'Neill (1988) clearly exposed the development of these resistances with settlement for piles and the curves was generated in form of normalized capacity-settlement curves as shown in the figure 4.1 below. Since, the study was inspired from the study of Reese and O'Neill (1988), the same way of presentation of the results is used. This presentation makes it possible to compare the findings with previous studies and eleminate case sensitivity as far as possible.

In this chapter, the results of generic finite element analyses in the form of normalized stress-displacement curves will be presented. However, in order to clarify the procedure, generation of a sample curve will be explained in the detail. In the following section, some of the important points in curve generation procedure will be discussed.

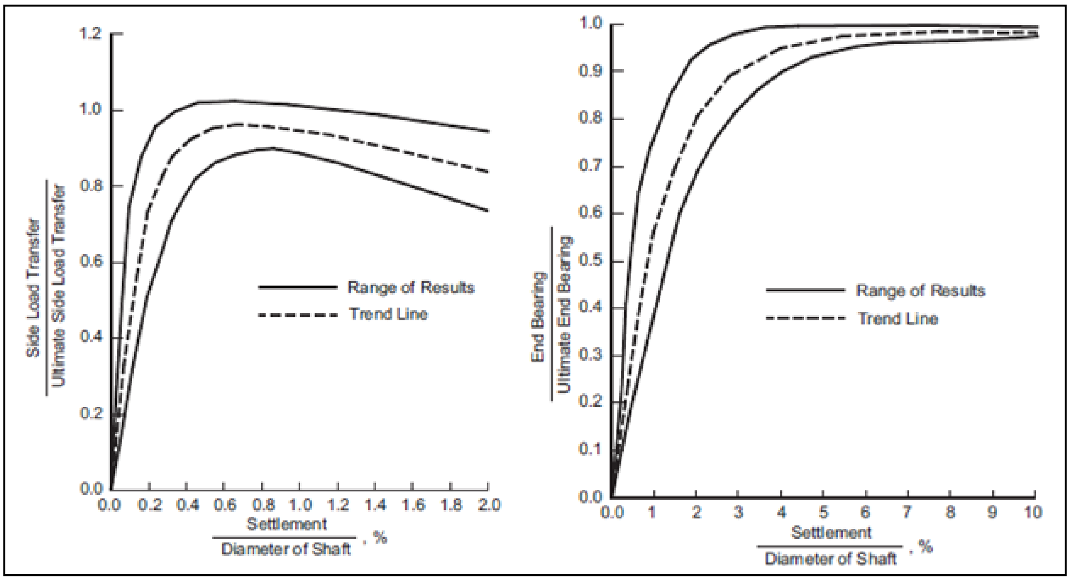

Figure 4.1 Normalized Load Transfer in side-shear and end-bearing capacity vs. Settlement in cohesive soils(After Reese and O’Neill, 1988)

4.1. Assessment of Load Displacement Curves

In the literature, no certain method for the assessment of aggregate pier (stone column) bearing capacity from load settlement curves exists. However, in performing field load test for aggregate piers, the procedure used for piles is commonly adopted. Therefore, using the guidelines prepared for piles in the assessment of field load tests may be applicable for aggregate piers. Some of the most commonly used methods to assess axial pile capacity are Davisson (1972), De Beer’s method (1967), De Beer and Wallays (1972), Brinch Hansen’s 90 percent criterion (1963), Mazurkiewicz (1972), Fuller and Hoy (1970), Butler and Hoy (1977), Vander Veen (1953). Yet, all these methods to define ultimate capacity are somehow judgmental and failure definition is not based on clear mathematical or engineering criteria.

In this thesis, in order to determine ultimate capacity in mobilized shear stress-displacement curve, a hyperbolic curve fitting procedure is adopted to provide robust algorithm and simplicity. The procedure which will be subsequently given is in the same way with assesment methods known as “Chin-Kondner and “modified Chin”.

The hyperbolic regression curve is in the form of;

$$\tau_{\mathrm{avg}} = \frac{x}{a+bx} \qquad (4.1)$$

where τ_{avg}, x, a and b are average shaft resistance, axial deformation and unknown constants of hyperbolic curve; respectively. The maximum shaft resistance can be obtained by taking limit of the Eq. 4.1.

$$(\tau_{avg})_{ult} = (\tau_{avg})_{max} = \lim_{x\to\infty}\left(\frac{x}{a+bx}\right) = \frac{1}{b} \qquad (4.2)$$

Meanwhile, the average shaft resistance is found by following equation :

$$\tau_{avg} = \frac{\sigma_{top} x A_{top} - \sigma_{tip} x A_{tip}}{A_{cyl}} \qquad (4.3)$$

where σ_{top}, σ_{tip}, A_{top}, A_{tip} and A_{cyl} are top stress, tip stress cross-sectional area of pier at the top or tip and cylindirical surface area of the pier. If we assume A_{top}, A_{tip} and A_{cyl} do not change during loading phase and $A_{\mathrm{top}} = A_{\mathrm{tip}}$;

$$\tau_{avg} = \frac{\sigma_{top} * \pi {r_0}^2 - \sigma_{tip} * \pi {r_0}^2}{2\pi \mathrm{r}_0 \mathrm{L}} \qquad (4.4)$$

Final simplified version is as follows:

$$\tau_{\mathrm{avg}} = (\sigma_{\mathrm{top}} - \sigma_{\mathrm{tip}}) * \frac{r_0}{2L} \qquad (4.5)$$

The last step in curve generation is to normalize shaft friction by ultimate friction (eq. 4.2) and top settlement by diameter. The final curve is in the form of normalized values of shaft friction and top or tip settlement.

It is important to note that some of the generated curves include author's extension lines (extrapolations). Also, it should be emphasized that the relation between shaft friction and settlement is *assumed to be hyperbolic as long as compliance is observed.*

4.2. Presentation of Results

In this section, the obtained normalized design curves will be presented. In order to clarify the assesment steps, the analysis results of L/D=3 will be shown in detail. Remaining results will be given in the Appendix section with other Plaxis outputs.

4.2.1. Generation of Lateral Confining Stress State

The installation of a single stone column was modeled as expansion of a cavity as specified previously. Here, results of the cavity expansion process will be given. The Figure 4.2 shows prescribed displacement of $\Delta r/r_0$=0.3 for initial radius of 0.5 m. It is important to note that applied displacements are uniformly distributed with depth (blue arrows in the figure below) in order to reflect the effect of construction-induced lateral stressing as numerically stable as possible.

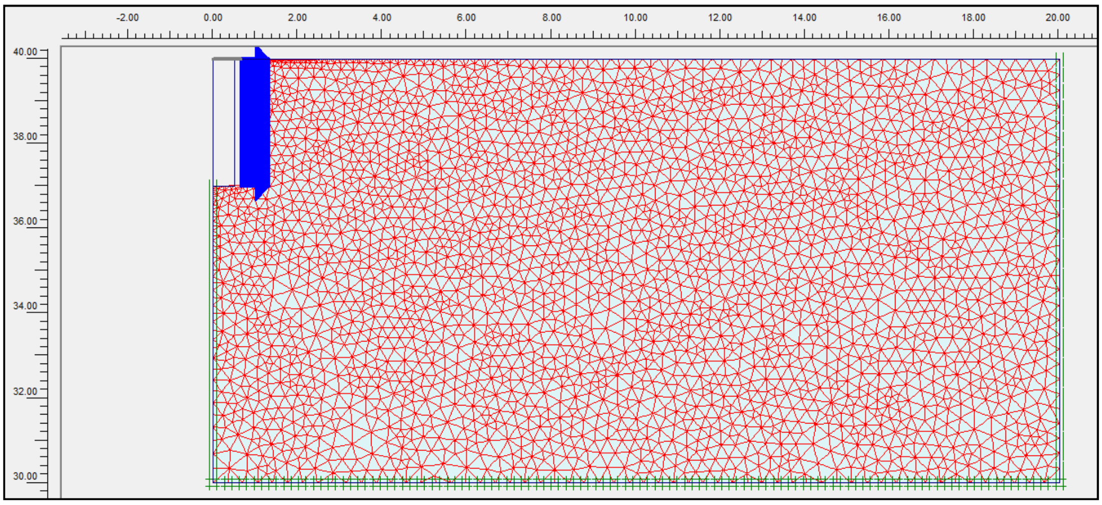

Figure 4. 2 Deformed shape after application of lateral displacement of $\Delta r/r_0$=0.3

Figure 4.3 shows the stress field developed after application of lateral displacement. As can be inferred from mean stress shadings in the figure, compressive state of stress was increased within the surrounding soil.

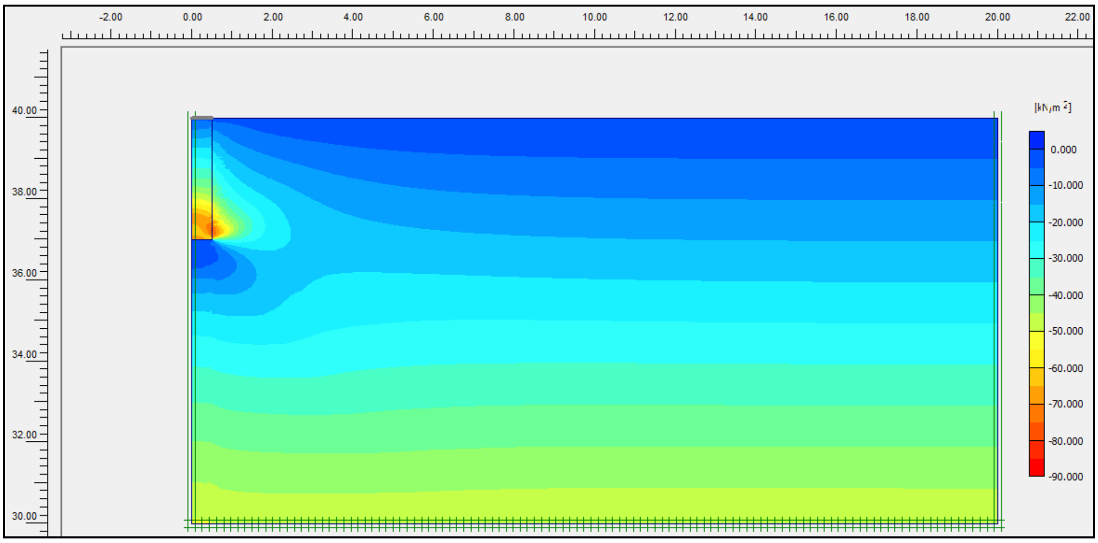

Figure 4.3 Lateral stresses around the pier of L/D=3 after $\Delta r/r_0$=0.3. (Note: Color scale on the right gives mean lateral stress with depth)

4.2.2. Mobilization Of Shaft Resistance

In this section, the results of the numerical simulations and derived shaft friction settlement response will be shown. Also, the normalization of the curves and determination of ultimate pier capacity will be clearly presented by using results of the aggregate pier, whose length to diameter ratio is 3.

4.2.2.1. Results for Aggregate Pier of L/D =3

The load settlement curve obtained from the analysis of a single isolated aggregate pier of L/D=3 is indicated as load displecement curves in tabular form in Table 4.1 and 4.2, also, in graphical form in Figure 4.4 and 4.5. The tables and the figures show top and tip stress versus settlement values in each calculation steps, which are given for lateral displacement ratio of 0.3. The “Sum-M-stage” shown in the Table 4.1, 4.2, in the Figure 4.4 and 4.5 represents the ratio of top load to applied total top load.

Table 4. 1 Top stage load vs. top displacement curve data in tabular form for L/D=3 and $\Delta r/r_0 = 0.3$

Point	Step	Uy [m]	Sum-Mstage	Phases
0	0	0.000	0.00	Phase I (Lateral displacement)
1	1	0.000	0.50	
2	2	0.000	1.00	
3	3	0.000	0.00	Phase II (Reversing of lateral stresses)
4	3	0.002	0.39	
5	4	0.004	1.00	
6	5	**0.004**	**0.00**	Phase III (Vertical loading)
7	5	0.035	0.20	
8	6	0.050	0.27	
9	7	0.058	0.29	
10	8	0.074	0.33	
11	9	0.105	0.38	
12	10	0.121	0.39	
13	11	0.137	0.41	
14	12	0.169	0.43	
15	13	0.185	0.44	
16	14	0.201	0.45	
17	15	0.217	0.47	
18	16	0.233	0.48	
19	17	0.264	0.49	
20	18	0.278	0.50	
21	19	0.291	0.50	
22	20	0.292	0.50	
23	21	0.292	0.51	
24	22	0.292	0.51	
25	23	0.292	0.51	
26	24	0.292	0.51	
27	25	0.292	0.50	
28	26	0.292	0.50	

Table 4.2 Tip stress vs. tip displacement curve data in tabular form for L/D=3 and $\Delta r/r_0 = 0.3$

Point	Step	Uy [m]	sig'-yy [kN/m2]	Phases
0	0	0.000	33.05	Phase I (Lateral displacement)
1	1	0.004	17.79	
2	2	0.001	3.26	
3	3	0.000	3.26	Phase II (Reversing of lateral stresses)
4	3	0.002	3.64	
5	4	0.006	4.53	
6	5	**0.006**	**4.53**	Phase III (Vertical loading)
7	5	0.029	17.60	
8	6	0.041	26.85	
9	7	0.047	32.22	
10	8	0.059	38.38	
11	9	0.084	47.48	
12	10	0.096	52.87	
13	11	0.108	58.40	
14	12	0.133	69.17	
15	13	0.145	74.77	
16	14	0.157	80.21	
17	15	0.169	85.56	
18	16	0.181	90.83	
19	17	0.202	100.56	
20	18	0.212	105.33	
21	19	0.221	109.63	
22	20	0.221	109.91	
23	21	0.221	109.93	
24	22	0.221	109.94	
25	23	0.222	109.97	
26	24	0.222	110.03	
27	25	0.222	110.10	
28	26	0.222	110.16	

In order to generate necessary shaft friction vs. settlement curve, Table 4.1 and 4.2 will be utilized. Since the procedure of curve generation was presented previously, the outcomes will be demonstrated in a graphical form.

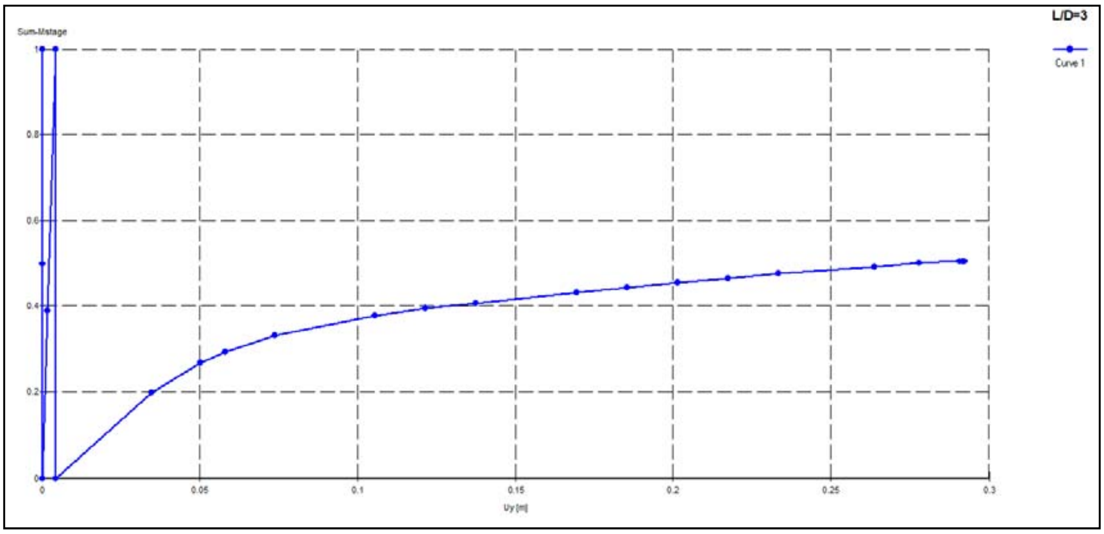

Figure 4.4 Top stage load ratio vs. top displacement curve of pier L/D=3 for $\Delta r/r_0 = 0.3$ (output of Plaxis 8.2)

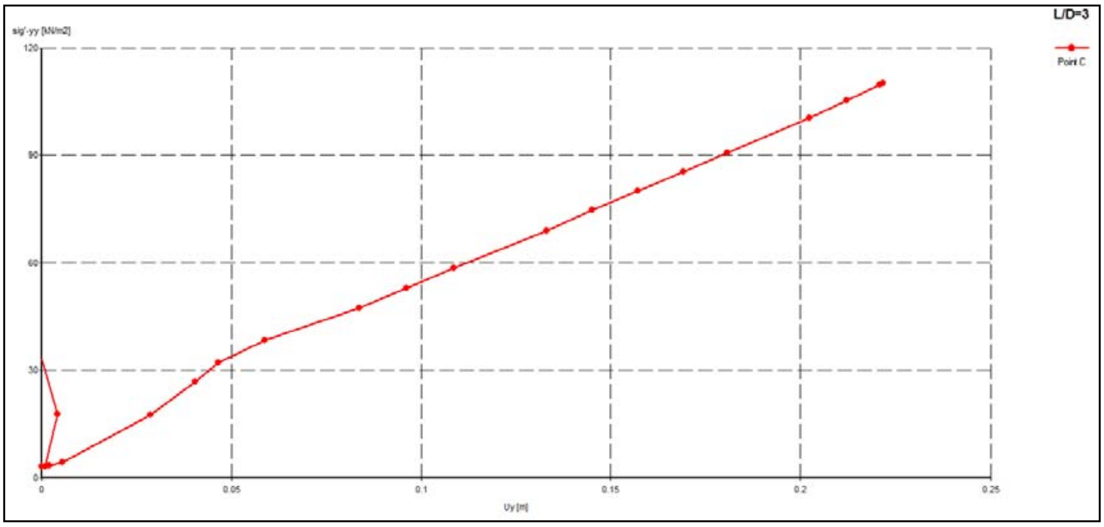

Figure 4.5 Tip stress vs. tip displacement curve for pier of L/D=3 and $\Delta r/r_0 = 0.3$ (output of Plaxis 8.2)

The fitted hyperbolic regression curves for each average shaft friction vs. settlement curves are shown as red dotted lines in the figure 4.6. As stated previously, the fitted hyperbolic curves are used to estimate ultimate shaft friction.

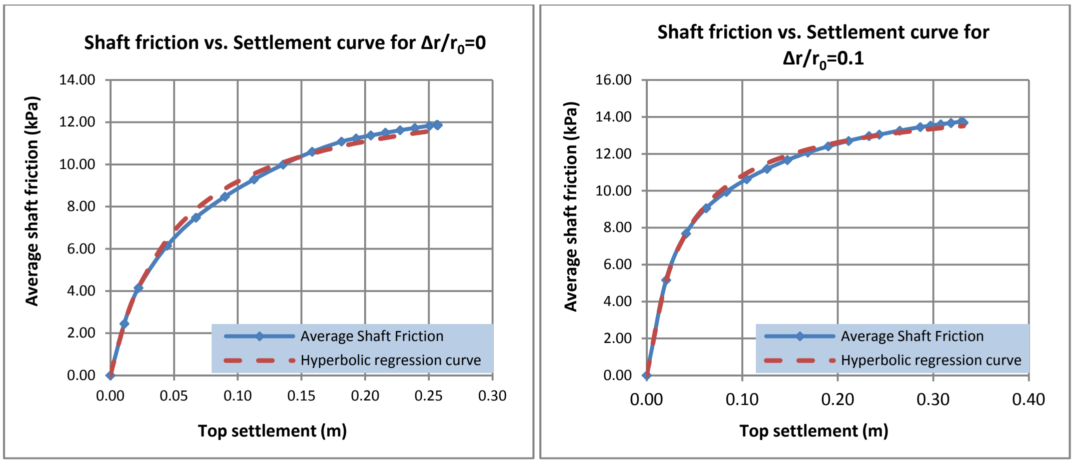

Figure 4.6 a) & b) Hyperbolic regression curves with shaft friction vs. settlement curves for cavity expansion ratio of 0 and 0.1.

As can be observed in the figure 4.7 a and b below, there is no need to fit a hyperbolic curve since ultimate average shaft friction can be easily determined by detecting the point beyond which shaft friction value remains constant or nearly constant (Figure 4.7 and 4.8). In addition, it is barely possible to fit a hyperbolic curve which sufficiently represents the original curve.

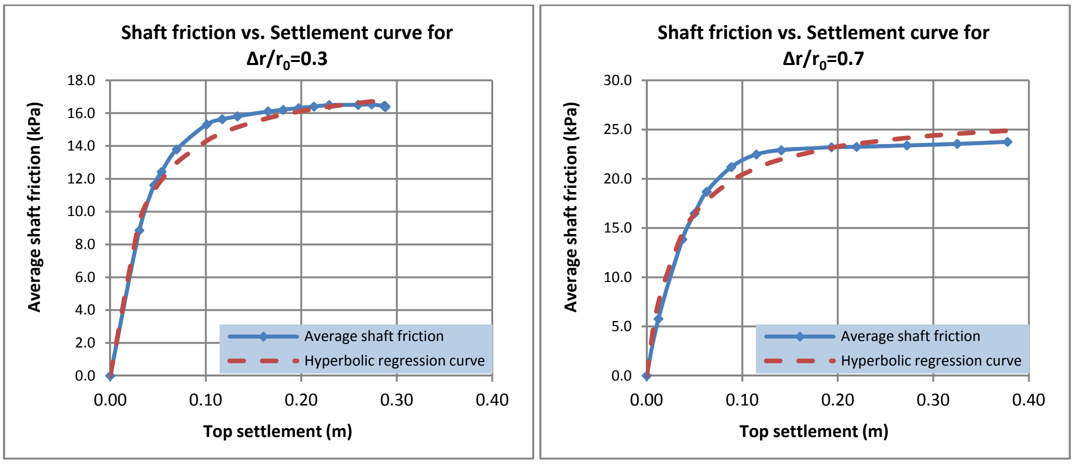

Figure 4.7 a) & b) Hyperbolic regression curves with shaft friction vs. settlement curves for cavity expansion ratio of 0.3 and 0.7.

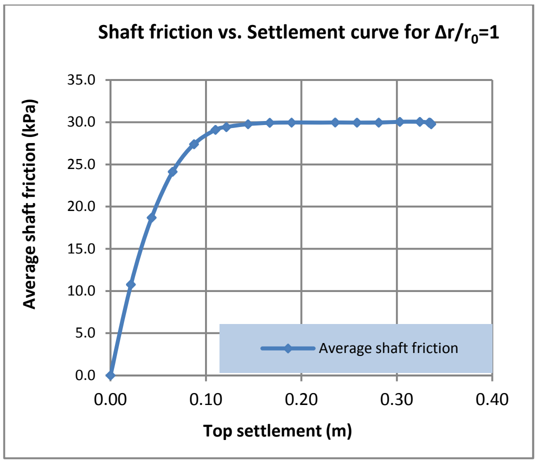

Figure 4.8 Shaft friction vs. settlement curves for cavity expansion ratio of 1.

Figure 4.9 demontrates summary of the average shaft friction mobilized in different confining stress conditions for aggregate pier of L/D=3.

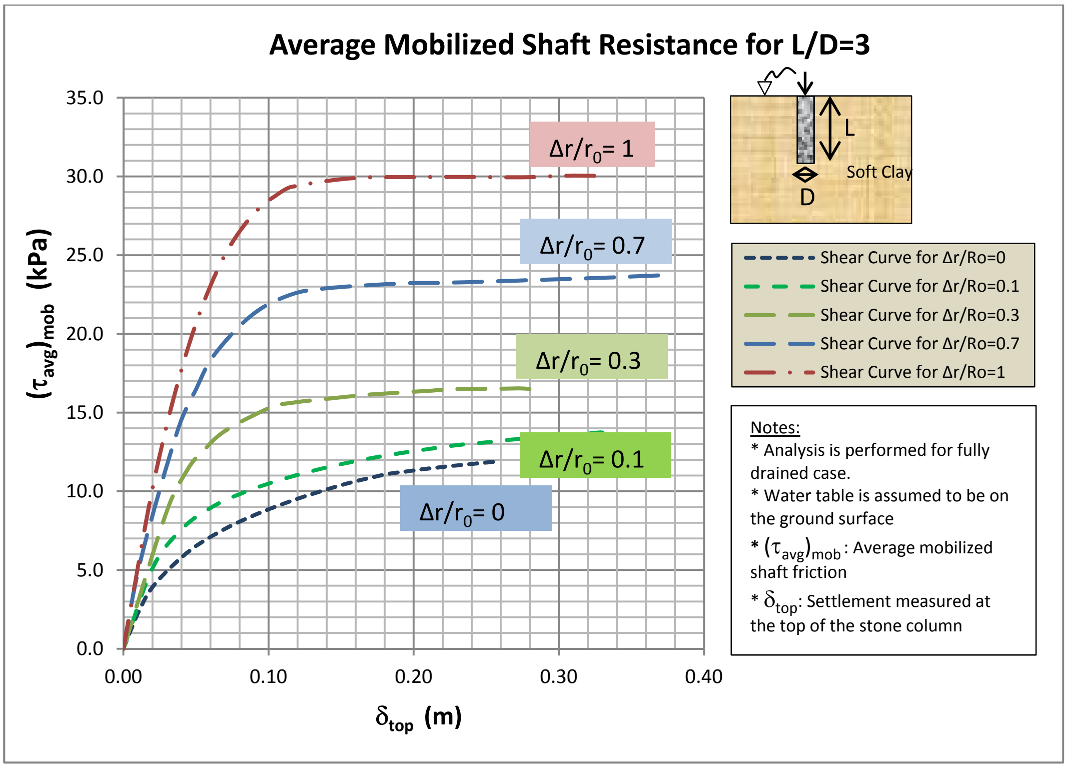

Notes:
* Analysis is performed for fully drained case.
* Water table is assumed to be on the ground surface
* $(\tau_{avg})_{mob}$: Average mobilized shaft friction
* δ_{top}: Settlement measured at the top of the stone column

Figure 4.9 Average shaft friction values for aggregate pier with L/D=3 and various cavity expansion ratios.

After generation of mobilized shaft friction vs. settlement curve, a normalization procedure was executed to eliminate case sensitive characteristics of the curves as seen in the Figure 4.10. For this purpose, average mobilized shaft friction is normalized by the ultimate value (1/b for hyperbolic fits, as Eq. 4.2, and maximum value in the rest of the curves); whereas top displacement is normalized by the column diameter.

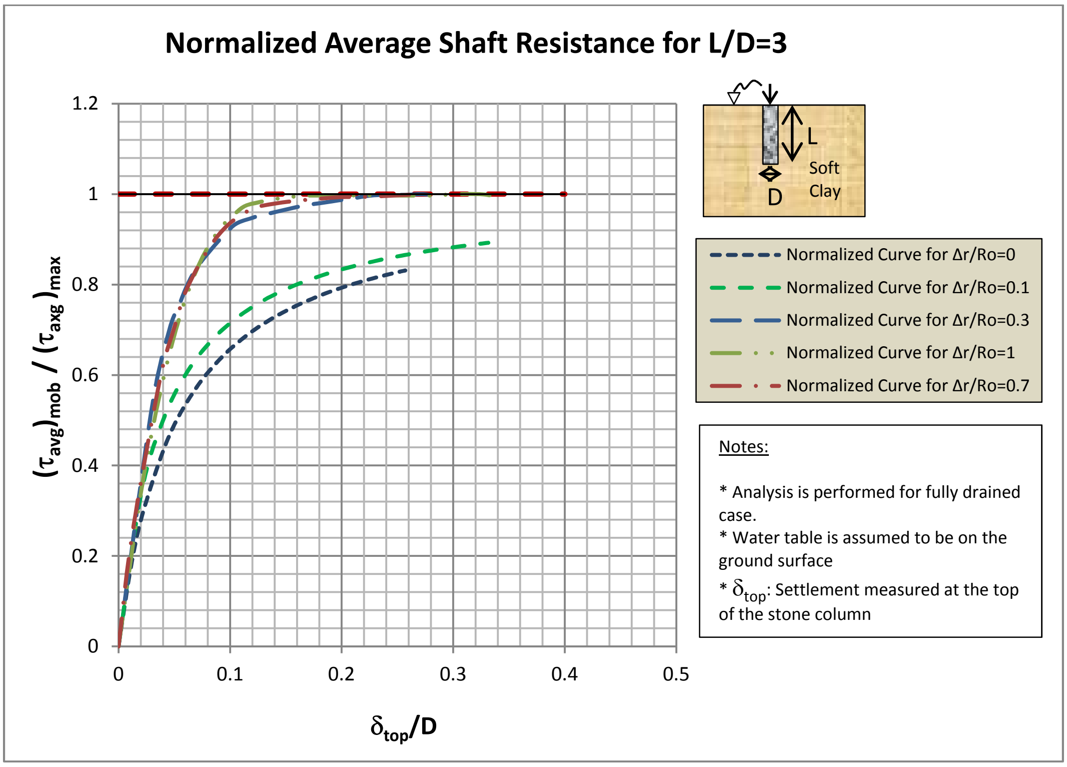

Figure 4.10 Normalized average shaft resistances of pier for L/D=3

Figure 4.10 shows the average normalized curves. Here, the curves after lateral expansion ratio of 0.3 are nearly overlapped. Since the discrepency between these curves is not significant from enginering point of view, a single representative curve will be used for the cases represented by these curves in the Figure 4.11.

Moreover, upper and lower threshold curves as given in Figure 4.12 can be defined as extreme minimum and maximum curves under different confining stress state. The main purpose of these curves is to define extreme boundaries in different confining stress conditions. Since there is always some uncertainty in confining stress state around a pier after installation, it may be necessary to utilize the mean curve.

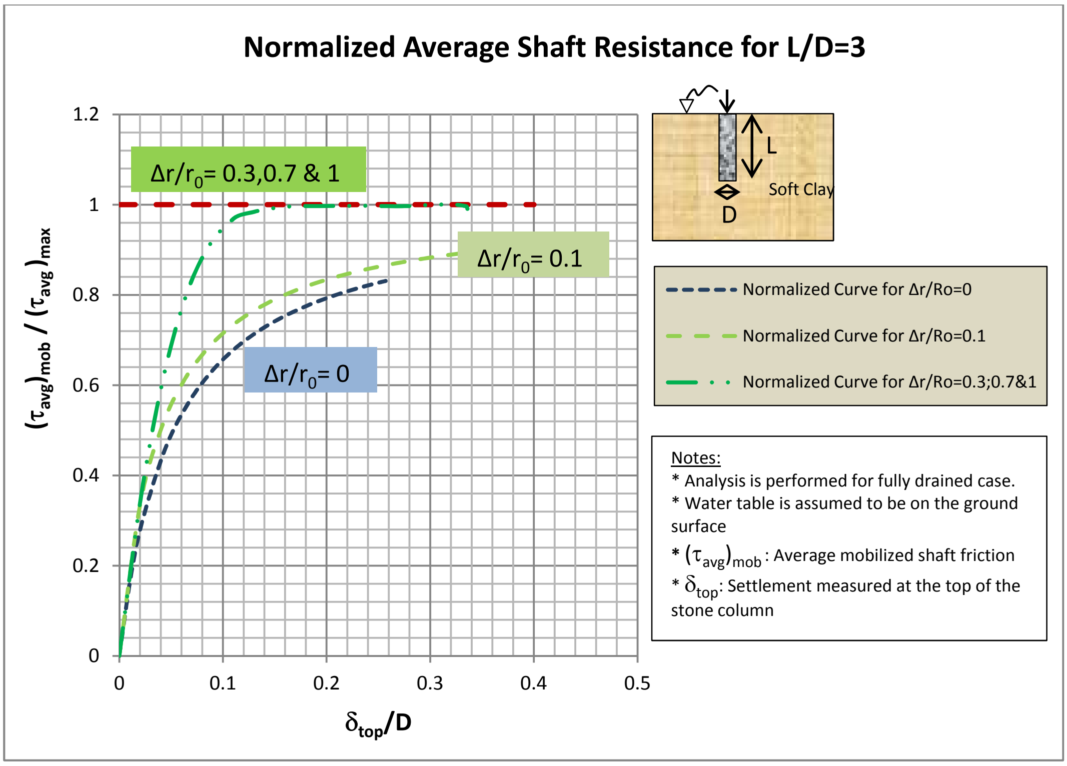

Figure 4.11 Normalized average shaft resistances after simplifying the overlapped curves

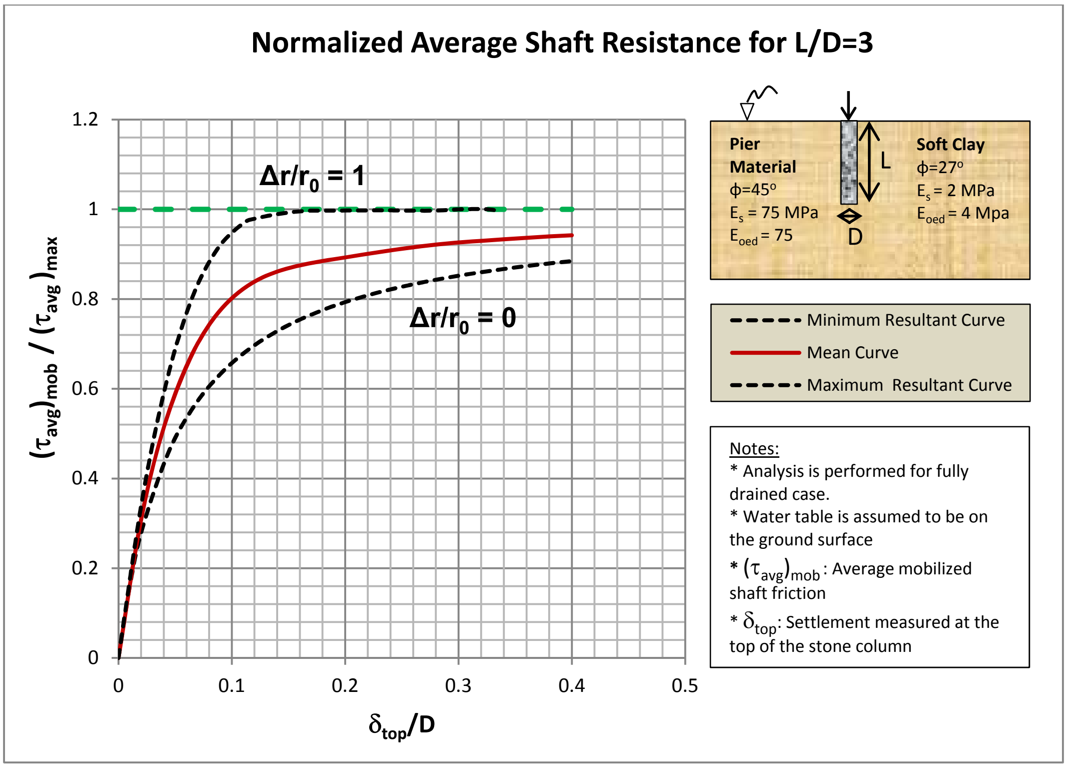

Notes:
* Analysis is performed for fully drained case.
* Water table is assumed to be on the ground surface
* $(\tau_{avg})_{mob}$: Average mobilized shaft friction
* δ_{top}: Settlement measured at the top of the stone column

Figure 4.12 Normalized mean curve with upper and lower threshold curves for L/D=3

The figure 4.13 (a and b) presents the deformed shape of the pier of L/D=3 ratio for $\Delta r/r_0$ =0.3 under ultimate vertical loading.

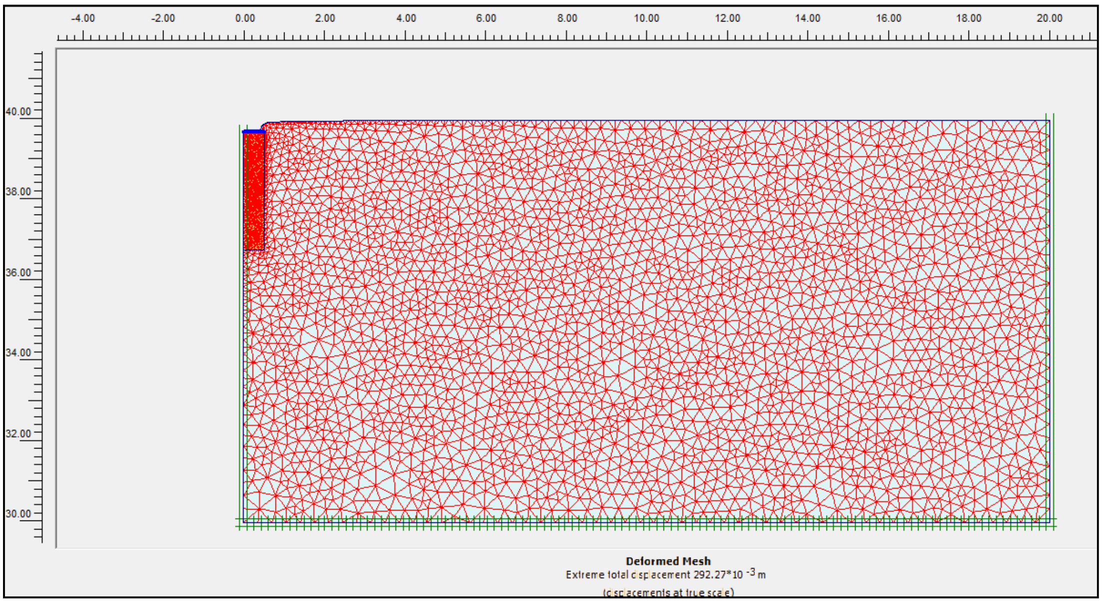
-4.00
-2.00
0.00
2.00
4.00
6.00
8.00
10.00
12.00
14.00
16.00
18.00
20.00
40.00
38.00
36.00
34.00
32.00
30.00

Deformed Mesh
Extreme total displacement 292.27*10^{-3} m
(displacements at true scale)

a)

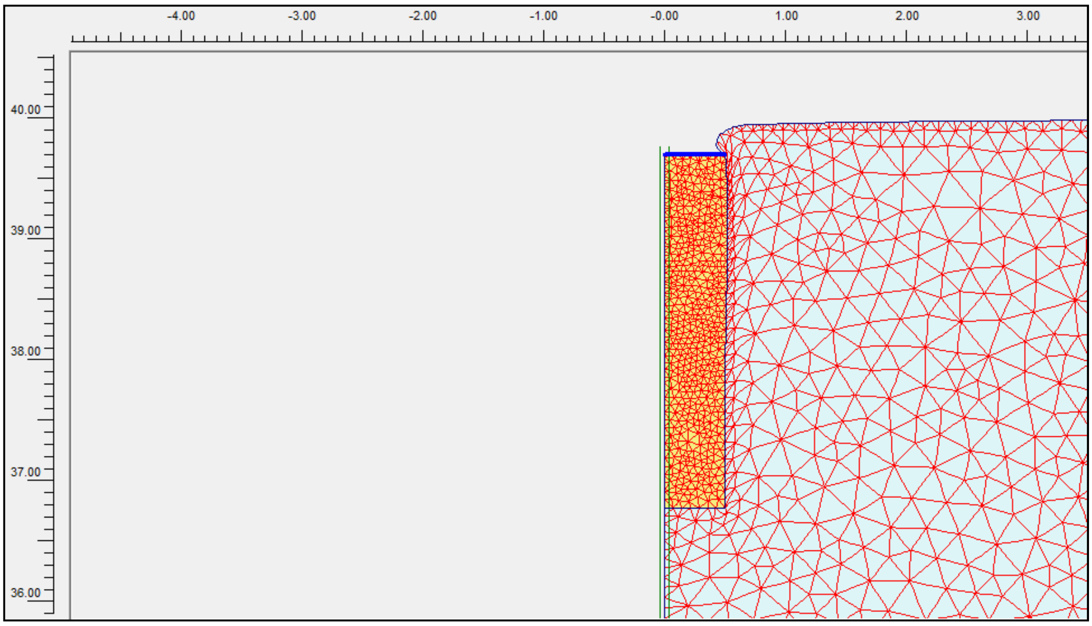
-4.00
-3.00
-2.00
-1.00
-0.00
1.00
2.00
3.00
40.00
39.00
38.00
37.00
36.00

b)

Figure 4.13 a) and b) Deformed mesh of aggregate pier of L/D=3 for $\Delta r/r_0$ =0.3 (Scale factor=1)

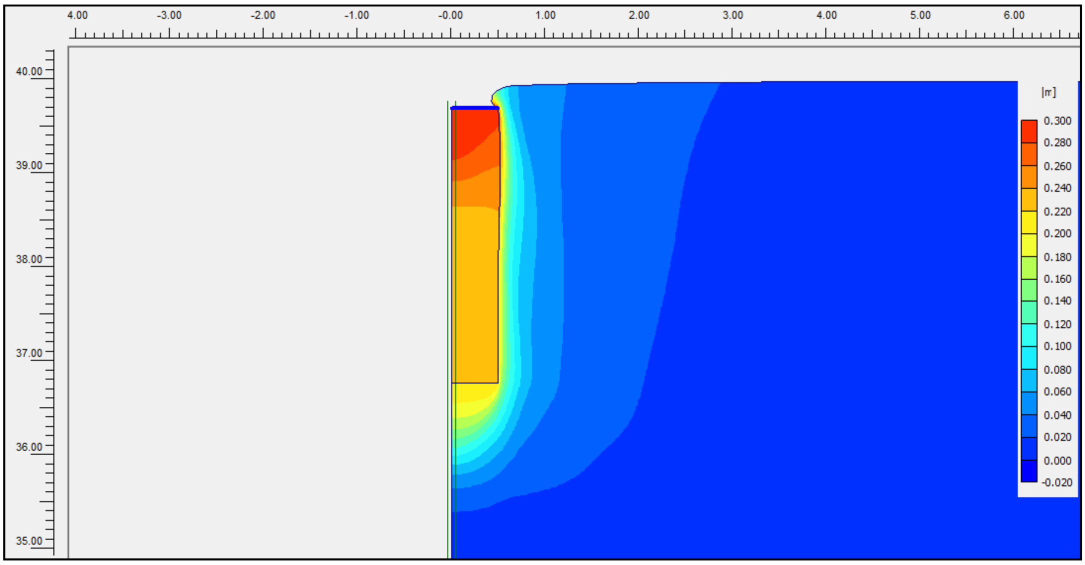

Figure 4.14 Total vertical displacement shading of aggregate pier of L/D = 3 for $\Delta r/r_0$=0.3

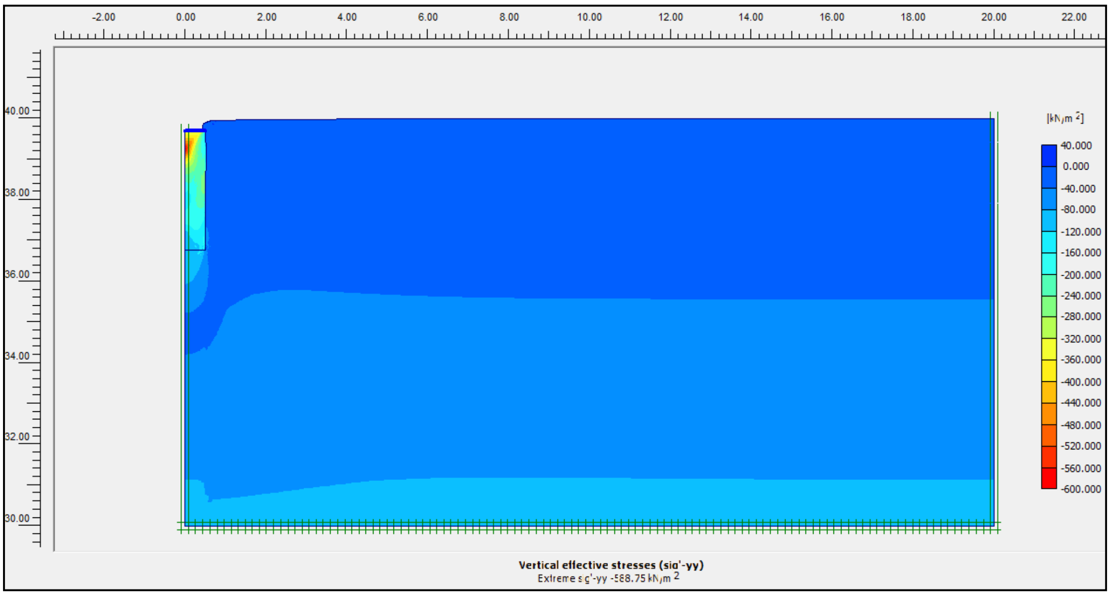
-2.00
0.00
2.00
4.00
6.00
8.00
10.00
12.00
14.00
16.00
18.00
20.00
22.00
40.00
38.00
36.00
34.00
32.00
30.00
[kN/m²]
40.000
0.000
-40.000
-80.000
-120.000
-160.000
-200.000
-240.000
-280.000
-320.000
-360.000
-400.000
-440.000
-480.000
-520.000
-560.000
-600.000
Vertical effective stresses (sig'-yy)
Extreme sig'-yy -588.75 kN/m²

Figure 4.15 Vertical effective stress at state of failure for L/D = 3 and $\Delta r/r_0$=0.3

The figure 4.14 illustrates mean displacement shadings of vertical settlement through depth at the state of failure. It can be inferred from the figure that the pier has a tendency of punch type of failure because while top displaces by 30 cm, tip moves by 22 cm. This mean that the large portion of the top settlement comes from the tip movement. Figure 4.15 presents the change of vertical effective stress with depth. As it can be seen in the figure, different mean stress shadings at the tip shows developed end bearing.

4.2.2. Mobilization of Tip Resistance

Normalized tip resistance curves will be presented in the following sections. Here, generated curve for L/D=3 will be shown. In the discussions section, mobilized tip resistances will be addressed in more detailed manner.

4.2.2.1. Aggregate Pier of L/D=3

The Figure 4.23 given below shows mobilized tip resistance of aggregate pier, whose length to diameter ratio is three. As can be seen from the graph, the tip resistance is mobilized in a rather linear manner. Therefore, a mean linear fit is decided to be used to represent the mobilization of tip resistance *up to half of the theoretically calculated ultimate tip resistance.* Therefore, suggested linear fitting is secant line approximation of true behaviour.

Developed tip resistances are normalized by ultimate capacity, which is used as a reference point . However, full development of tip resistance was found to be not possible after numerical analysis. Therefore, in order to perform normalization, ultimate tip resistance is estimated using conventional Terzaghi bearing capacity formula for rigid circular footings:

$$(\sigma'_{tip})_{max} = (\sigma'_{tip})_{ult} = 1.3c'N_c + qN_q + 0.4\gamma'BN_\gamma - \sigma'_0 \qquad (4.6)$$

$$(\sigma'_{max})_{tip} /2 = (1.3*1*29.24+3*(19–10)*(15.9-1)+0.4*(19-10)*1*11.6)/2$$

$$= 241 \text{ kPa}$$

Figure 4.16 shows developed tip resistance and settlement values for different cavity expansion ratios. It is believed that a least square regression fit may be representative of the response for all cases and factor of safety values greater than 2.0. Therefore, a least-square linear fit will be used to demonstrate tip resistance development. The linear fit is shown in Figure 4.17 with respective equation.

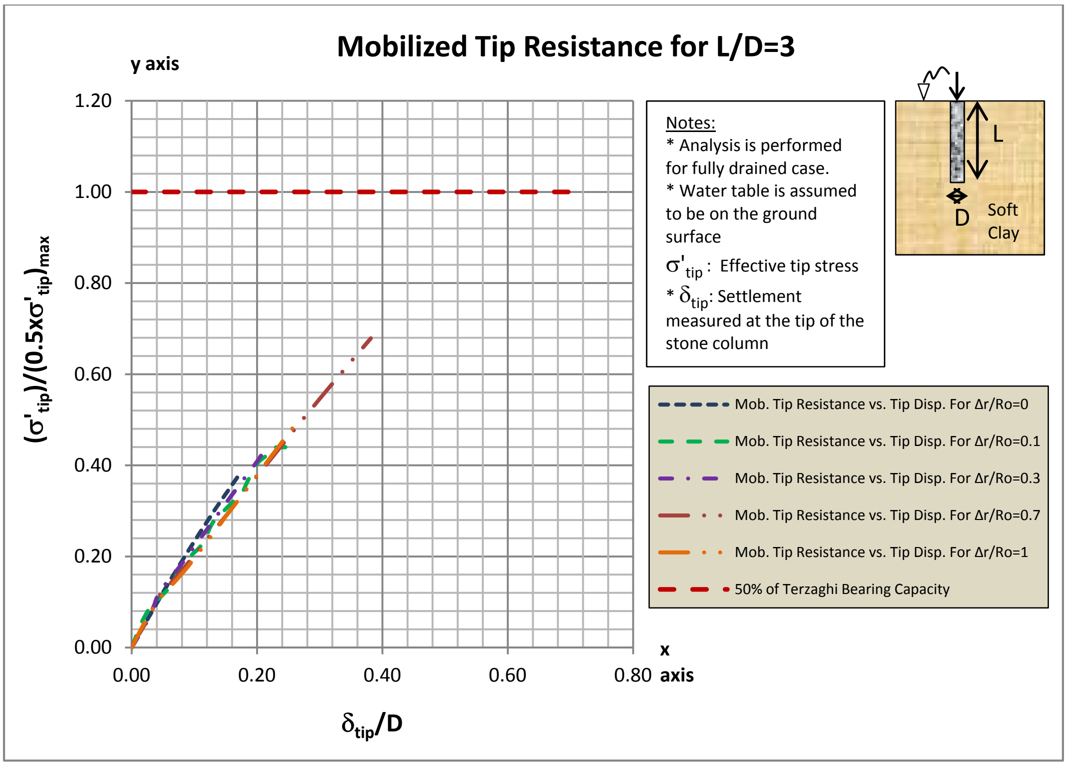

Figure 4.16 Tip Resistances mobilized in different confining state of stresses for L/D=3

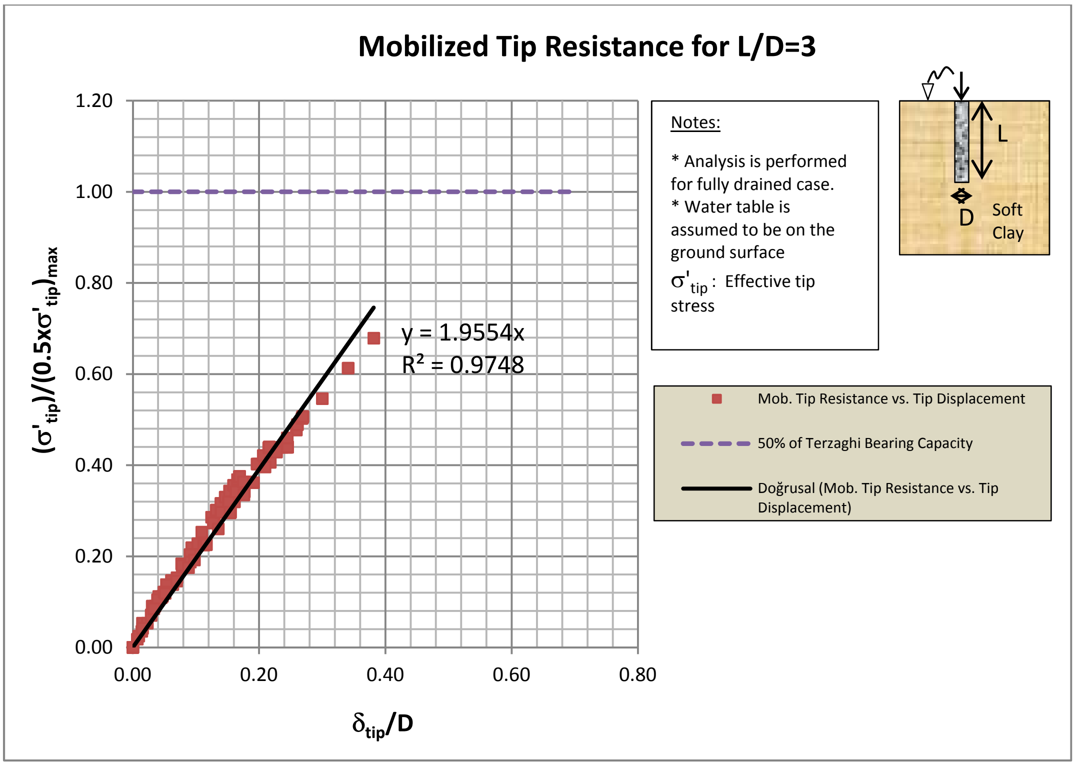

Figure 4.17 Linear regression to normalized tip resistances

CHAPTER 5.

DISCUSSION OF RESULTS

5.1. Mobilization of Shaft Friction

Analysis results showed that, increase in confining stress state around aggregate pier affects shaft friction vs. settlement curves positively. Pre-mobilization of radial effective stresses cause incerase in shaft frictions and decrease in vertical settlements (Figure 5.1). The same trend can be seen in normalized curves (Figure 5.4). However, while radial confining stress has a great influence on shaft friction and causes increase in both stiffness as well as mobilized capacity as shown in Figure 5.2, a similar trend cannot be seen in the normalized curves given in Figure 5.3. The main reason is that the characteristic shape of shaft friction vs. settlement curves depends on the interaction between pier and surrounding soil. Therefore, it can be inferred from the curve that the pier of L/D ratio of three behaves more like a granular pile since lateral expansion action resulting from loading is less significant. It means that increasing lateral confining stress around pier makes the behavior *more brittle* than pier installed without cavity expansion as seen in Figure 5.4. Therefore, improvement in shaft resistance can be observed in normalized curves.

On the other hand, in figure 5.2, shaft friction vs. settlement curves of the pier, with L/D of 6, are hardening i.e. shaft friction continues to increase untill failure since pier still resists vertical loading with shaft shear but lateral expansion influences the development of shear stresses. It makes the determination of ultimate shaft resistance very difficult and therefore, a hyperbolic curve fitting procedure was introduced previously. However; besides all, increasing of confining stresses makes the pier behavior *more ductile*. This tendency can be seen more clearly in normalized curves (Figure 5.3) but less obvious in the curves generated for pier of L/D=9 (Figure 5.5).

Nevertheless, normalized graph of pier L/D=6 may lead to a misconception that mobilized shaft resistance is lower in higher confining stress state but the normalized curves give just *the portion of the ultimate capacity* and *rate of mobilization.*

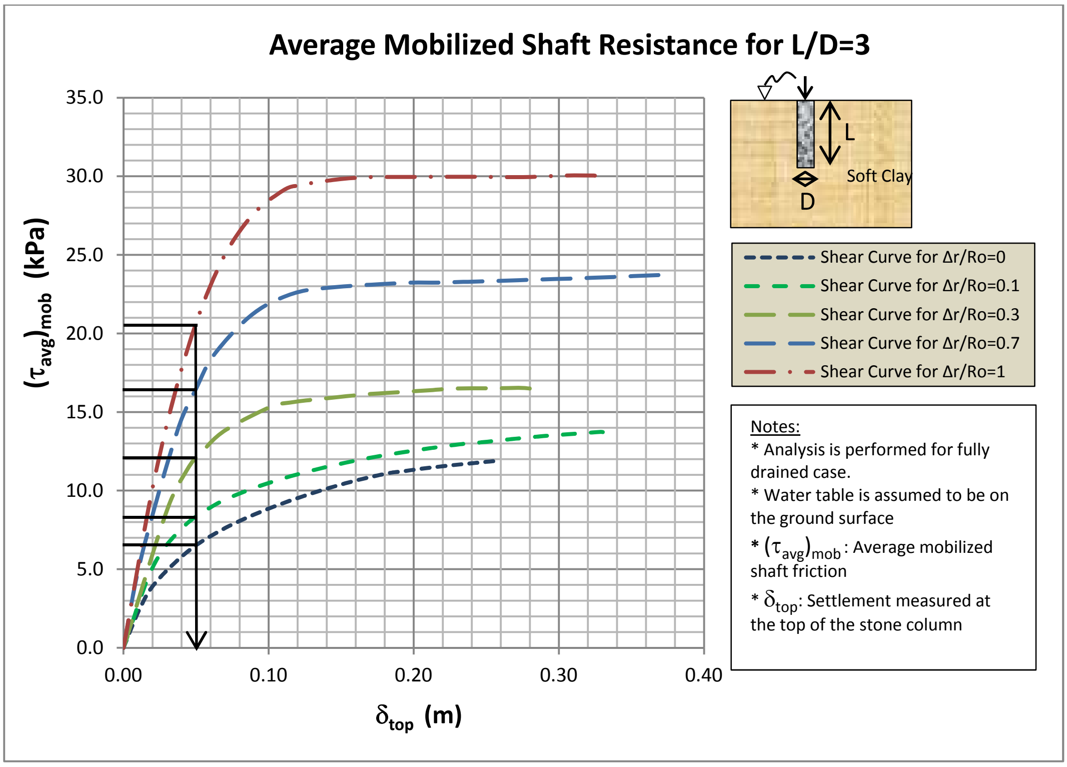

Notes:
* Analysis is performed for fully drained case.
* Water table is assumed to be on the ground surface
* $(\tau_{avg})_{mob}$: Average mobilized shaft friction
* δ_{top}: Settlement measured at the top of the stone column

Figure 5.1 Mobilized shaft friction of pier L/D=3

It is important to note that for the piers, whose L/D ratio is nine or higher, a formal trend cannot be observed, instead, some curves move back and forth (figure 5.5). The main reason is difficulty of assessing ultimate shaft resistance. Since as L/D ratio increases, the main mechanism of failure become bulging and therefore, the column fails before full mobilization of shaft resistance. In addition this, the problem may result from numerical instability, despite using advanced “update mesh” option. This problem and uncertainty which is associated with installation (or construction induced confining stress) modeled by expanded cavity is overcome by introducing maximum, minimum and mean curves. (See Figure 4.3, 4.11 and Figures in Appendix-A).

Considering stone column constitutive modeling, as lateral confining pressure increases, the stiffness of stone column is expected to increase. As it is evident from resistance vs. settlement curves, this expected behavior was observed exactly (Figures from 4.1 to 4.9 and Figures in Appendix-A). It means that “Hardening Soil” model successfully simulates desired field conditions to certain extent. Moreover, expected increase in vertical load capacity due to confining stress increment was clearly detected in generated curves (figure 4.1, 5.1, 5.3 and others).

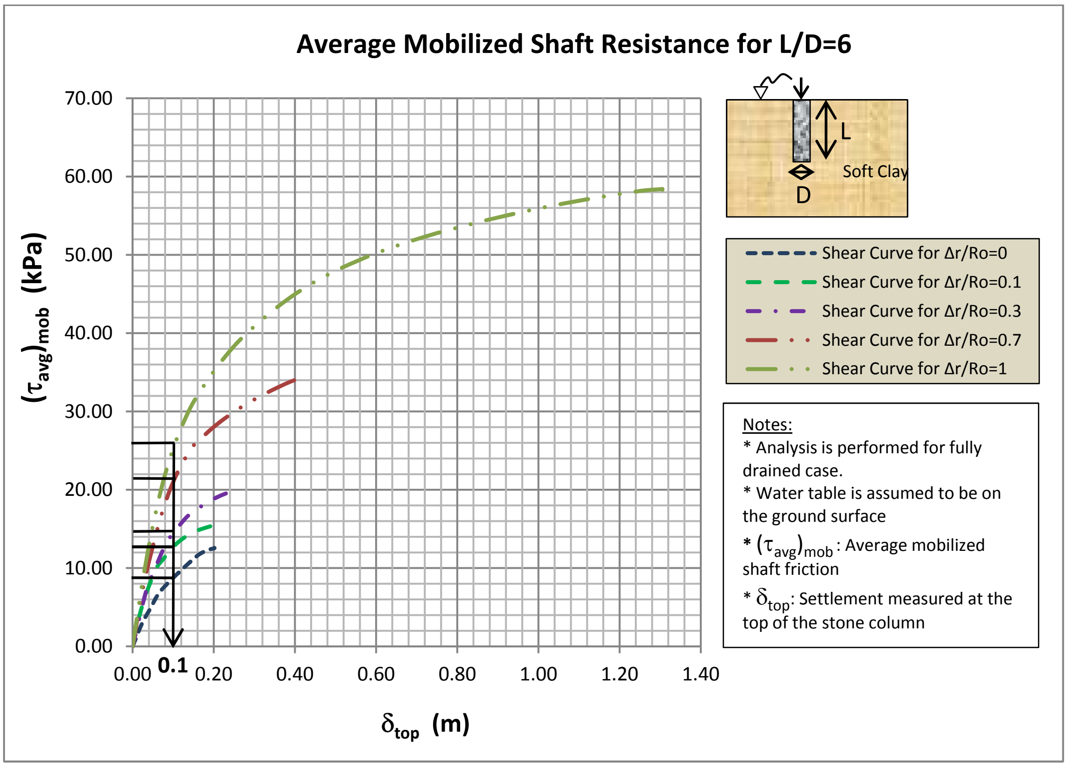

Notes:
* Analysis is performed for fully drained case.
* Water table is assumed to be on the ground surface
* $(\tau_{avg})_{mob}$: Average mobilized shaft friction
* δ_{top}: Settlement measured at the top of the stone column

Figure 5.2 Mobilized shaft friction of pier L/D=6

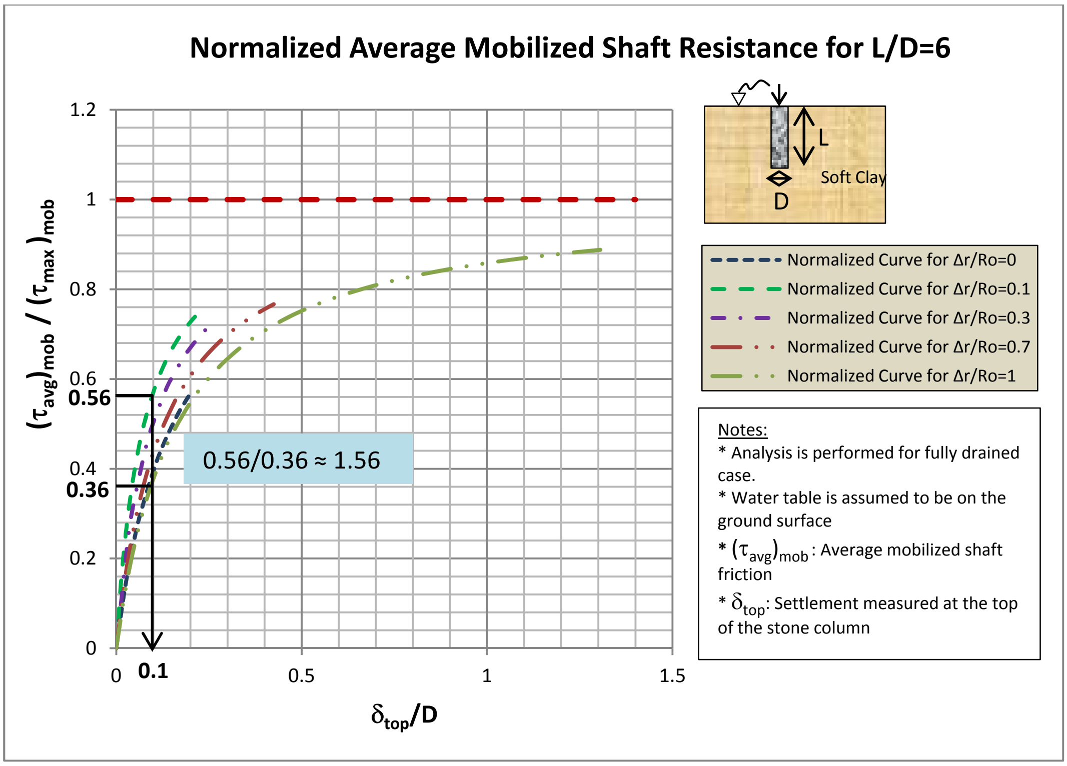

Notes:
* Analysis is performed for fully drained case.
* Water table is assumed to be on the ground surface
* $(\tau_{avg})_{mob}$: Average mobilized shaft friction
* δ_{top}: Settlement measured at the top of the stone column

Figure 5.3 Normalized mobilized shaft friction of pier L/D=6

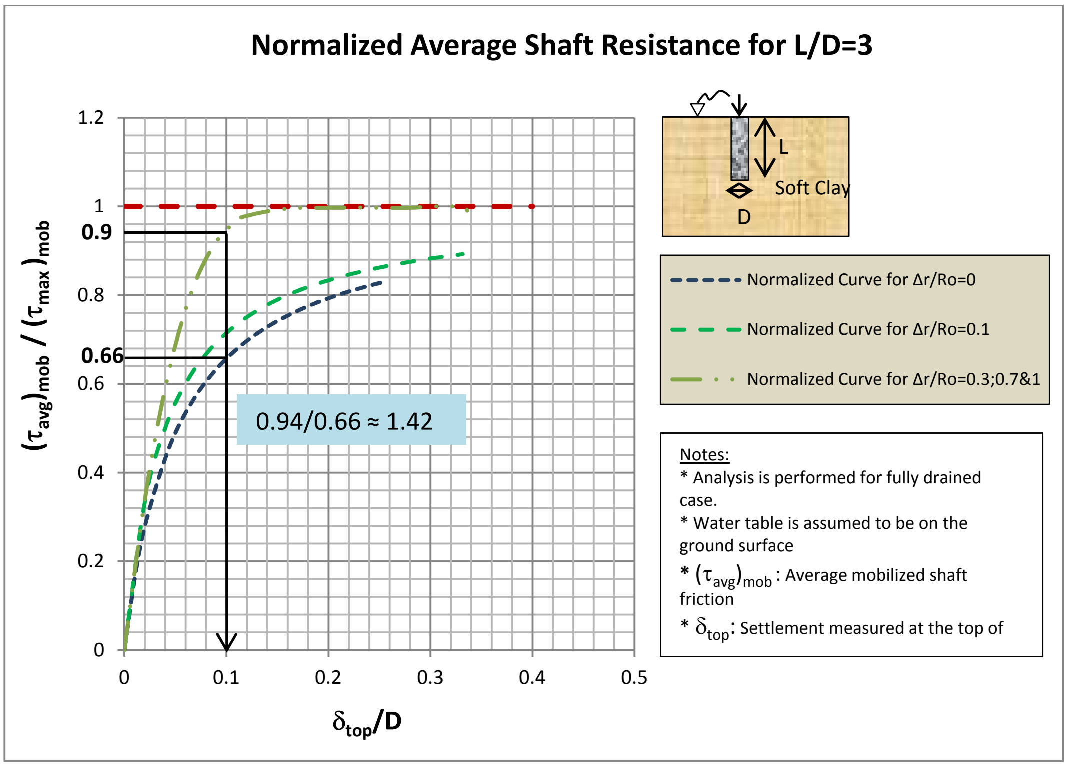

Notes:
* Analysis is performed for fully drained case.
* Water table is assumed to be on the ground surface
* $(\tau_{avg})_{mob}$: Average mobilized shaft friction
* δ_{top}: Settlement measured at the top of

Figure 5.4 Normalized mobilized shaft friction of pier L/D=3

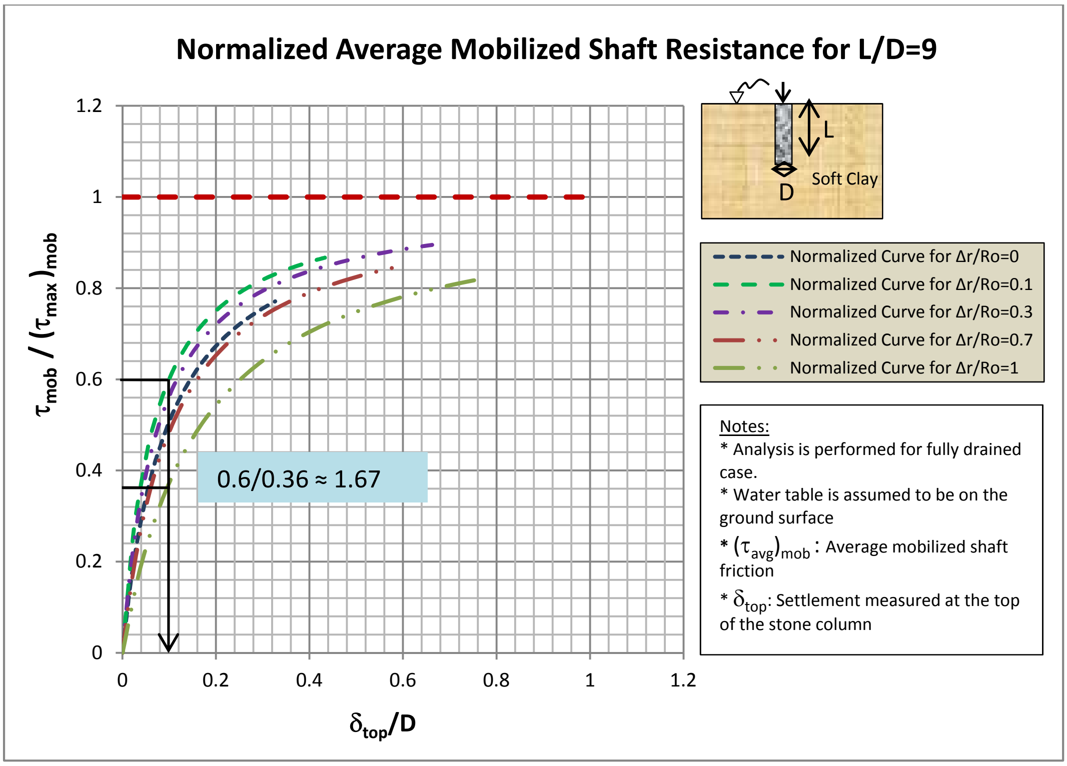

Figure 5.5 Normalized mobilized shaft friction of pier L/D=9

There is no significant influence of construction method or confining stress state on normalized capacity vs settlement curves up to normalized shaft friction capacity ratio of 0.4 for aggregate piers whose length to diameter ratio is up to 4. Since, this ratio corresponds to a factor of safety of 2.5, for the piers whose L/D ratio is less than four, effect of confining stresses on normalized frictional capacity development versus settlement behaviour is less important. However, as seen from the curves genarated for L/D ratio of 6 or higher, the same conclusion is not valid. (Figures 5.3 and 5.5)

Furthermore, consistent with the literature, bulging is observed to be the main mechanism of failure in ultimate state in piers, whose L/D ratio is larger than four, as can be seen in Figure a.5 in appedix section.

Also, significant changes in stiffness and horizontal stresses in a certain zone around the columns are observed during the installation process. The influence radius of lateral displacement is about 10D which is consistent with the value stated by Randolph et al. (1978) and Castro and Karstunen (2010) (Figure a.5 etc).

Figure 5.6 illustrates the mean normalized shaft friction vs. normalized top settlement for aggregate piers of different L/D ratios. As L/D ratio increases, there should be more deformation to mobilize average shaft friction. However, it can be eliminated by further normalizing top settlement with length of the column (Figure 5.7). The new normalized settlement term can be defined as "*settlement ratio" of aggregate pier* ($\delta_{top}/(D*L)$) (Figure 5.7).

Moreover, although the curves resembles to each other, the shape of the curve reveals that long stone columns show more ductile behavior compared to short columns.

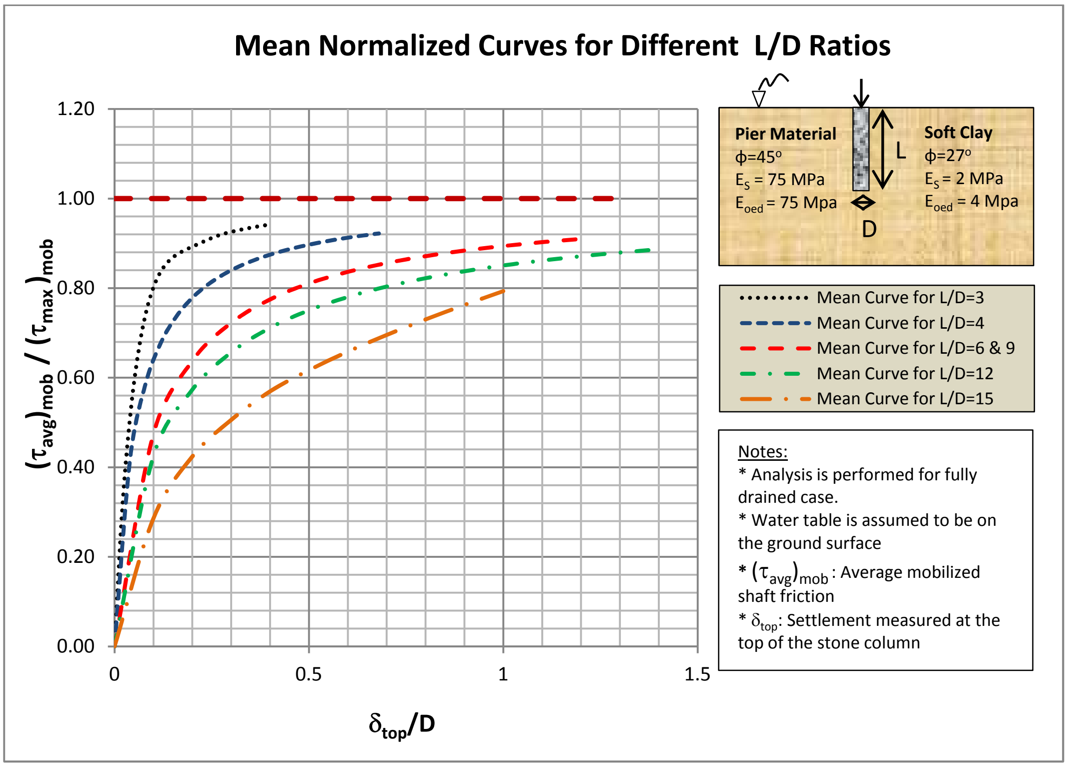

Mean Normalized Curves for Different L/D Ratios

Notes:
* Analysis is performed for fully drained case.
* Water table is assumed to be on the ground surface
* $(\tau_{avg})_{mob}$: Average mobilized shaft friction
* δ_{top}: Settlement measured at the top of the stone column

Figure 5.6 Normalized mean curves for different L/D ratios

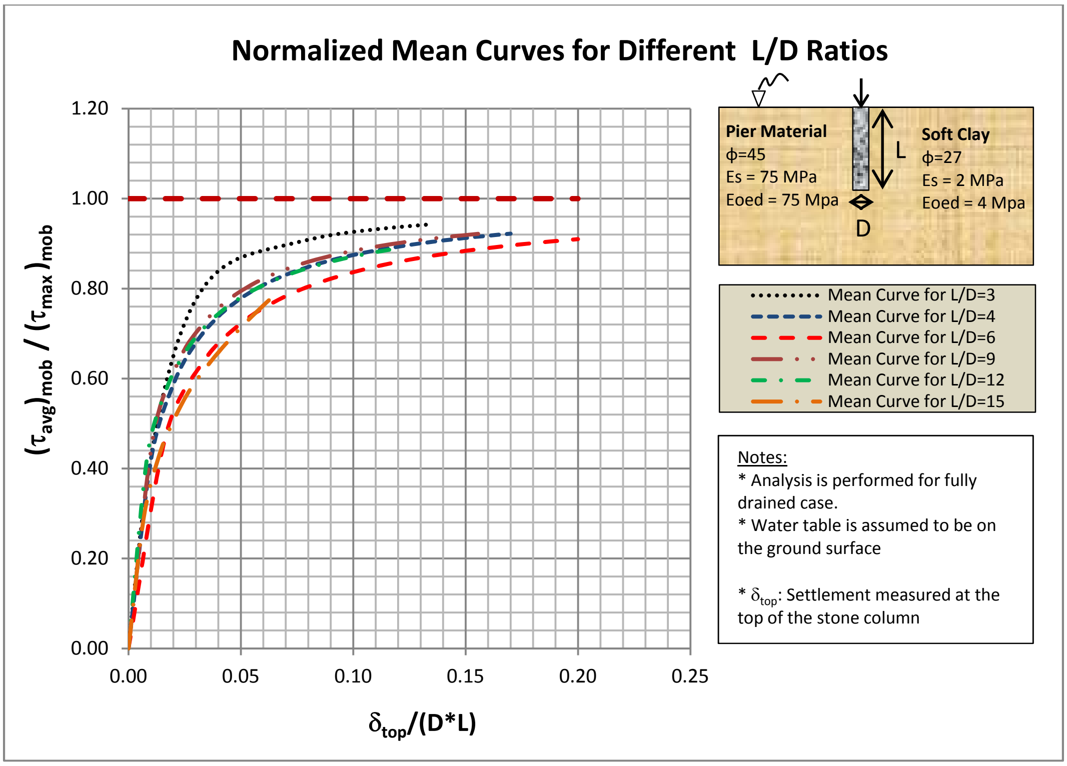

Figure 5.7 Normalized mean curves for different L/D ratios

In figure 5.8, a single representative mean curve is given to estimate mobilized capacity of a single aggregate pier in any confining stress state. The curve can be used as a first estimation for any type of aggregate pier. Also, in the figure 5.9, the mean representative curve is given with the standard deviation values separately in the graphical form. It can be observed as given in the figure, standard deviation incerases up to $\delta_{top}/(D*L) = 0.05$ where it reaches a maximum value of 0.08 and remains constant.

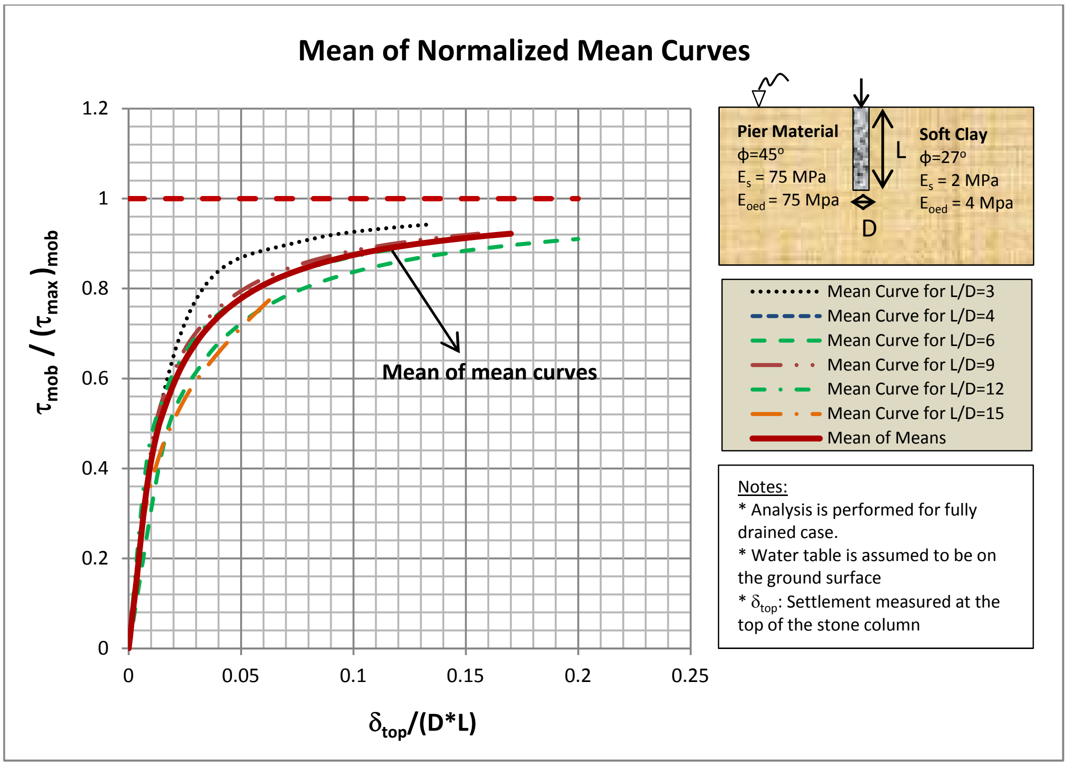

Figure 5.8 Mean of normalized mean curves

As seen from the Figure 5.9, in order to mobilize of 40 % of maximum shaft fricition (F.S. = 2.5), a settlement ratio of 0.01 is sufficient. Assuming an aggregate pier diameter of 0.5 m and length of 7.5 m :

$$\delta_{top}/(D*L) = 0.01 \qquad\qquad \delta_{top} = 0.0375 \text{ m} = 3.75 \text{ cm}$$

This value seems to be little bit higher than expected field response by investigating various field load tests. However, the design curve were generated from analysis of fully drained case. It means that the settlement value reflects expected consolidation settlement, i.e., anticipated long term behaviour. Here, it should be emphasized that *generated graphs can not be compared with any existing study or field load tests since there is no given data for tip stresses obtained by field load test in the literature.*

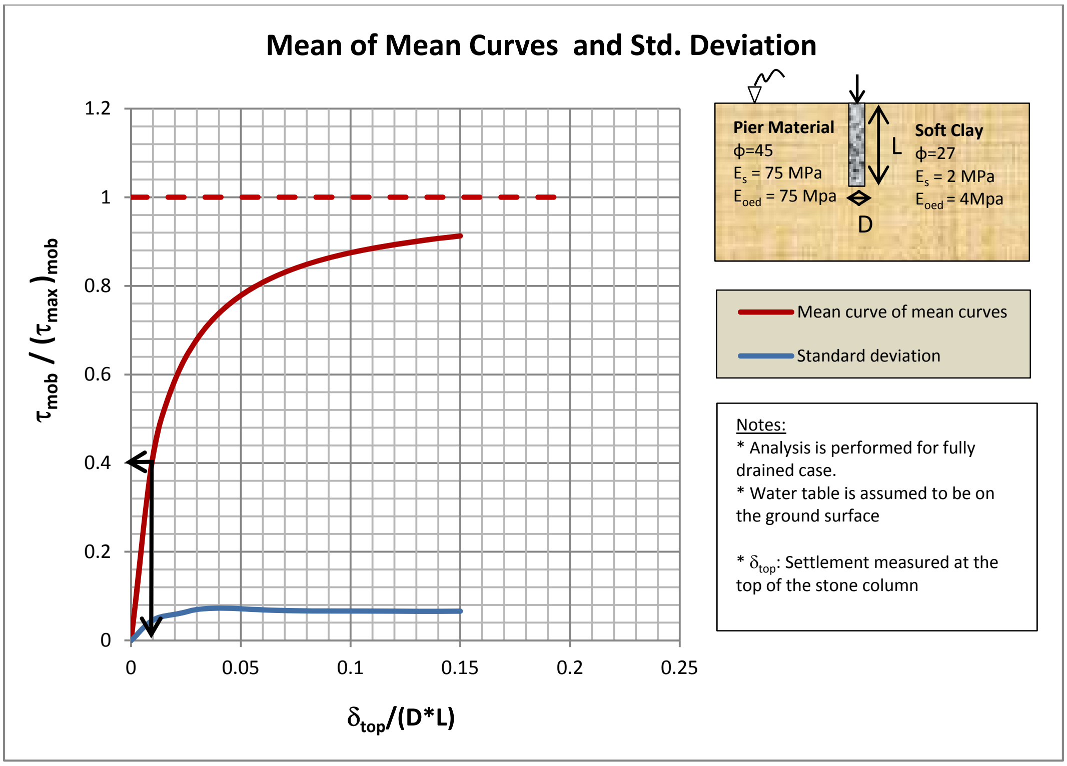

Figure 5.9 Mean of normalized mean curves with standard deviation

Moreover, as can be seen in Figure 5.10 for the pier of L/D=3; as the cavity expansion and resultantly confining stress increases, the maximum shaft friction increases. Also, the relation between calculated maximum shaft friction and cavity expansion is observed as sufficiently linear. However, this response can not be obtained in the pier of L/D=15 (Figure a.40 in Appendix-A). The main reason may be due to the fact that a representative maximum shaft friction value can not be obtained since a sufficient hyperbolic relation cannot be detected in the stress-displacement curve of the pier of L/D=15 (Figure a.37 in Appendix-A).

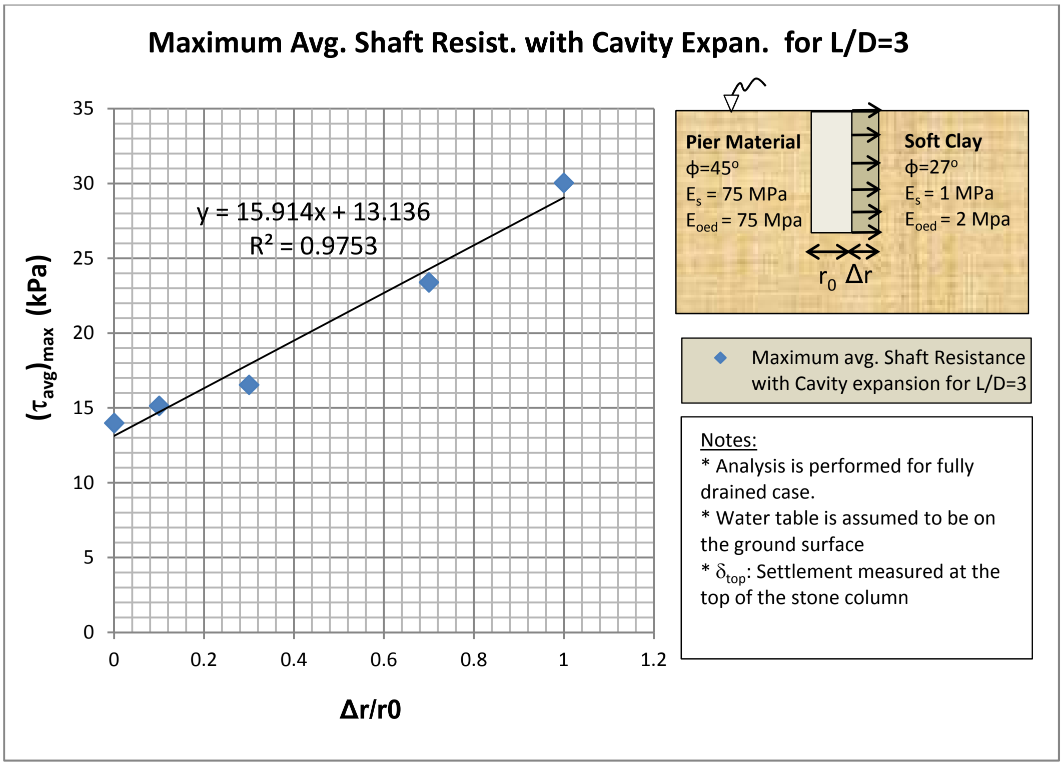

Figure 5. 10 Mobilization of shaft friction with cavity expansion for the pier of L/D=3

5.2. Mobilization of Tip Resistance

As the lateral confining pressure increases, more tip resistance is mobilized. On the other hand, maximum mobilized tip resistance reaches just about 30 % of ultimate capacity even for aggregate pier whose L/D ratio is 3 (Figure 5.11). The maximum mobilized tip resistance for aggregate pier of L/D=6 is 5 % of maximum estimated tip resistance if developed tip resistance for $\Delta r/r_0 = 1$ is excluded (Figure 5.12). Developed tip resistance in aggregate pier of L/D=9 is just 2.5 % of estimated tip capacity. Therefore, it does not seem to be necessary to obtain tip resistances in aggregate pier whose L/D ratio is larger than nine. However, it was observed that degree of mobilization rises with increasing radial confining pressure as shown in the Figure 5.13. It should be noted that in mobilized tip resistance vs. settlement graph of zero confining stress is not presented in Figure 5.13 because tip resistance response could not be obtained.

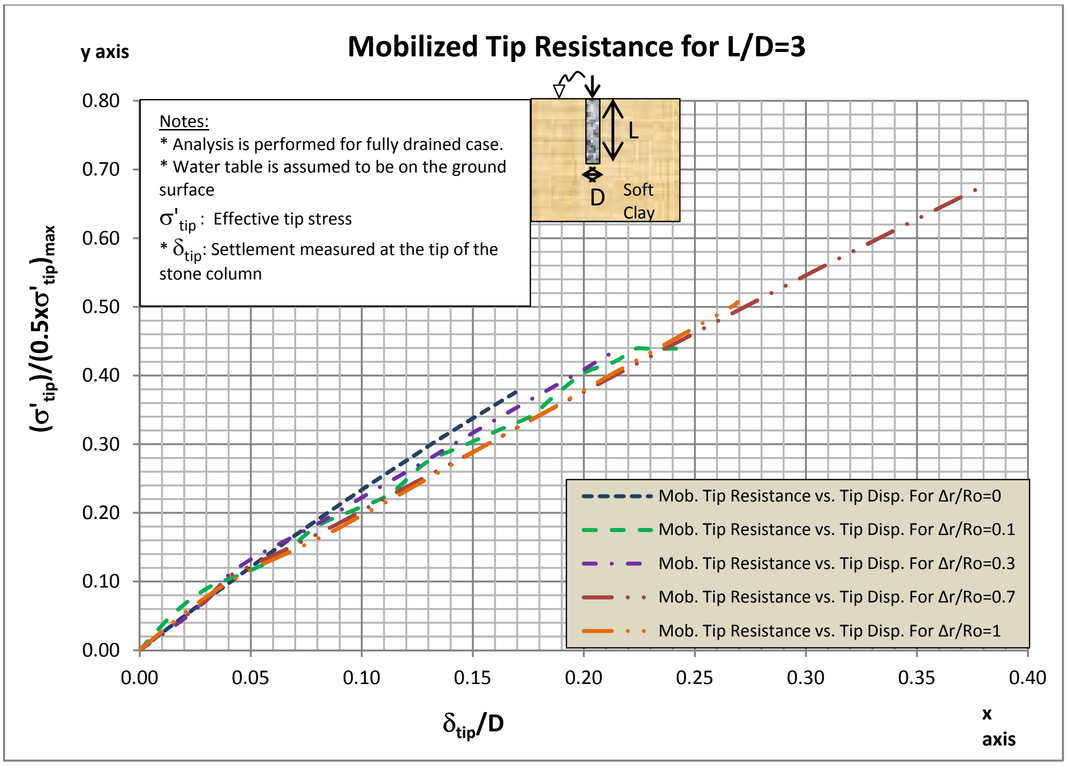

Figure 5.11 Mobilization of tip resistance in different state of confining stresses for pier of L/D=3

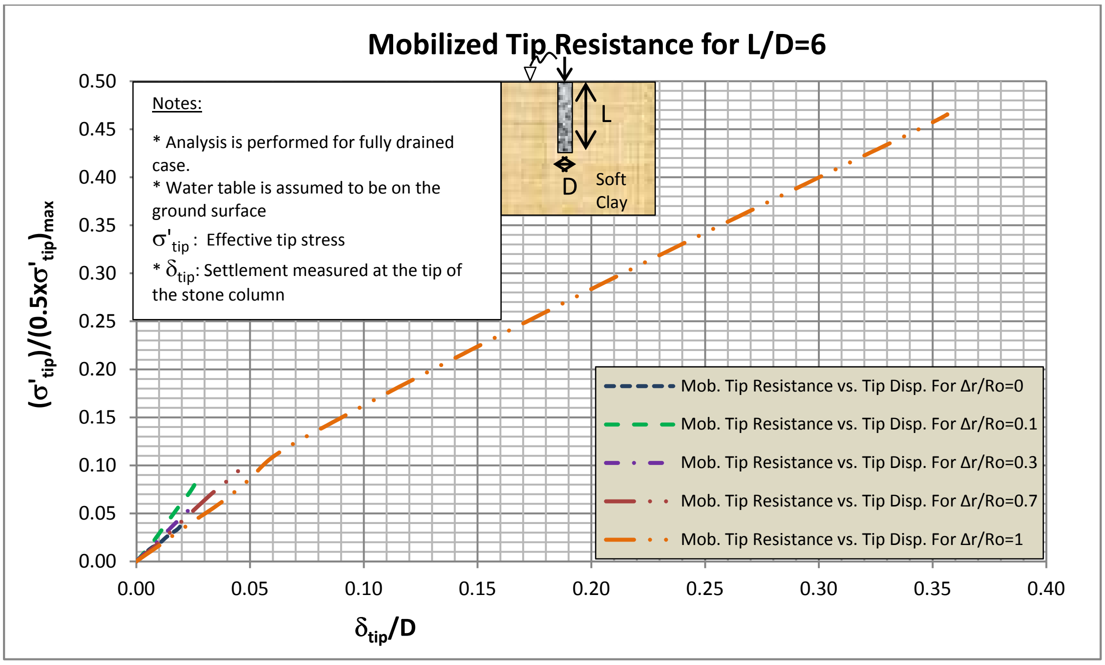

Figure 5. 12 Mobilization of tip resistance in different state of confining stresses for pier of L/D=6

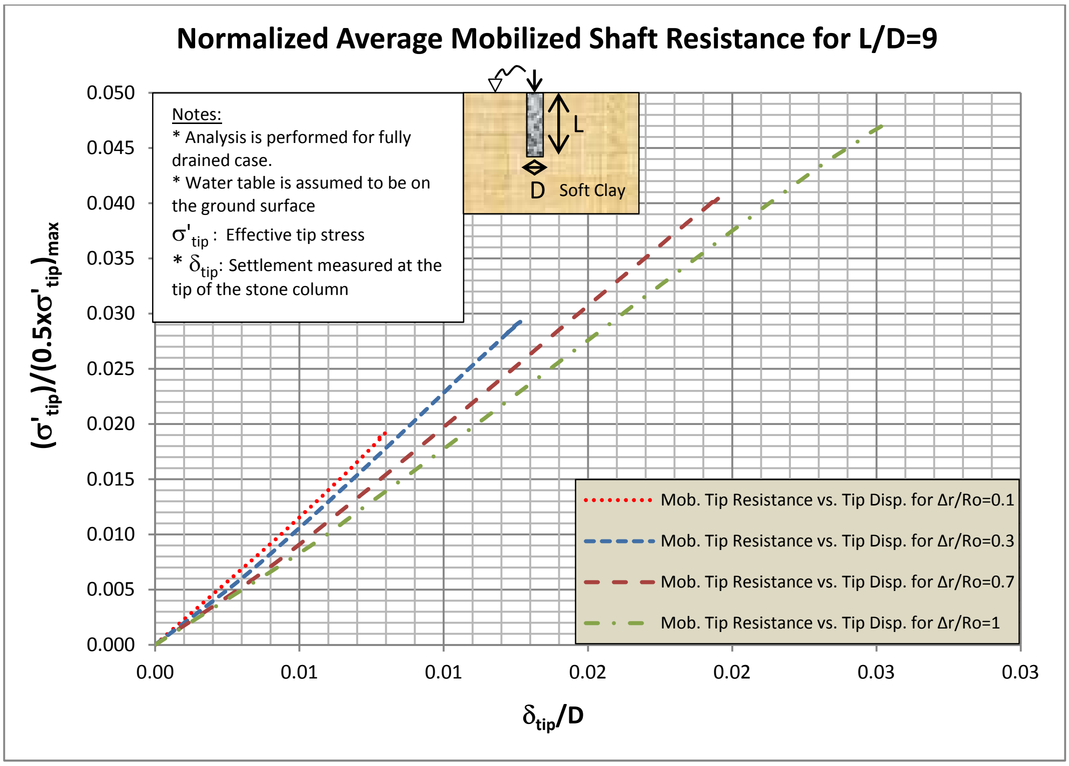

Figure 5.13 Mobilization of tip resistance in different state of confining stresses for pier of L/D=9

As can be seen in the figures 5.11, 5.12 and 5.13, the linear fitting, as specified previously in chapter 4, sufficiently represent the behavior. In addition to linear fits of all aggregate piers of different L/D ratio, a mean of linear fits is introduced in the figure 5.14. Also, standard deviation curve is given in the same graph. In the same way, this line represents average normalized tip resistance mobilization through normalized settlement. However, it is important to emphasize again that the maximum mobilized value of one gives the half of the theoretically calculated maximum tip resistance.

As in the shaft friction, required average tip settlement can be tested with a simple calculation. Again, assuming a pier diameter of 0.5 m and length of 7.5 m:

- F.S. = 2.5 → of 40 % of maximum shaft friction.
- A settlement ratio of 0.22 is required.

$\delta_{tip}/D = 0.22$ $\delta_{tip} = 0.11$ m = **11 cm**

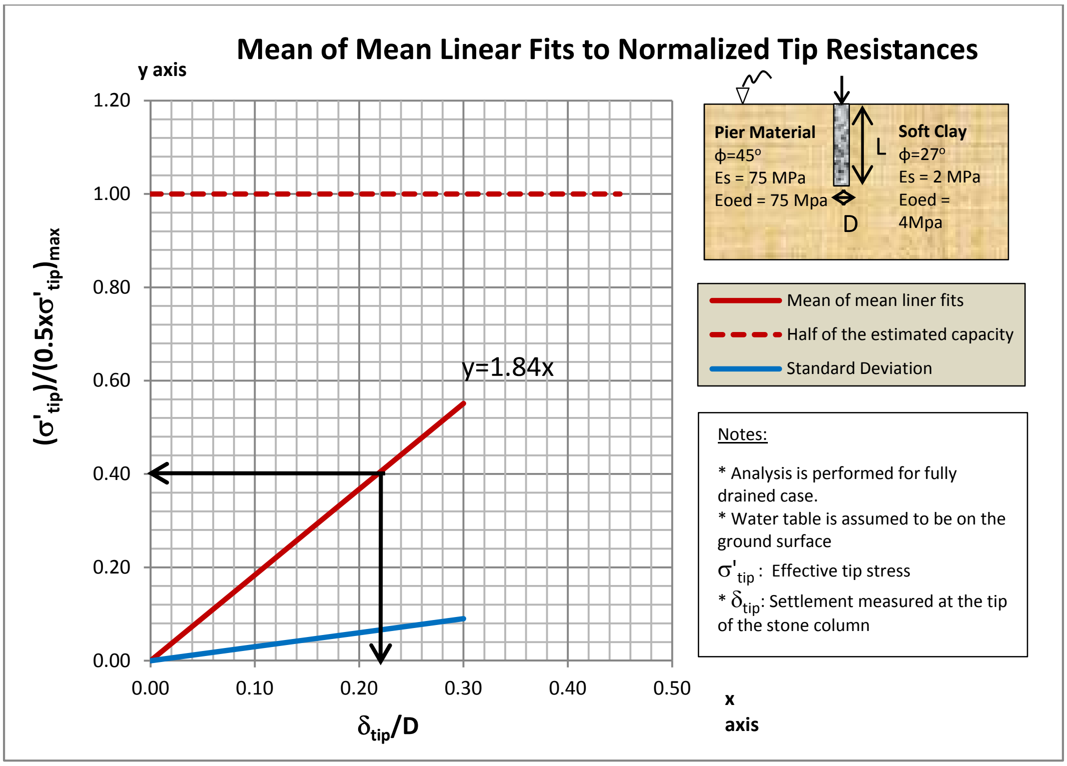

Figure 5.14 Mean mobilized tip resistance with standard deviation

The analysis shows that it is not practically possible to move the tip of a aggregate pier whose L/D ratio is 15 but this simple calculation shows how difficult to mobilize tip resistance in permissible settlement limit for an aggregate pier, whose L/D ratio is 15.

5.3. Mobilization of Modulus of Subgrade Reaction

Mobilized modulus subgrade reaction is expressed as the slope of the vertical stress settlement curve from origin to particular stress point which corresponds to desired settlement value. Since value of the subgrade modulus is deformation (or stress) dependent, the following values are obtained for settlement value of 2.5 cm.

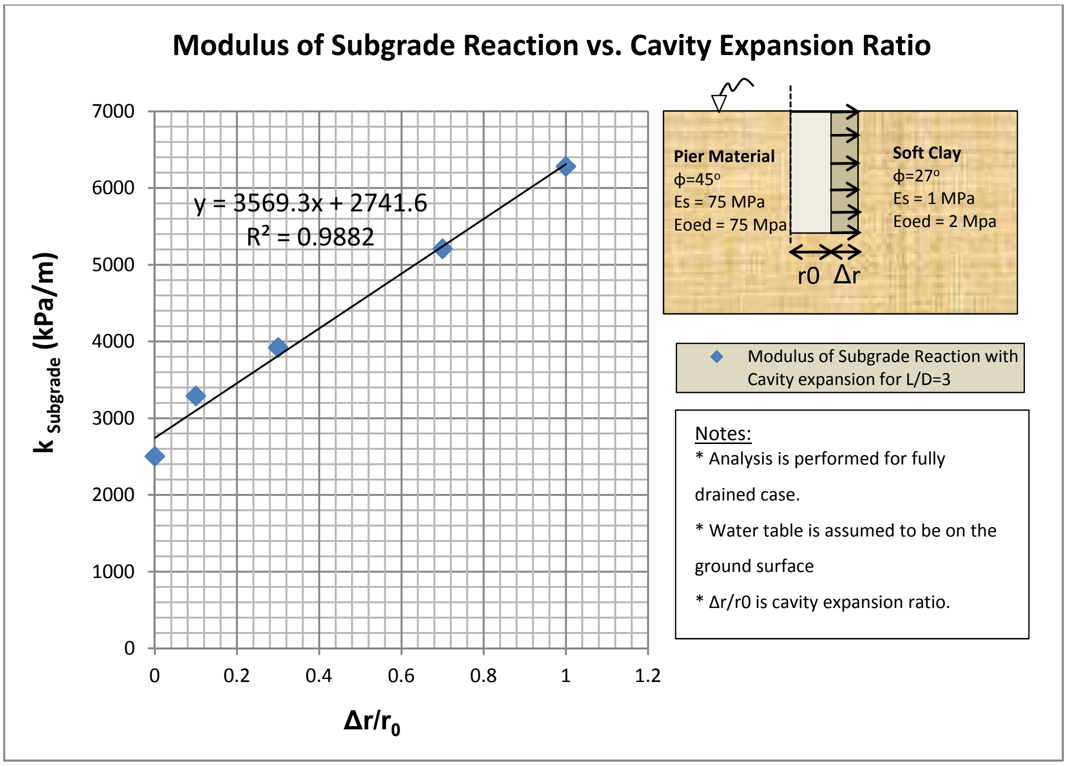

Figure 5. 15 Change in modulus of subgrade reaction vs. cavity expansion for L/D=3

As it can be seen from Figure 5.15 for pier of L/D=3, modulus of subgrade reaction increases as cavity expansion ratio increases. The same linear trend can be observed in the piers of L/D = 4 and 6. However, the linear relation cannot be obtained in the piers of which L/D is higher than 6. (Figure 5.16). In addition to this, no further incerase in modulus of subgrade reaction is obtained in the piers which has L/D ratio higher than 9 (Figure 5.16).

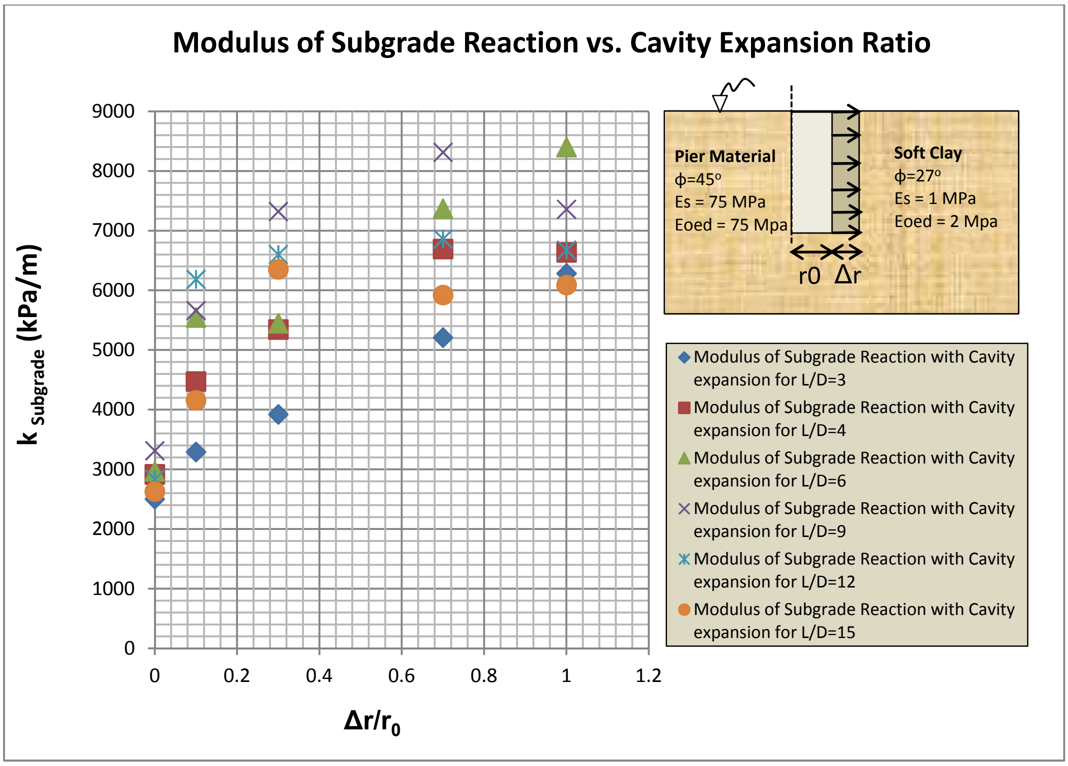

Figure 5.16 Change in modulus of subgrade reaction vs. cavity expansion ratio for pier of L/D=3, 4, 6, 9, 12 and 15

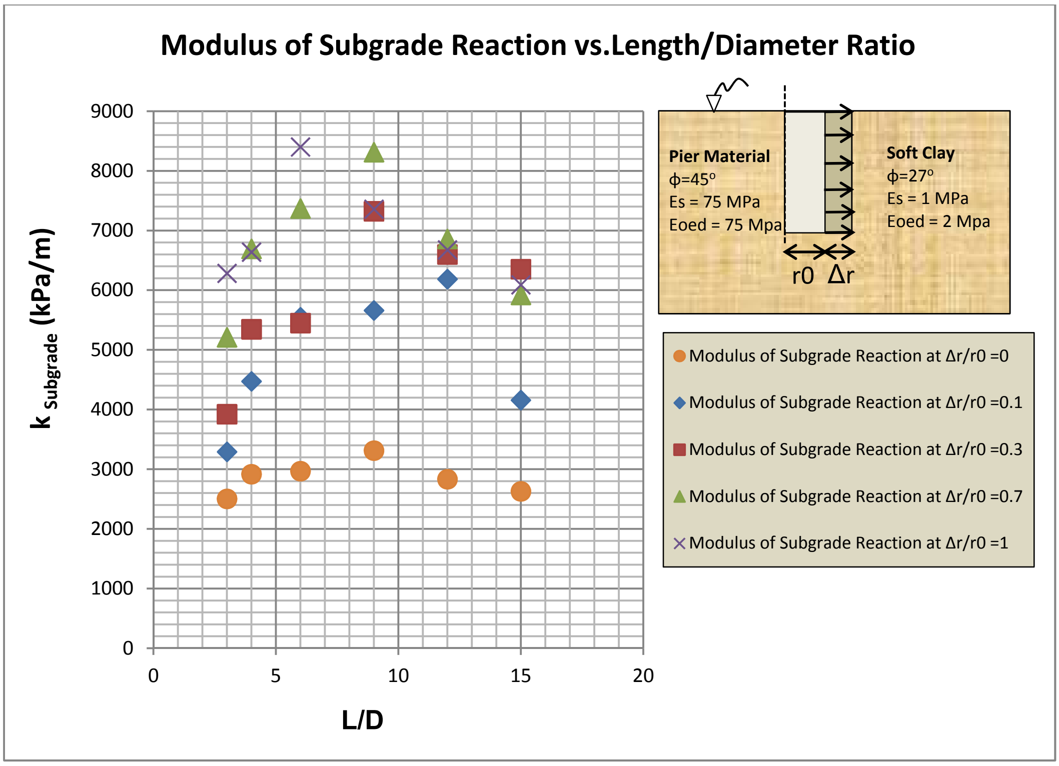

Figure 5.17 Change in modulus of subgrade reaction for pier of different L/D ratios

5.4. Mobilization of Lateral Stress (K*)

Change in lateral stress condition can be easily compared with initial lateral stress state by introducing the ratio as:

$$K^*/K_0 = (\sigma'_h)_f/(\sigma'_h)_0 \qquad (5.1)$$

where K^* is coeficient of lateral stress which defines the state of the soil in between in situ lateral stress and passive state and also; $(\sigma'_h)_f$ and $(\sigma'_h)_0$ are final lateral effective stress and initial in situ lateral effective stress, respectively. In situ lateral stress (lateral stress at rest) of a normally consolidated soil can be estimated by using following relation suggested by Jaky (1948):

$$(\sigma'_h)_0 = K_{0*}(\sigma'_0)_v \qquad (5.2)$$

$$K_0 = 1\text{-}\sin\varphi' \qquad (5.3)$$

where K_0, $(\sigma'_0)_v$ and φ'are lateral stress coefficient at rest, vertical effective stress and drained angle of shearing resistance, respectively. Here, it is important to note that from numerical analysis radial effective stresses are obtained. Also, the radial stresses are given for average embedment depth of the aggregate pier.

In Figure 5.18, the change in lateral stress condition is presented for pier of L/D=3 . As lateral displacement (cavity expansion) increases lateral stress coefficient ratio increases. The final ratio is larger than the ratio obtained by using rankine passive state coefficient K_p ($K_p = (1+\sin\varphi) / (1-\sin\varphi)$).

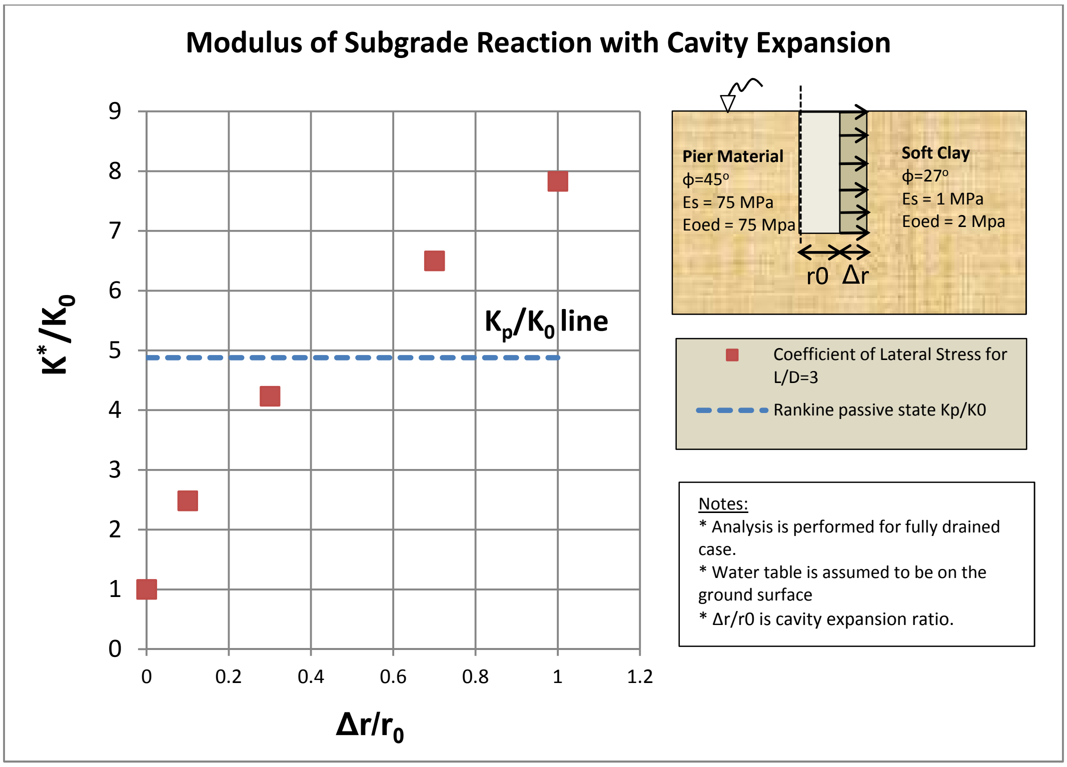

Figure 5. 18 Change in lateral stress state with cavity expansion for L/D=3

CHAPTER 6.

CONCLUSION AND RECOMMENDATIONS

This study has highlighted the influence of method of installation to the overall performance of stone columns. The type of installation and its effect on mobilization of shaft and tip resistances were simulated as expanded granular piers. In order to create different construction induced confining stresses, different cavity expansion ratios ($\Delta r/r_0$) were utilized. As a final product, average normalized shaft friction–settlement solutions of aggregate piers of different sizes in different confining stress states were developed to help implementation of performance based design. Also, contribution of tip resistance to overall load carrying capacity was specified.

Even though widely followed design methodology includes assesment steps of i) determination of ultimate lateral capacity of matrix soil, ii) penalizing the capacity with a factor of safety, then iii) checking for permissible settlements; it does not enable the designer to check how axial resistance in an aggregate pier is mobilized with induced settlements. Actual portrait should involve the determination of mobilized shaft resistance that is developed as a function of vertical displacement. This vertical displacement results from the movement of the column relative to surrounding soil, as well as lateral and vertical deformation of the column itself. The gap was filled by this study which clearly presents the relation between normalized settlement of the pier and average normalized shaft friction as well as tip resistance inspired from the study performed for piles by Reese and O’Neill (1988).

For this purpose, solutions which can be utilized as a design guideline during preliminary design stage was generated in the figure 6.1 and 6.2. The chart solution presents a mean curve with plus and minus one standard deviation range. Two solutions were prepared on the basis of finite-element simulations. First one shows the development of normalized shaft friction vs. normalized top settlement and the other one presents normalized tip resistance vs. normalized tip settlement. Here, it is significant to note that the produced solutions are only for the cases which are smilar with the aggregate material and soft soil given on the right side of the graph. Although dimensional sensitivity of the results are attempted to reduce by introducing normalization, mobilized capacity ratio for a particular normalized settlement value is highly sensitive to stiffness ratio of aggregate and soft soil.

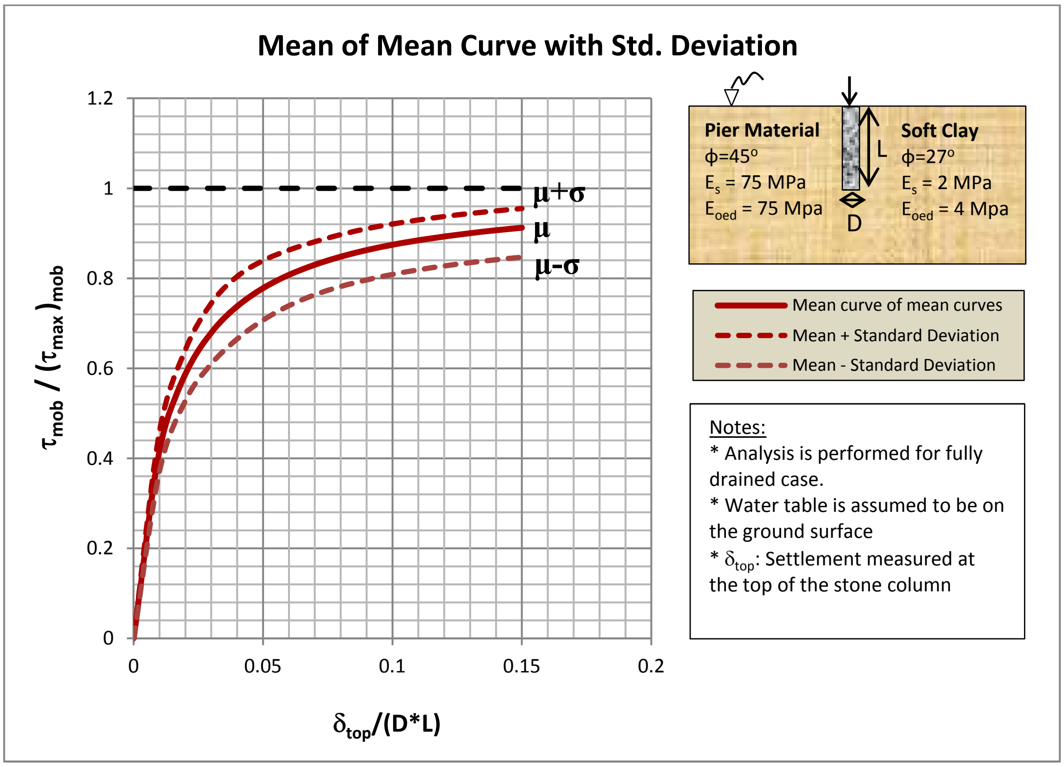

Notes:
* Analysis is performed for fully drained case.
* Water table is assumed to be on the ground surface
* δ_{top}: Settlement measured at the top of the stone column

Figure 6.1 Mean normalized mobilized shaft resistance with one standard deviation range

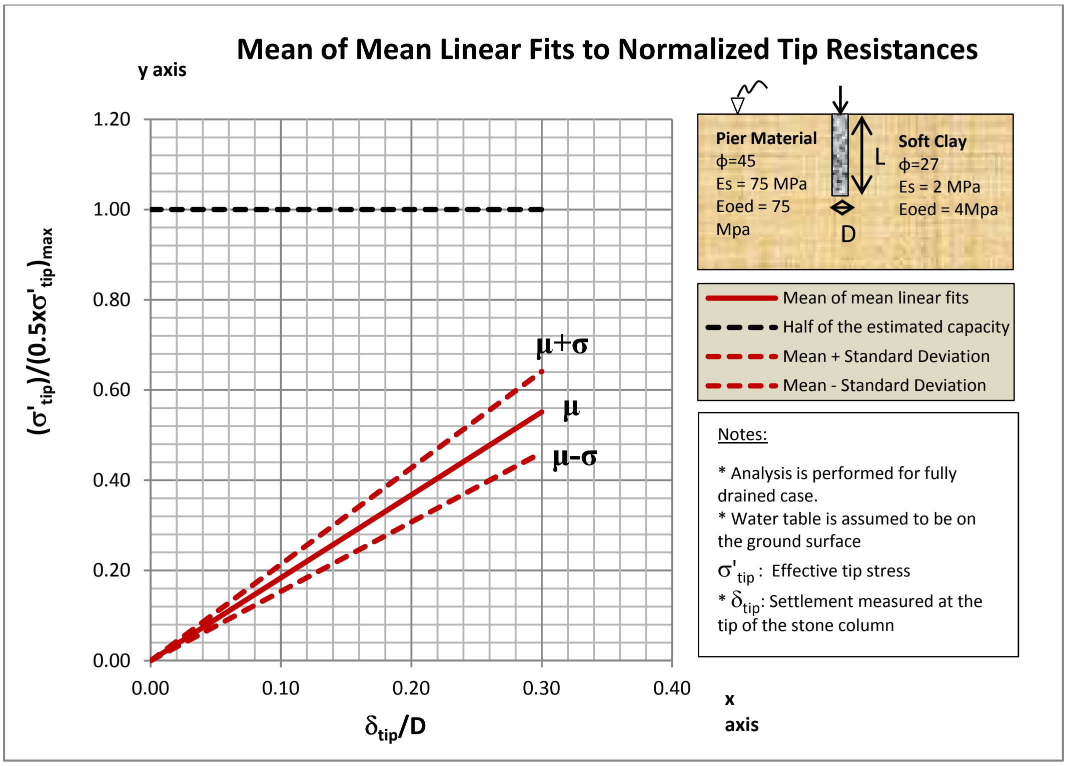

Figure 6.2 Mean mobilized tip resistance with one standard deviation range

In addition, some other specific conclusions based on the assessment of analysis results of the study are as follows:

1. The mobilized shaft resistance of an aggregate pier in a soil depends remarkably on the behavior of native soil–aggregate pier interaction. As a result, it is *believed that the application of advanced constitutive models can cause more realistic predictions on shaft load-displacement response*.

2. Development of shaft resistance increases as confining stresses increases. Therefore, *disregarding of installation effects gives rise to underestimation of pier capacity as well as overestimation of real settlement.* Illustration of this mobilized shaft resistance as a function of expansion ratio (i.e: $\Delta r/r_0$) is shown in figure 6.3 for L/D =3.

3. No appreciable tip resistance is developed even in short aggregate piers (L/D<5). In addition, to obtain full mobilization of tip resistance, vertical deformation that cannot be tolerated by most of the engineering structures is necessary. Therefore, *it is not practically possible to utilize tip resistance in pier design.*

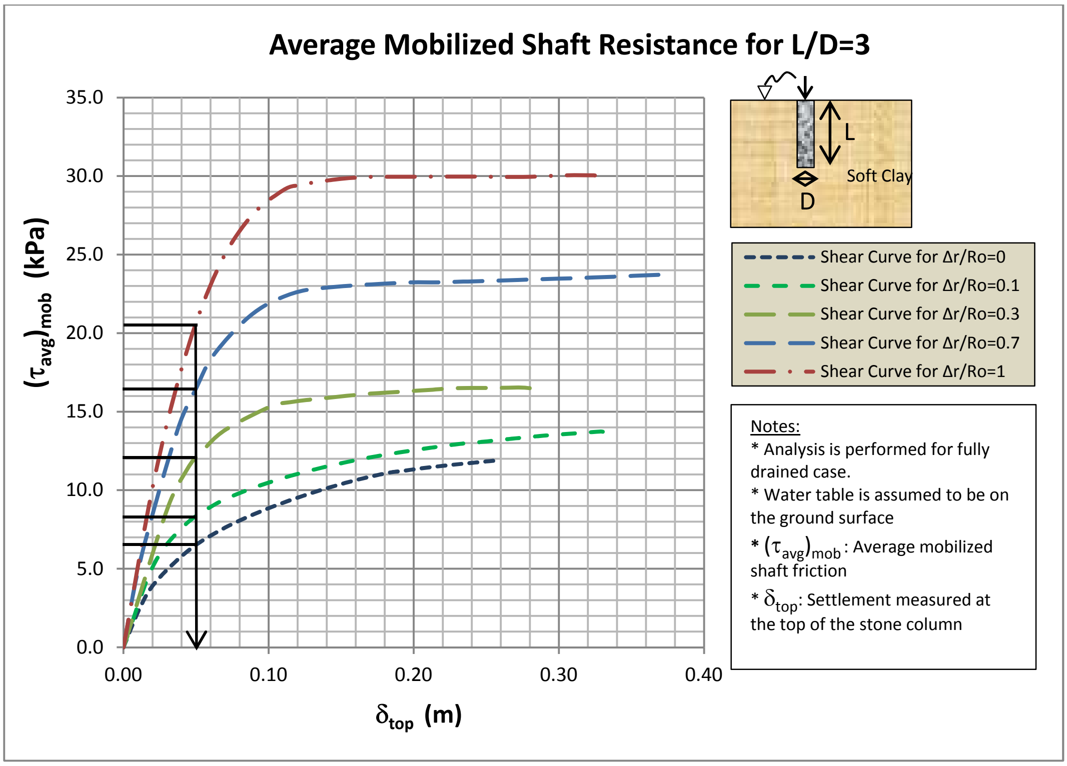
Average Mobilized Shaft Resistance for L/D=3

Notes:
* Analysis is performed for fully drained case.
* Water table is assumed to be on the ground surface
* $(\tau_{avg})_{mob}$: Average mobilized shaft friction
* δ_{top}: Settlement measured at the top of the stone column

Figure 6.3 Mobilized shaft resistance as a function of expansion ratio

6.1. Recommendations for Future Studies

1. The shaft friction mechanism, which is main load carrying mechanism but not the mechanism of failure in ultimate state, has been overlooked until now. Therefore, this mechanism is intended to be brought to focus in this thesis by finite element based numerical simulations. However, it should be noted that little experimental evidence exists about confining stress state around stone columns. Field tests should be performed especially under either drained or undrained conditions to verify the results of this study.

2. In the scope of this thesis, resistance mobilization in aggregate piers under monotonically increasing centric axial load was examined and dynamic effects of installation are excluded. Hence, dynamic installation effects need to be studied.

3. The most appropriate method of installation and length to diameter ratio can be determined by optimizing cost and maximum benefit (capacity for a certain specified lateral displacement) for a certain stress range and concentration ratio. As a part of future research studies, economical aspects of different aggregate piers can be assessed.

REFERENCES

Babu, M. R. D., Nayak S., Shivashankar, R. (2012). A Critical Review of Construction, Analysis and Behaviour of Stone Columns. Geotech. Geol. Eng. , 31:1–22, Springer.

Barksdale, R.D., and Bachus, R.C. (1983). Design and Construction of Stone Columns. Report No. FHWA/RD-83/026, National Technical Information Service, Virginia, USA.

Bolton M.D. (1986). Strength and Dilatancy of Sands. Geotechnique, Vol 36, No 1, pp 65-78.

Brinkgreve, R.B.J. (2005). Selection of Soil Models and Parameters for Geotechnical Engineering Application. Soil Constitutive Models, pp. 69-98.

Brinkgreve, R.B.J., Vermeer, P.A. (2002). PLAXIS-Finite Element Code for Soil and Rock Analysis. Version 8.2 Manuals, PLAXIS B.V., Balkema, Rotterdam.

Castro J. and Karstunen M. (2010). Numerical simulations of stone column installation. Can. Geotech. J. Vol. 47, pp. 1127-1138. NRC Research Press.

Chin, F.K. (1970). Estimation of the Ultimate Load of Piles Not Carried to Failure. Proc.2ndSoutheast Asia. Conference on soil Engineering, pp. 81-90.

Datye K. R and Nagaraju S.S. (1975). Installation and testing of rammed stone columns. In: Proceedings, 5th Asian regionalconference on soil mech. and found. Eng., Bangalore, India, pp 101–104

Ehsan R. (2013). A Study of Geotechnical ConstitutiveModels Used in Plaxis 2D. G&S Papers Competition.

Elshazly H.A., Hafez D., Mosaad M. (2006). Back calculating vibro-installation stresses in stone columns reinforced grounds. J Ground Improv 10(2). pp.47–53.

FHWA-HRT-13-068. (2013). Friction Angles of Open- Graded Aggregates From Large-Scale Direct Shear Testing.

Gibson, R. E. (1953). Experimental determination of the true cohesion and true angle of internal friction in clays. Proc. 3rd International Conference on Soil Mechanics and Foundation Engineering, Zurich, Switzerland, 1, 126−131.

Handy, R. L. (2001). Does Lateral Stress Really Influence Settlement. Journal of Geotechnical and Geoenvironmental Engineering, ASCE, Vol. 127, No. 7, pp.623-626.

Jaky, J. (1948). Pressure in silos. Proc., 2nd Int. Conf. on SoilMechanics and Foundation Engineering, Rotterdam, The Netherland. Vol 1, pp.103–107.

Keller Brochure 10-02 E. Deep Vibro Techniques.

Kirsch, F. (2008). Evaluation of ground improvement by groups of vibro stone columns using field measurements and numerical analysis. Proceedings of the Second International Workshop on Geotechnics of Soft Soils, Scotland, pp 241–248.

Kirsch, K. and Kirsch, F. (2010). Ground improvement by deep vibratory methods. Spon Press.

Mitchell, J.K. (1982). Soil Improvement-State-of–the Art Report. Proceedings of the 10th Int. Conf. on SMFE, Stockholm. Vol.4, pp.509-565.

Mosoley, M.P., and Priebe, H. J. (1993). Vibro Techniques Ground Improvement. Chapman and Hall.

Randolph, M. F., Carter, J. P. and Wroth, C. P. (1979). Driven piles in clay-the effects of installation and subsequent consolidation. Geotechnique 29, No. 4, 361-393.

Reese, L. C., and O'Neill M. W. (1988). Drilled Shaft: Construction Procedures and Design Methods. FHWA-HI-88-042, Federal Highway Administration, Washington, D.C.

Prakash, S., Sharma H. D. (1990). Pile Foundations in Engineering Practice. John Wiley & Sons, Inc.

Van Impe W. F. and Madhav M. R. and Wandercry J.P. (1997). Considerations in Stone Column design. Ground Imrovement Geosystems. Thomas Telford, London, pp. 190-196.

Sentez İnşaat. (n.d.). Retrieved 5 May 2012, from http://sentezinsaat.com.tr/geopier-sistemi.html

Vibroflotation. (n.d.). Retrieved 3 Sep. 2013, from http://www.vibroflotation.com/Vibro/vibroflotation_fr.nsf/site/Stone-Columns.Dry-Stone-Columns

Vibroflotation. (n.d.). Retrieved 10 Nov. 2013, from http://www.vibroflotation.com/Vibro/vibroflotation_fr.nsf/site/Stone-Columns.Wet-Stone-Columns

Vibro Menard (n.d.). Retrieved 10 Dec. 2013, from http://vibro.co.uk/index.php?option=com_content&view=article&id=4&Itemid=19

Zetaş (n.d.). Retrieved 8 Feb. 2014, from http://www.zetas.com.tr/index.php?id=222000&dil=EN

APPENDIX A

OUTPUTS OF AGGREGATE PIERS OF L/D=4, 6, 9, 12 AND 15

Aggregate Pier of L/D = 4:

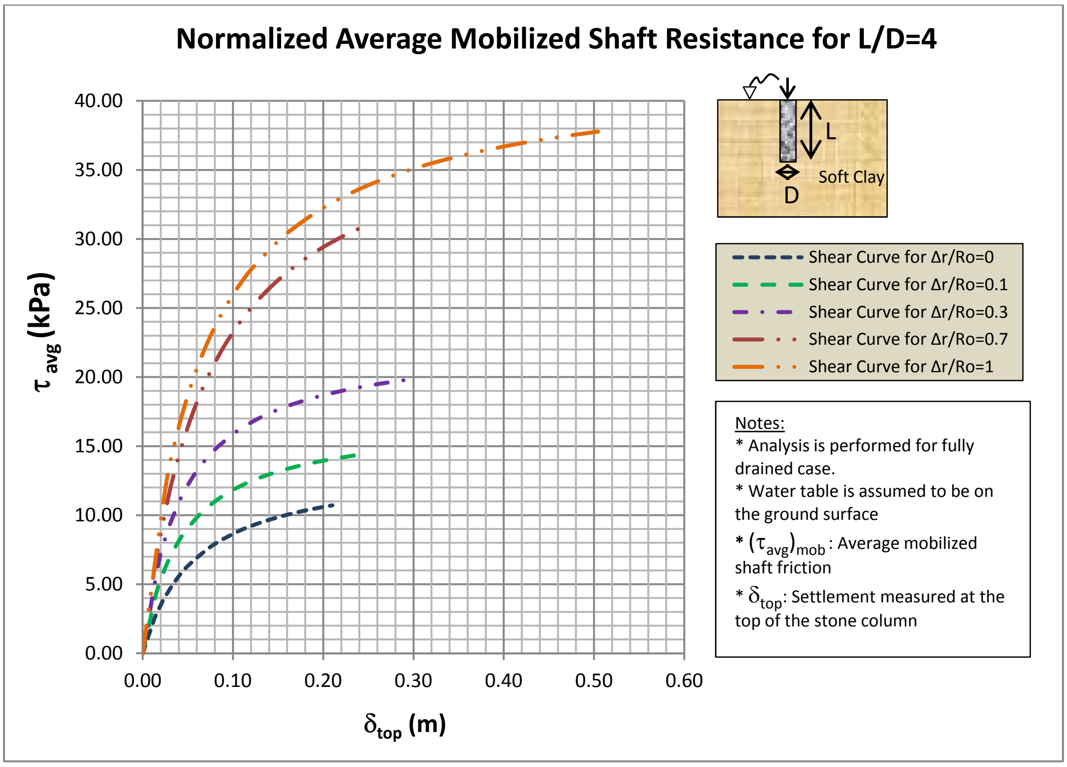

Notes:
* Analysis is performed for fully drained case.
* Water table is assumed to be on the ground surface
* $(\tau_{avg})_{mob}$: Average mobilized shaft friction
* δ_{top}: Settlement measured at the top of the stone column

Figure a. 1 Average shaft resistance for aggregate pier for L/D=4

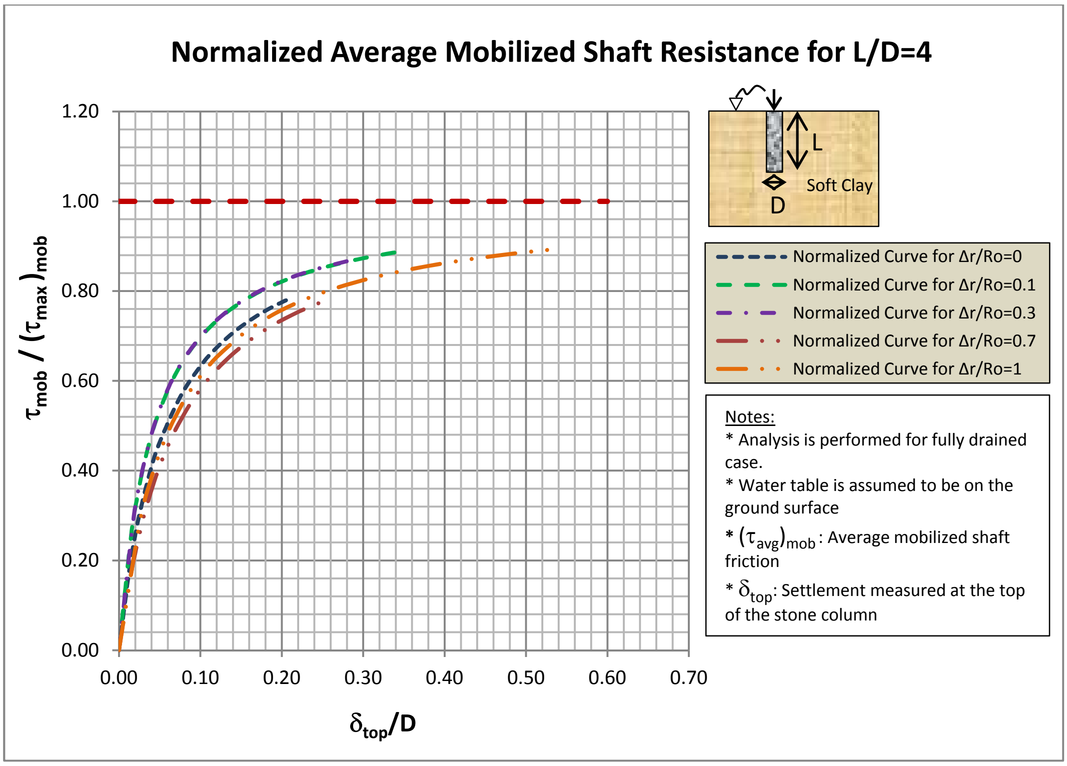

Figure a.2 Normalized average shaft resistances for L/D=4

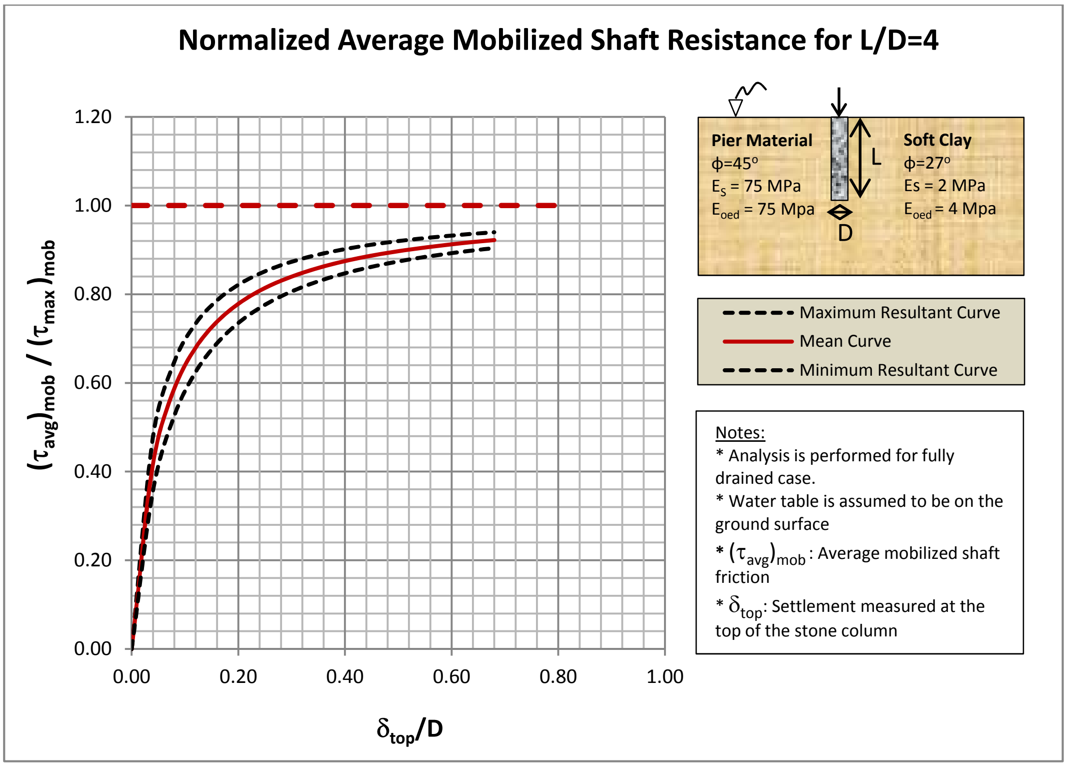

Figure a.3 Average normalized curve with upper and lower threshold curves for L/D=4

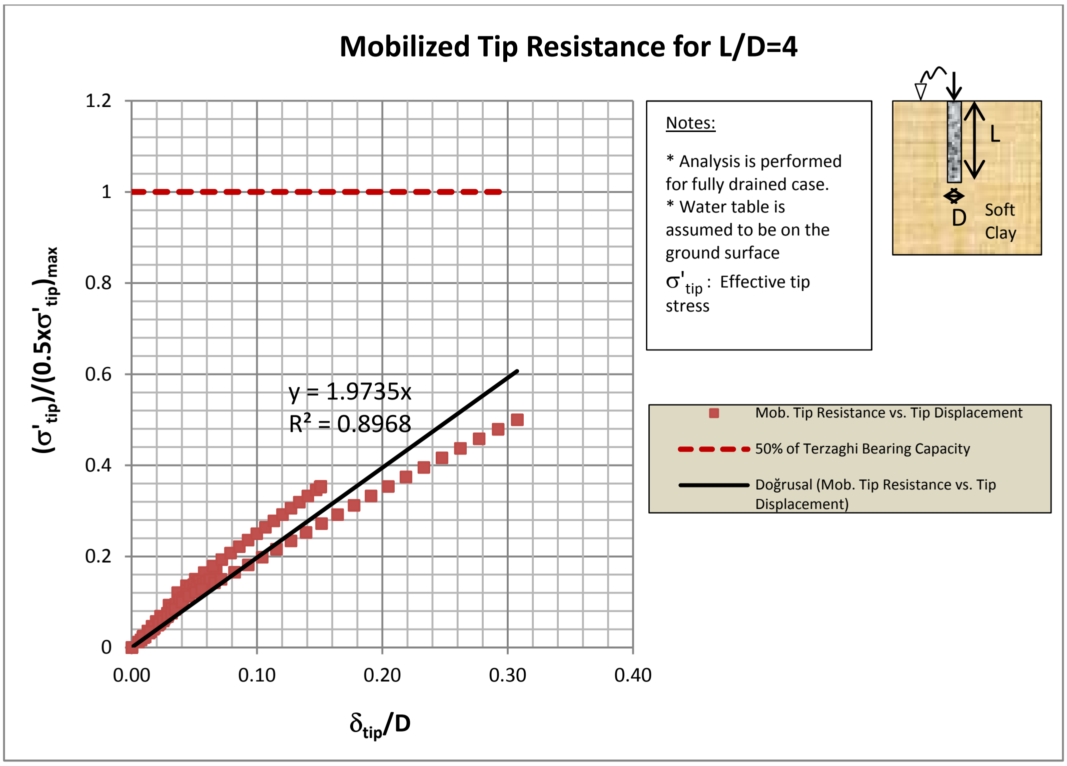

Figure a.4 Normalized tip resistances of aggregate pier of L/D=4

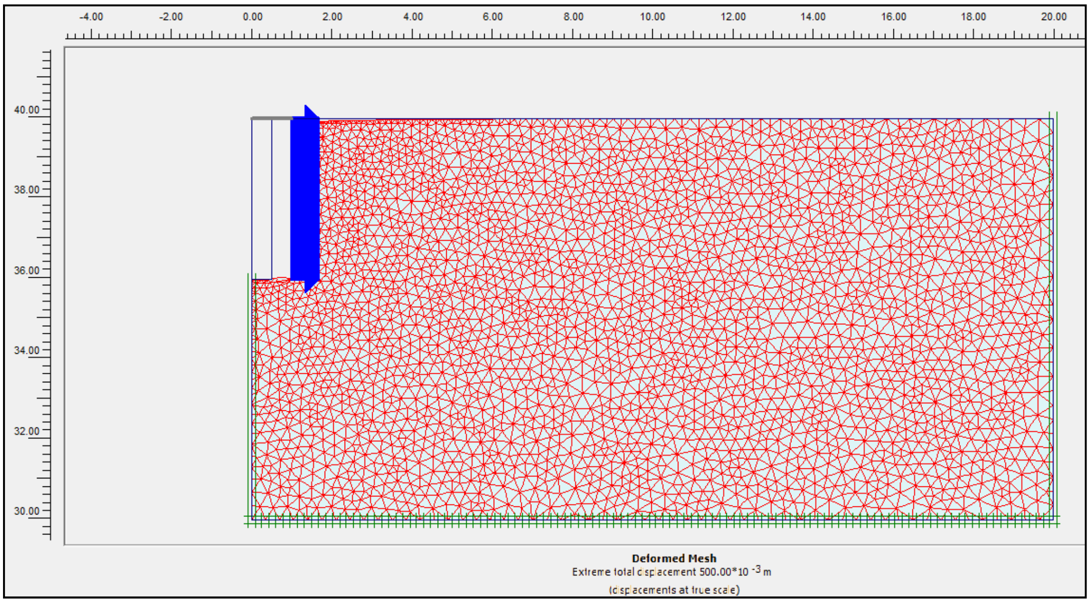
-4.00
-2.00
0.00
2.00
4.00
6.00
8.00
10.00
12.00
14.00
16.00
18.00
20.00
40.00
38.00
36.00
34.00
32.00
30.00
Deformed Mesh
Extreme total displacement 500.00*10⁻³ m
(displacements at true scale)

Figure a.5 Deformed shape after application of lateral displacement ($\Delta r/r_0 = 1$) to pier of L/D=4

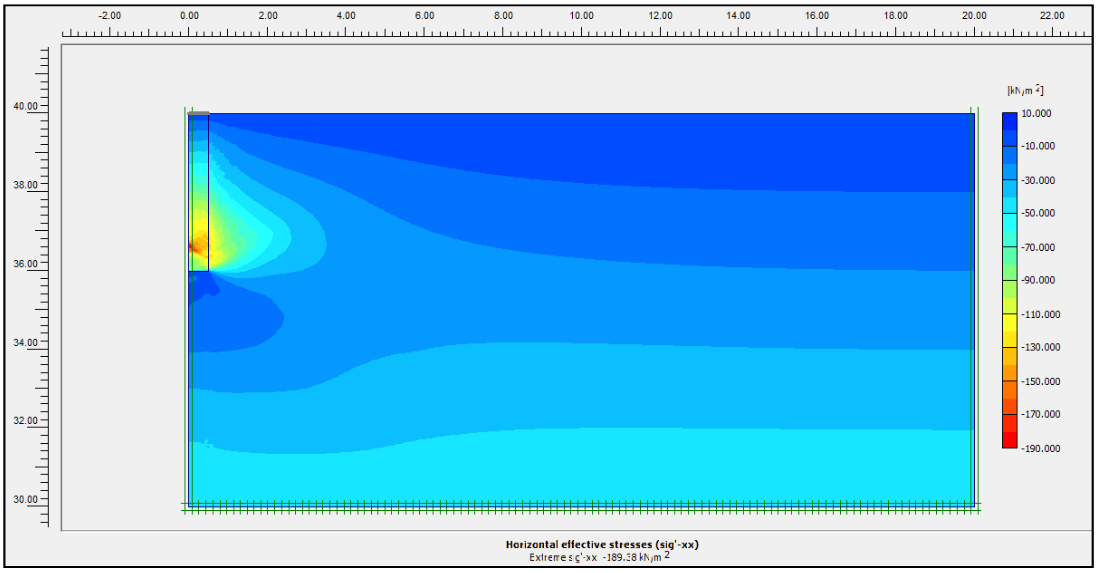

Figure a.6 Confining stresses around the pier of L/D=4 for $\Delta r/r_0 = 1$

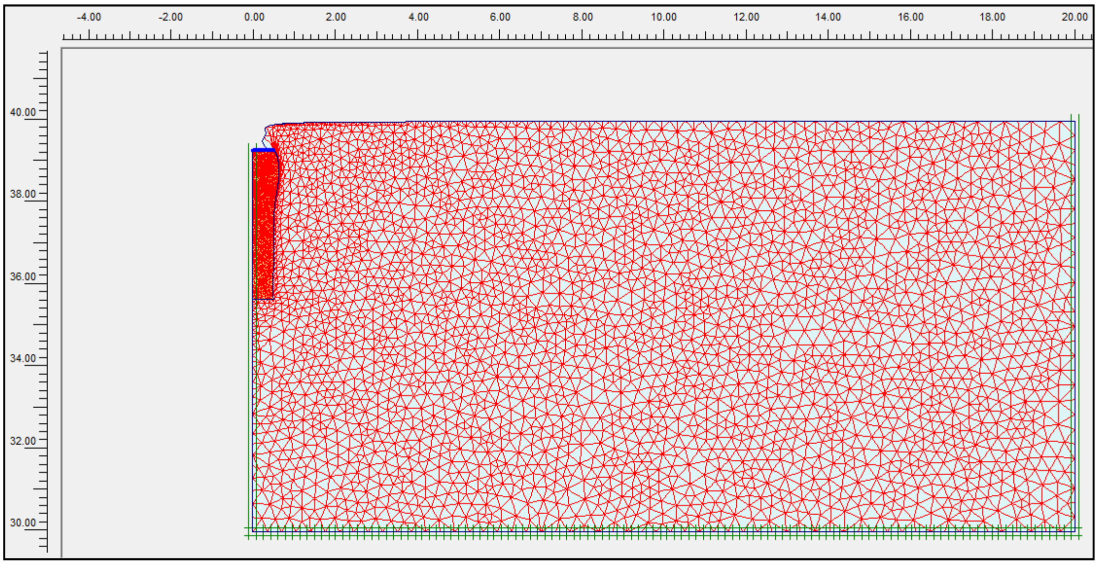
-4.00
-2.00
0.00
2.00
4.00
6.00
8.00
10.00
12.00
14.00
16.00
18.00
20.00
40.00
38.00
36.00
34.00
32.00
30.00

Figure a.7 Deformed mesh of aggregate pier of L/D=4 for $\Delta r/r_0 = 1$ (Scale factor=1)

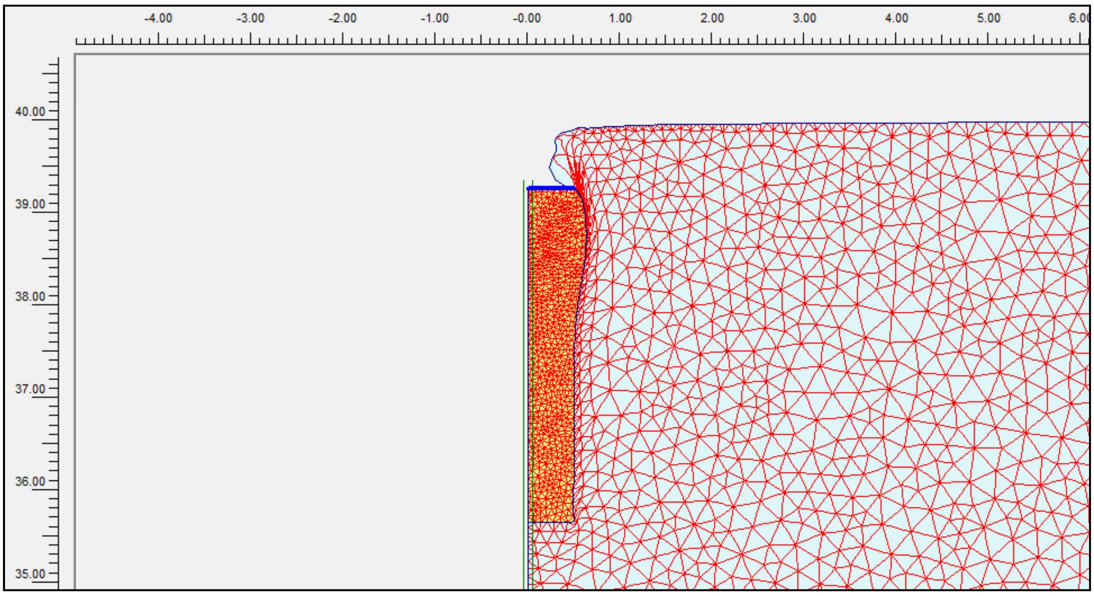
-4.00
-3.00
-2.00
-1.00
-0.00
1.00
2.00
3.00
4.00
5.00
40.00
39.00
38.00
37.00
36.00
35.00

Figure a.8 Deformed mesh of aggregate pier of L/D=4 for $\Delta r/r_0$ =1 (Scale factor=1)

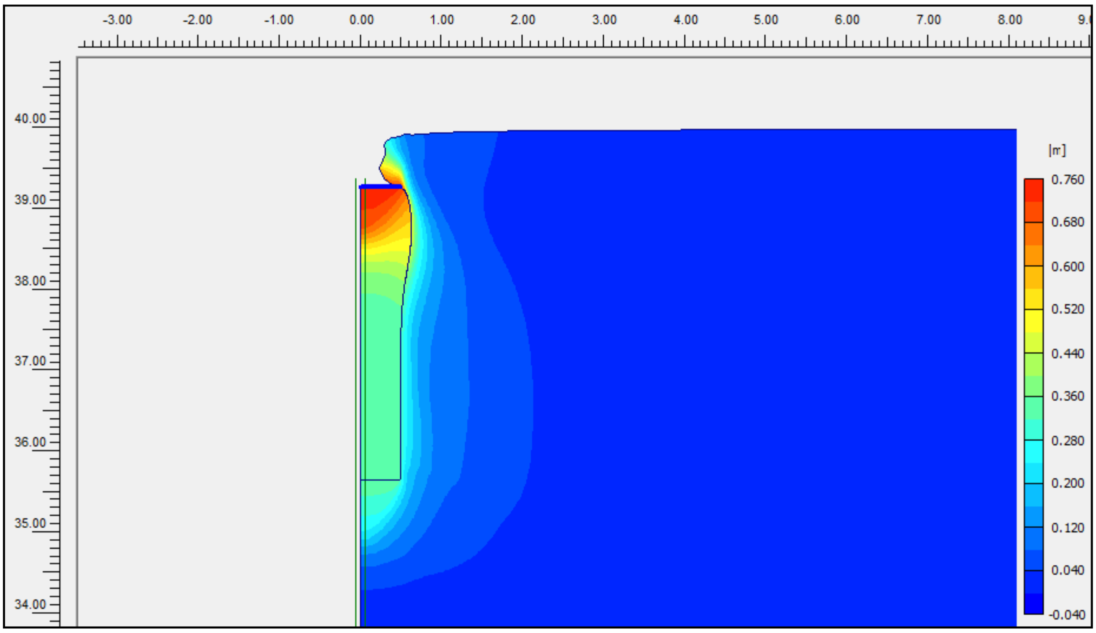

Figure a.9 Total displacement shading of aggregate pier of L/D=4 for $\Delta r/r_0$ =1

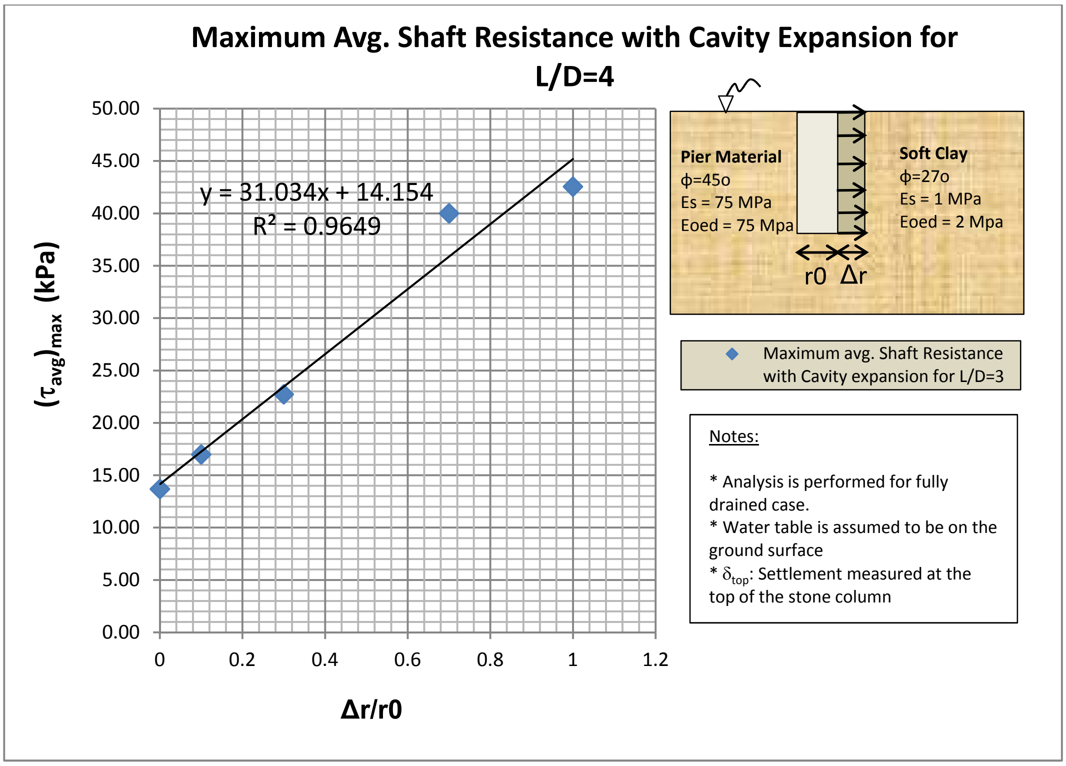

Notes:

* Analysis is performed for fully drained case.
* Water table is assumed to be on the ground surface
* δ_{top}: Settlement measured at the top of the stone column

Figure a.10 Maximum average shaft resistance vs. cavity expansion ratio for L/D=4

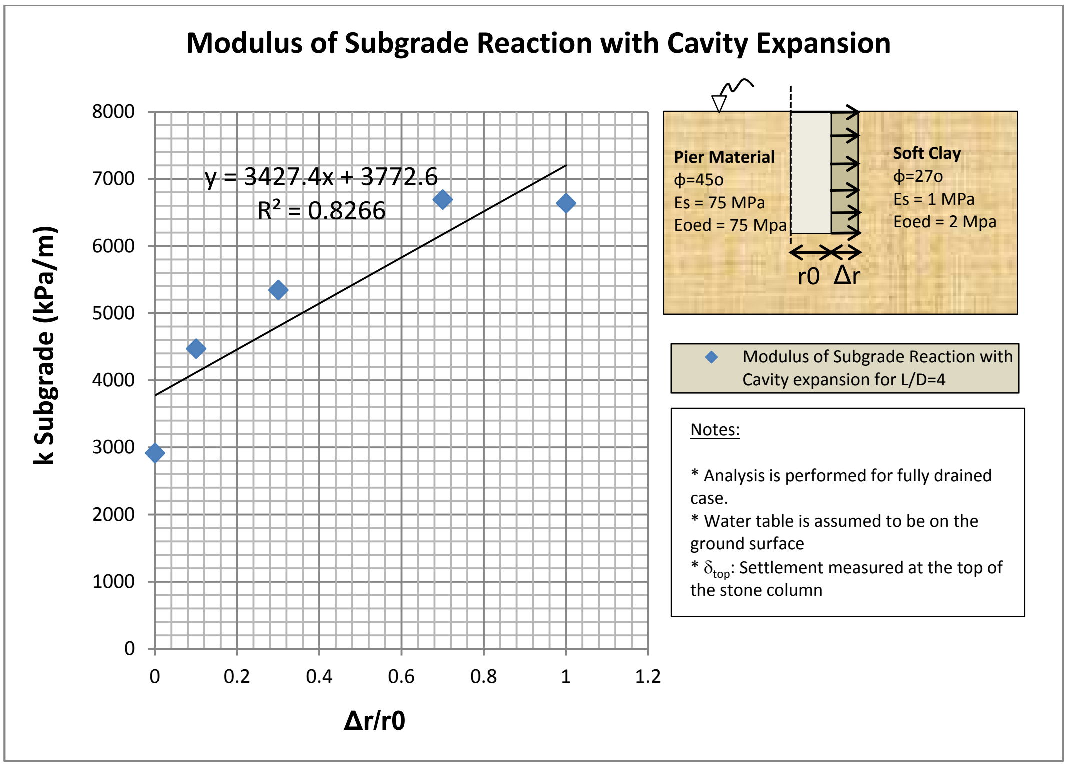

Notes:

* Analysis is performed for fully drained case.
* Water table is assumed to be on the ground surface
* δ_{top}: Settlement measured at the top of the stone column

Figure a.11 Modulus of subgrade reaction vs. cavity expansion ratio for L/D=4

Aggregate Pier of L/D =6:

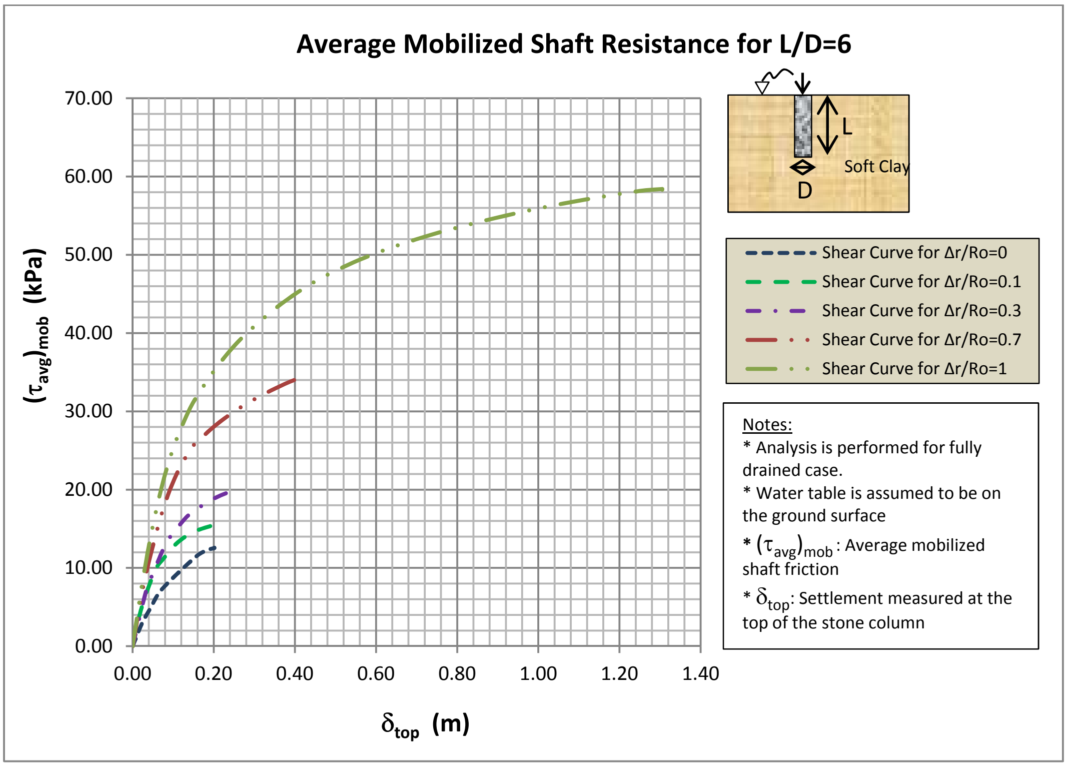

Figure a.12 Average shaft resistance for aggregate pier for L/D=6

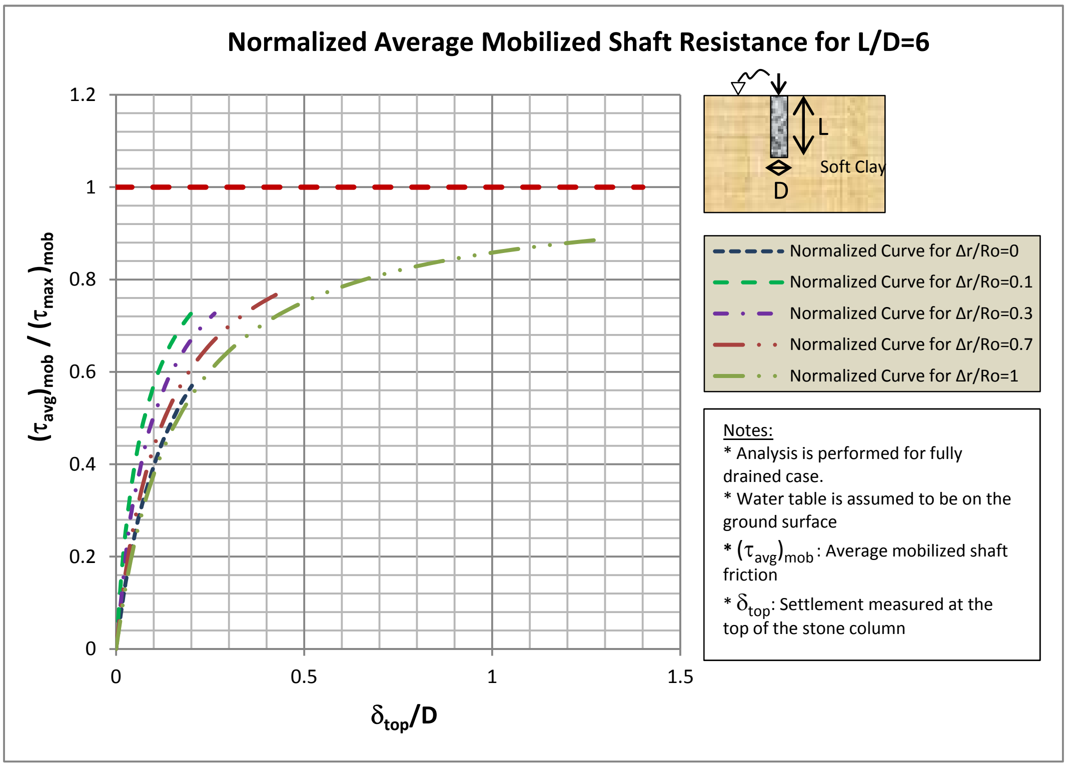

Figure a.13 Normalized average shaft resistances of pier for L/D=6

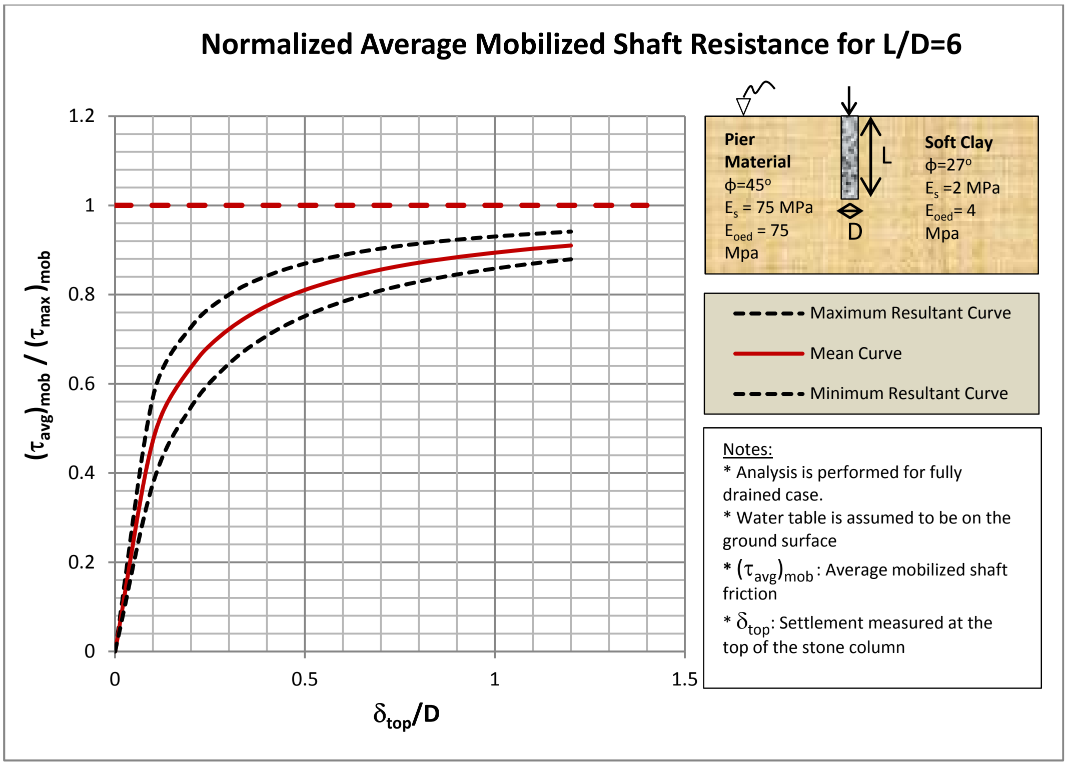

Notes:
* Analysis is performed for fully drained case.
* Water table is assumed to be on the ground surface
* $(\tau_{avg})_{mob}$: Average mobilized shaft friction
* δ_{top}: Settlement measured at the top of the stone column

Figure a.14 Normalized mean curve with upper and lower threshold curves for L/D=6

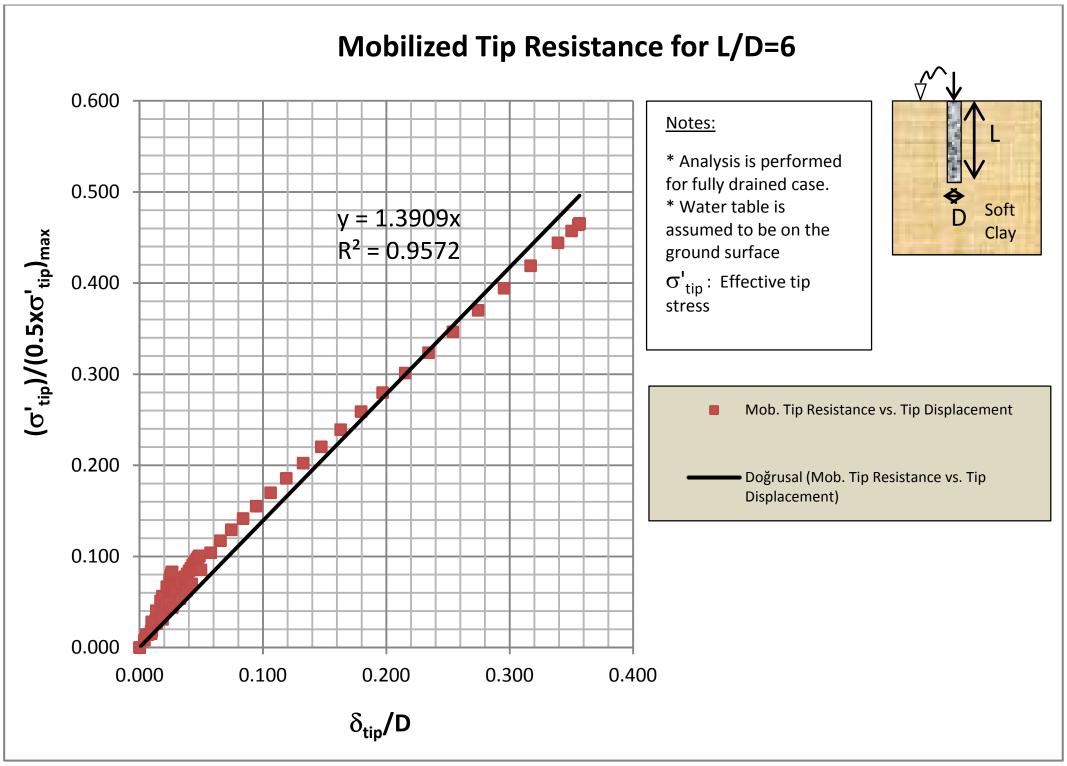

Notes:
* Analysis is performed for fully drained case.
* Water table is assumed to be on the ground surface
σ'_{tip} : Effective tip stress

Figure a.15 Normalized tip resistances of aggregate pier of L/D=6

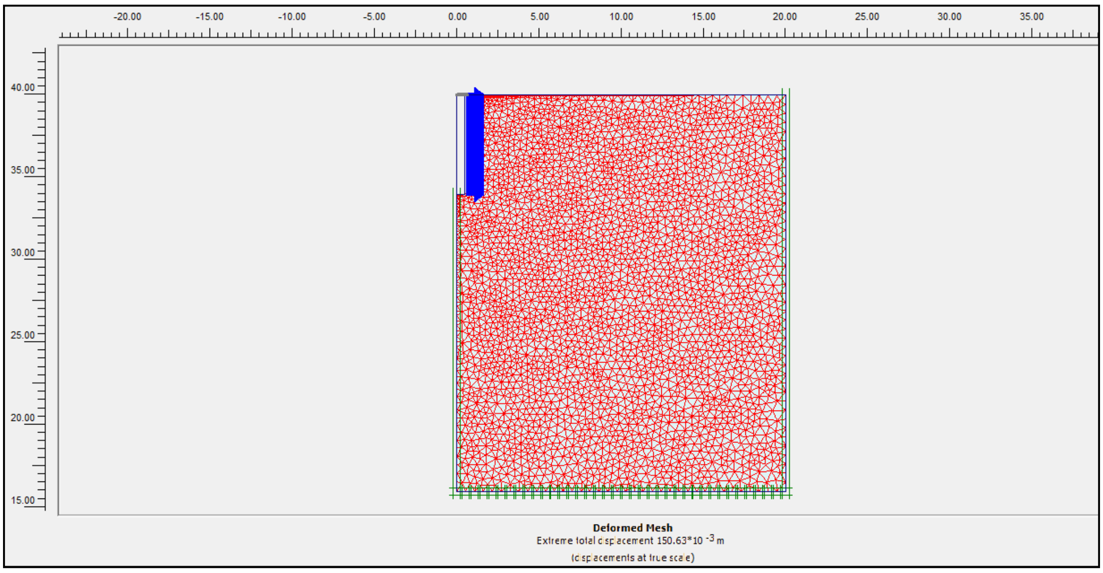
-20.00
-15.00
-10.00
-5.00
0.00
5.00
10.00
15.00
20.00
25.00
30.00
35.00
40.00
35.00
30.00
25.00
20.00
15.00
Deformed Mesh
Extreme total displacement 150.63*10 -3 m
(displacements at true scale)

Figure a.16 Deformed shape after application of lateral displacement of $\Delta r/r_0$ =0.3

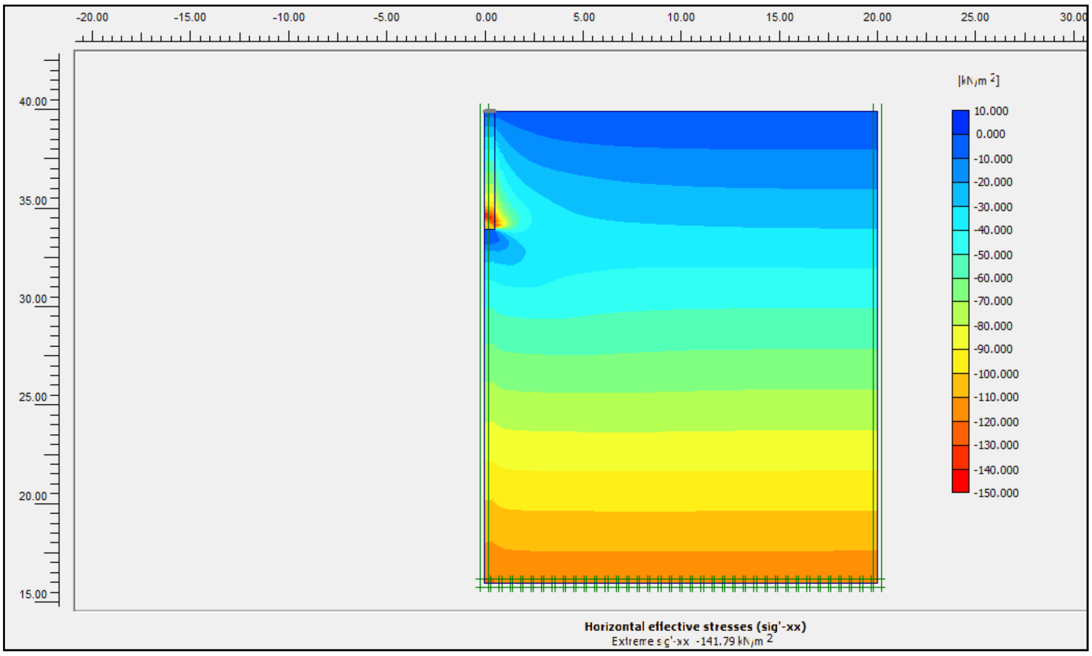

Figure a.17 Confining stresses around the pier of L/D=6 after installation

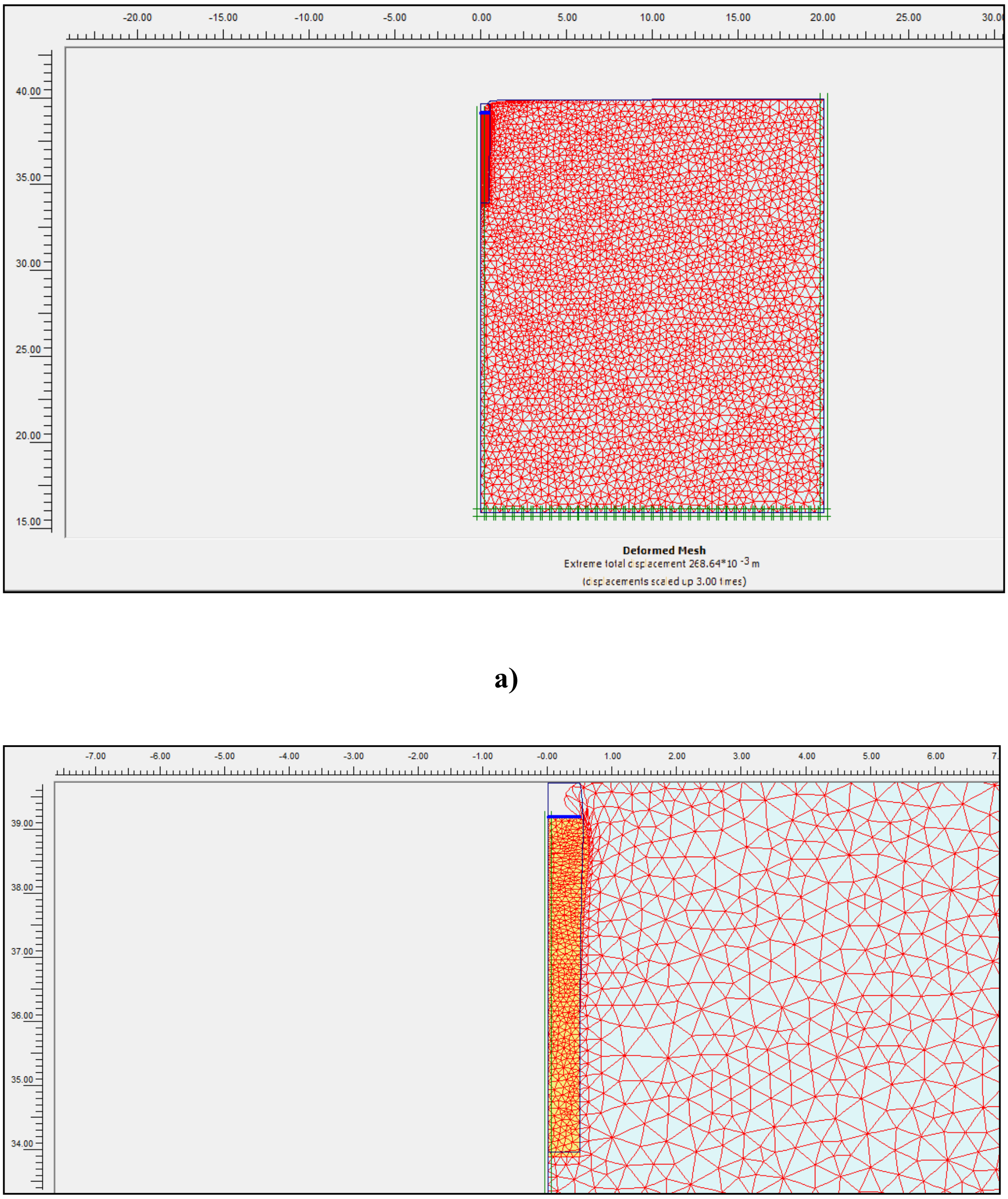
-20.00
-15.00
-10.00
-5.00
0.00
5.00
10.00
15.00
20.00
25.00
30.00
40.00
35.00
30.00
25.00
20.00
15.00
Deformed Mesh
Extreme total displacement 268.64*10^-3 m
(displacements scaled up 3.00 times)
-7.00
-6.00
-5.00
-4.00
-3.00
-2.00
-1.00
-0.00
1.00
2.00
3.00
4.00
5.00
6.00
39.00
38.00
37.00
36.00
35.00
34.00

a)

b)

Figure a. 18 a) and b) Deformed mesh of aggregate pier of L/D=6 for $\Delta r/r_0$ =0.3 (Scale factor=3)

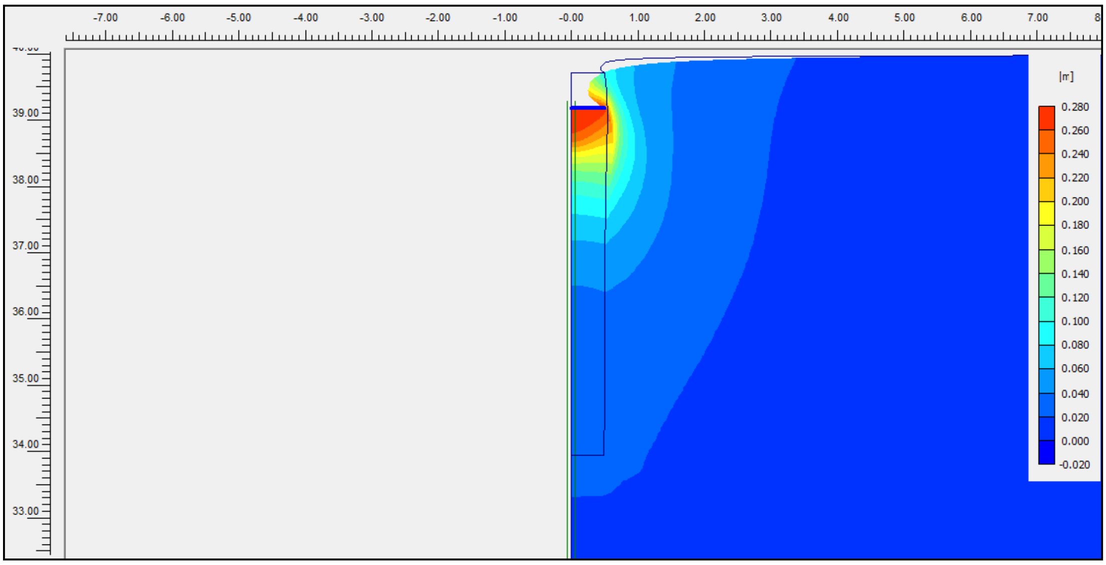

Figure a.19 Total displacement shading of aggregate pier of L/D=6

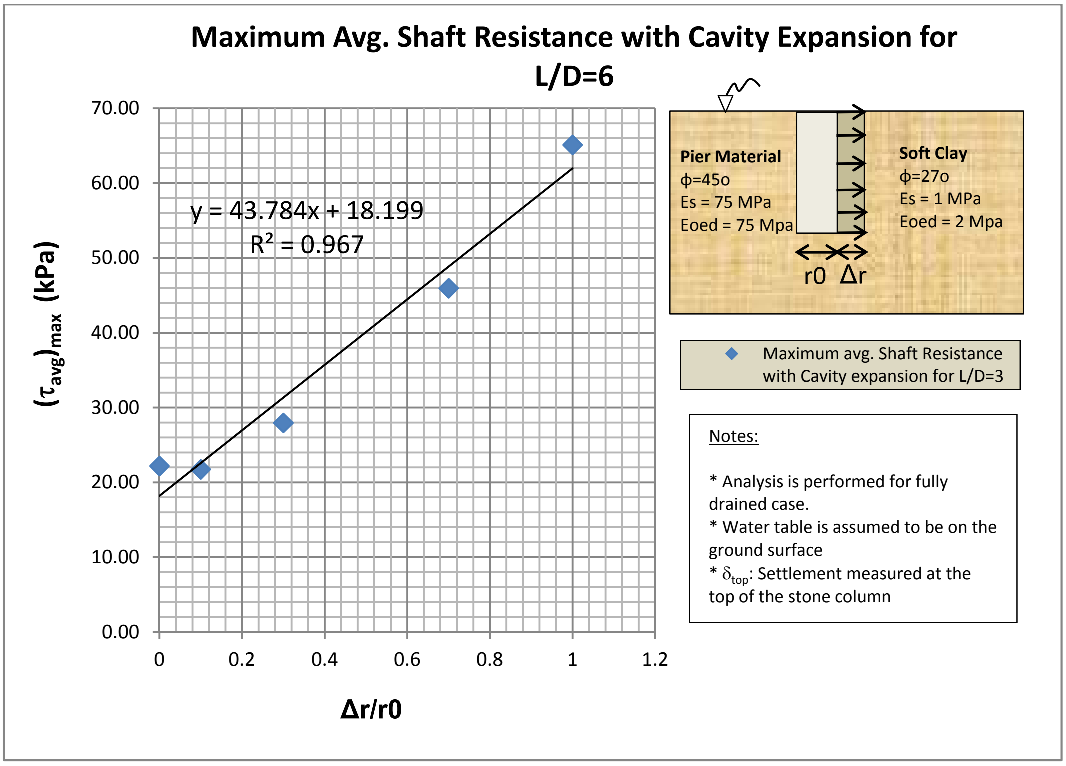

Notes:

* Analysis is performed for fully drained case.

* Water table is assumed to be on the ground surface

* δ_{top}: Settlement measured at the top of the stone column

Figure a.20 Maximum average shaft resistance vs. cavity expansion ratio for L/D=6

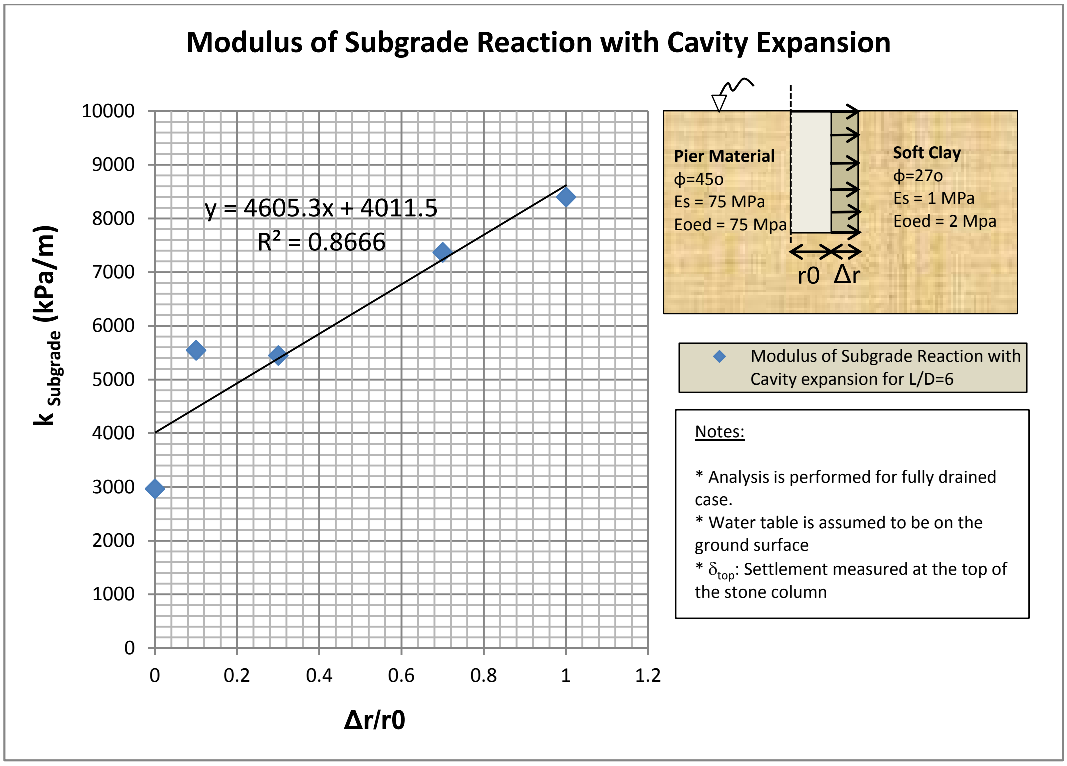

Figure a. 21 Modulus of subgrade reaction vs. cavity expansion ratio for L/D=6

Aggregate Pier of L/D = 9:

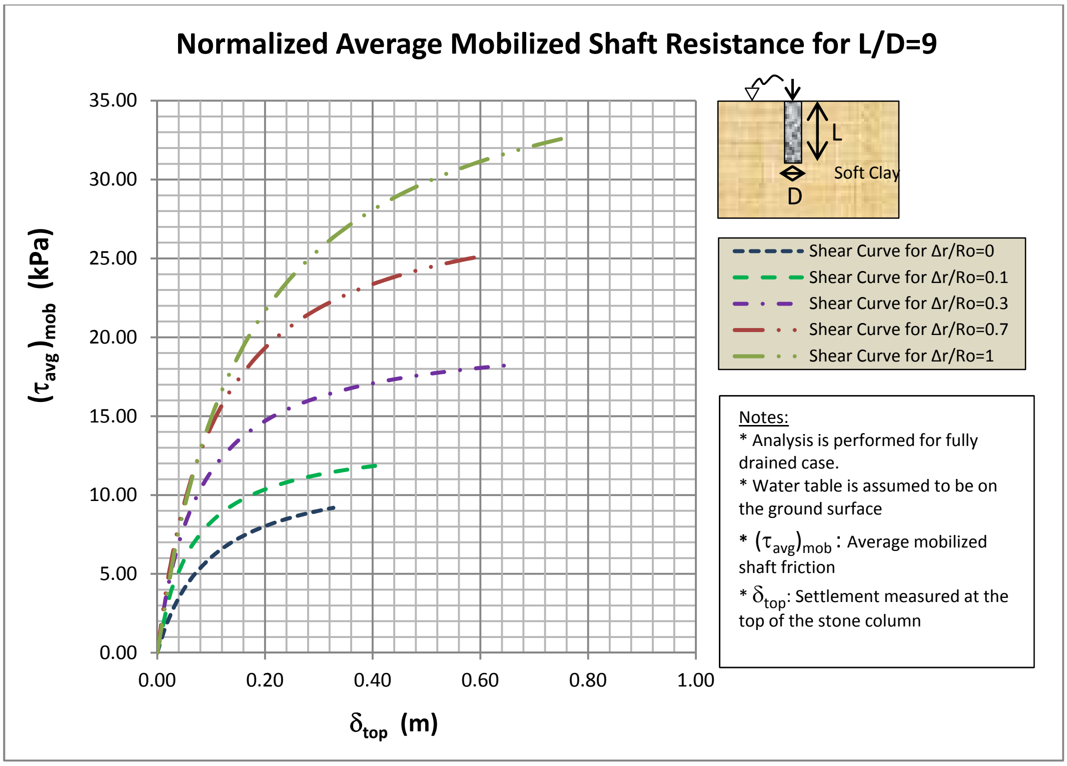

Figure a. 22 Average shaft resistance for aggregate pier for L/D=9

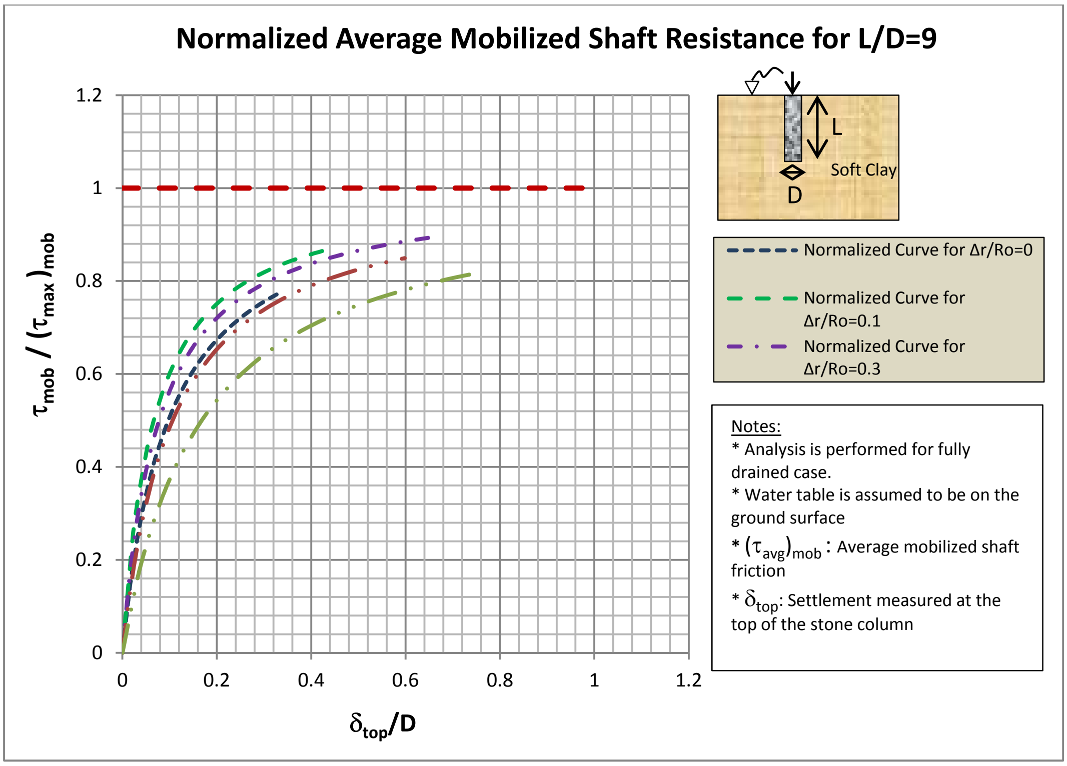

Figure a.23 Normalized average shaft resistances for L/D=9

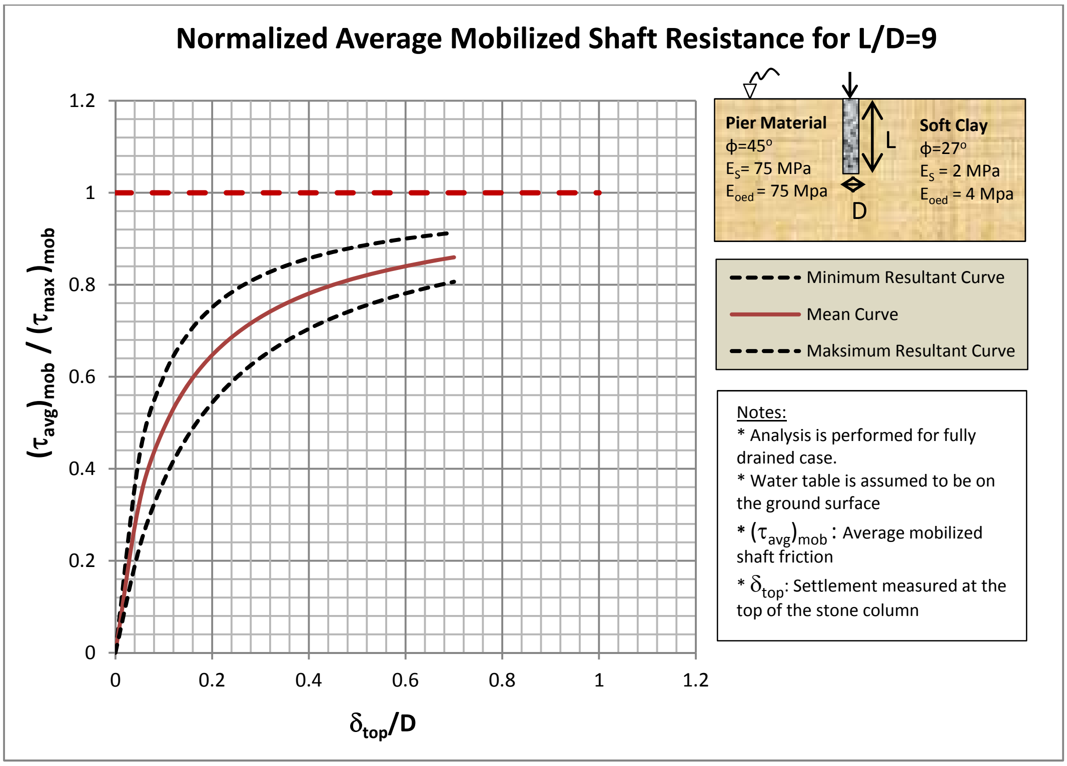

Figure a.24 Average normalized curve with upper and lower threshold curves for L/D=9

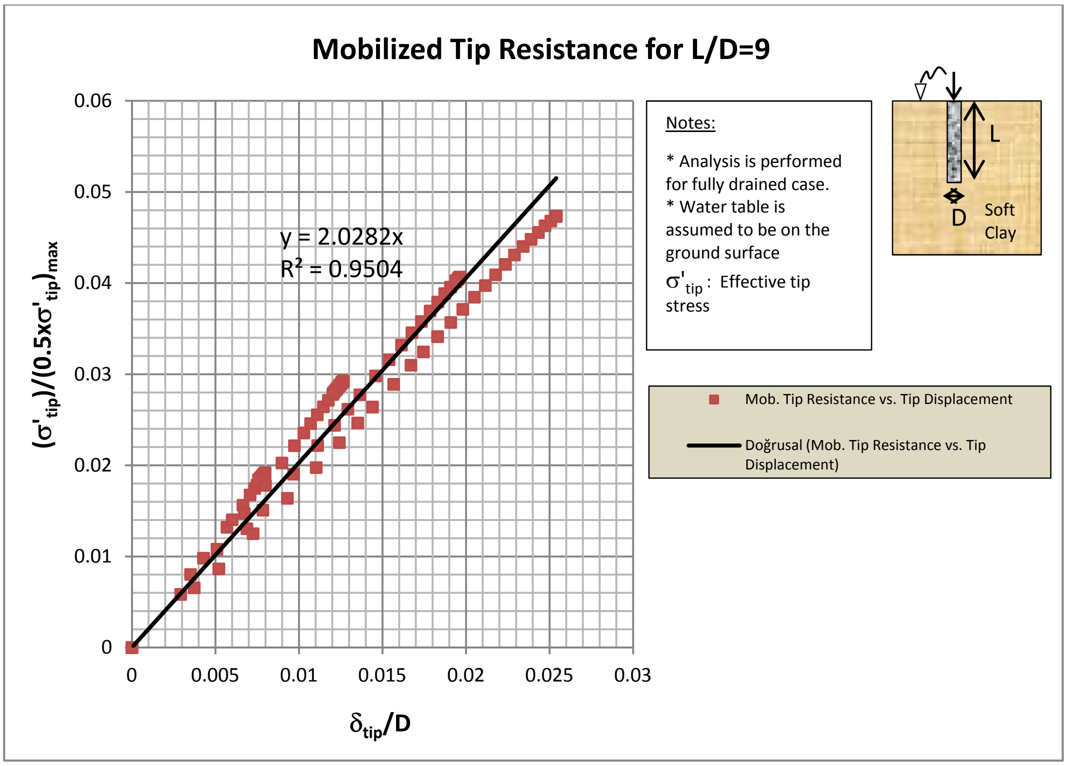

Figure a.25 Normalized tip resistances of aggregate pier of L/D=9

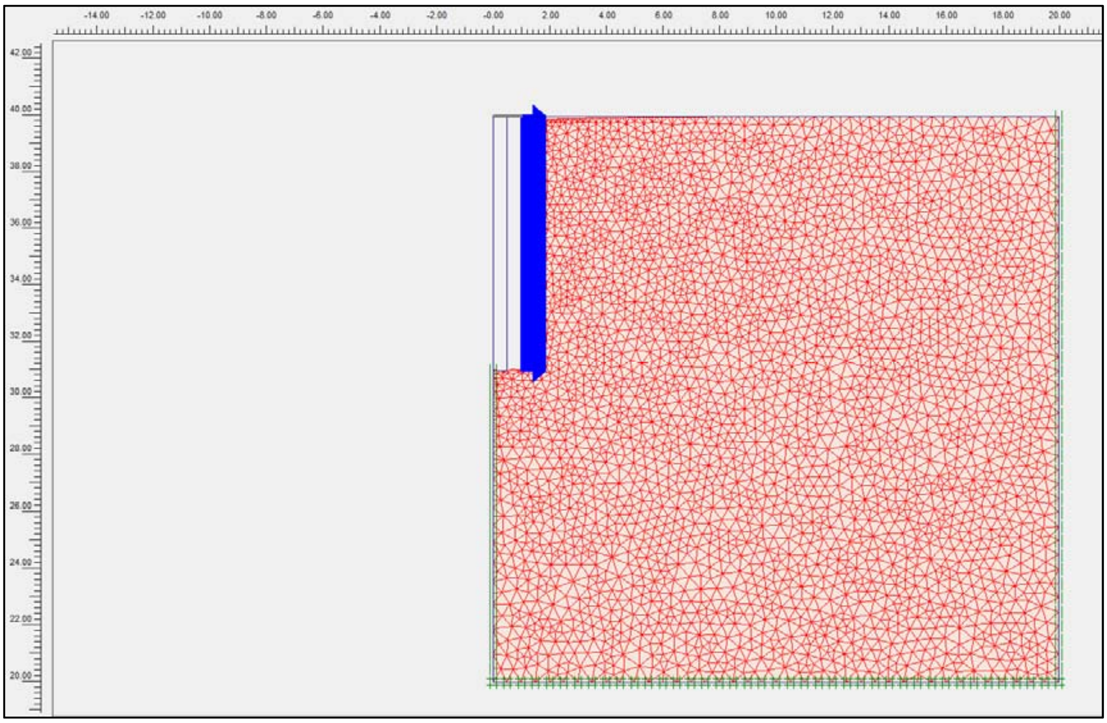
-14.00
-12.00
-10.00
-8.00
-6.00
-4.00
-2.00
-0.00
2.00
4.00
6.00
8.00
10.00
12.00
14.00
16.00
18.00
20.00
42.00
40.00
38.00
36.00
34.00
32.00
30.00
28.00
26.00
24.00
22.00
20.00

Figure a.26 Deformed shape after application of lateral displacement ($\Delta r/r_0 = 1$) to pier of L/D=9

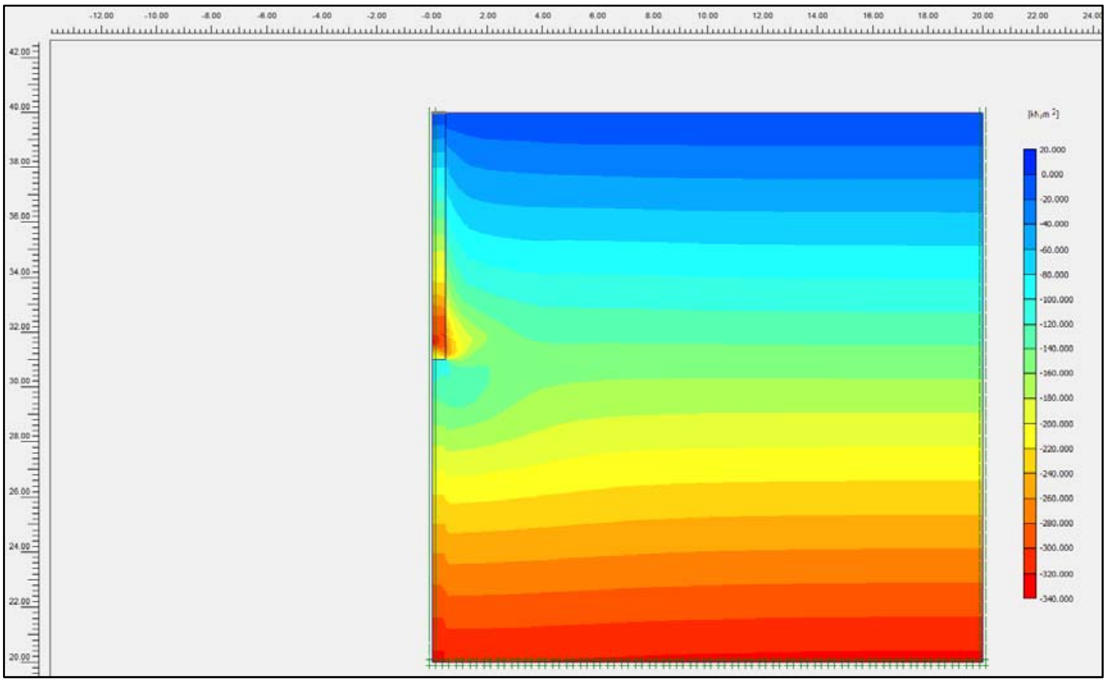

Figure a.27 Confining stresses around the pier of L/D=9 for $\Delta r/r_0$ =1

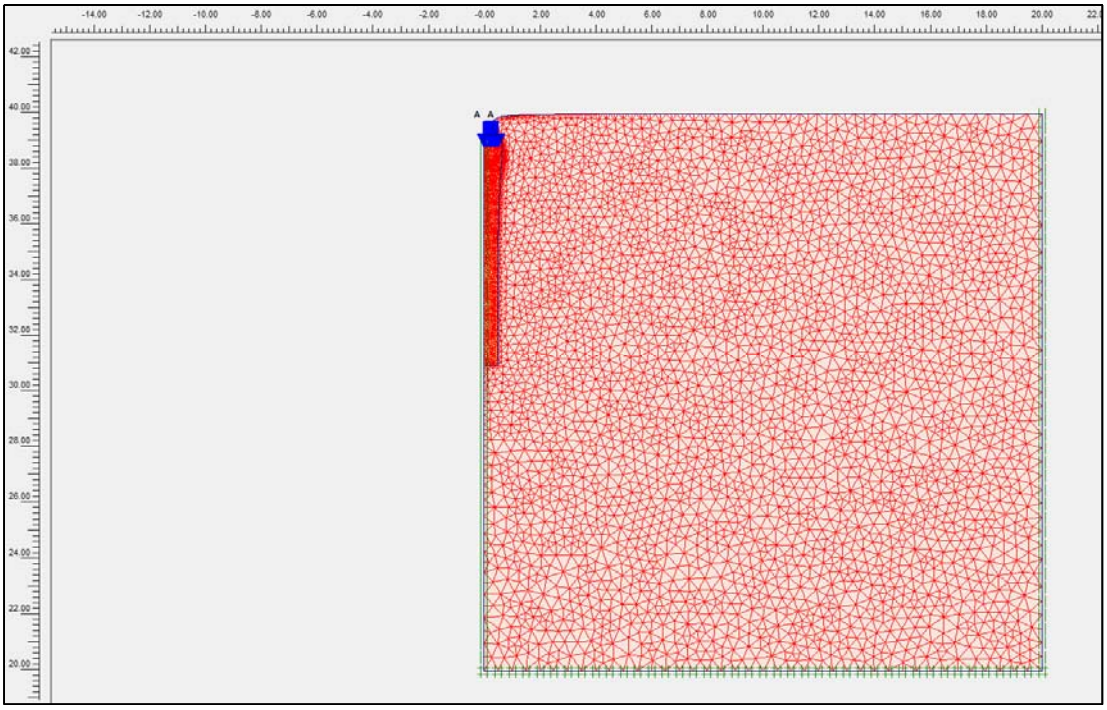
-14.00
-12.00
-10.00
-8.00
-6.00
-4.00
-2.00
0.00
2.00
4.00
6.00
8.00
10.00
12.00
14.00
16.00
18.00
20.00
42.00
40.00
38.00
36.00
34.00
32.00
30.00
28.00
26.00
24.00
22.00
20.00
A
A

a)

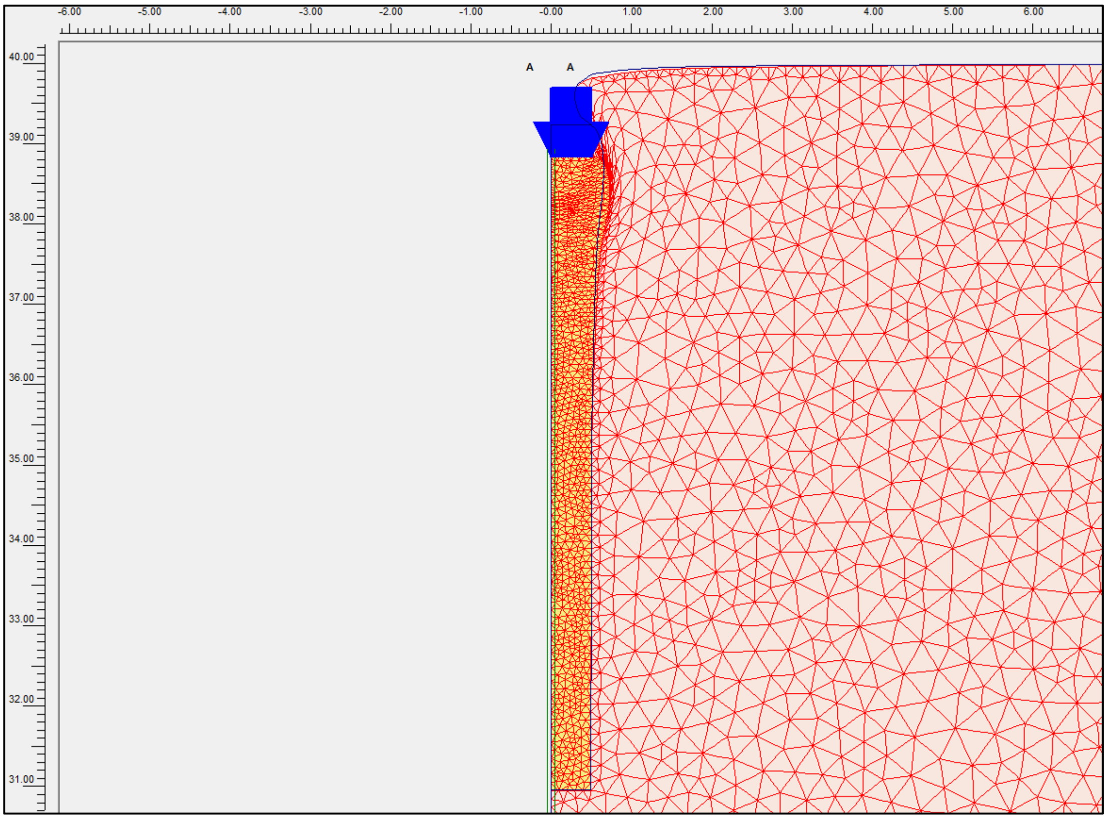

Figure a.28 a) and b) Deformed mesh of aggregate pier of L/D=9 for $\Delta r/r_0$ =1 (Scale factor=1)

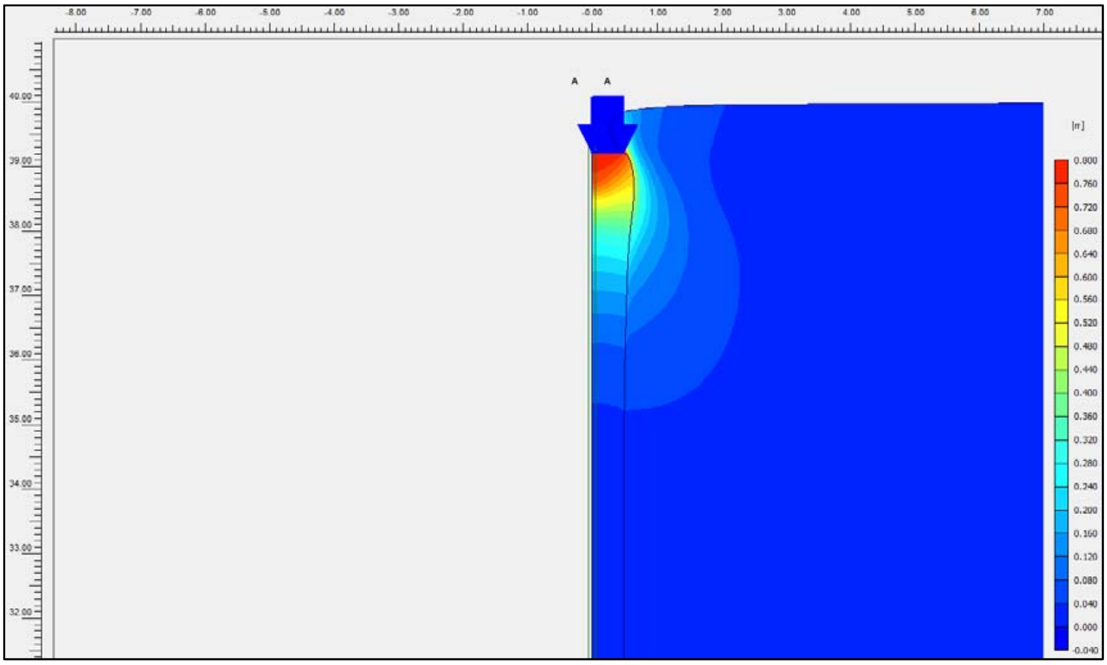

Figure a.29 Total displacement shading of aggregate pier of L/D=9 for $\Delta r/r_0$ =1

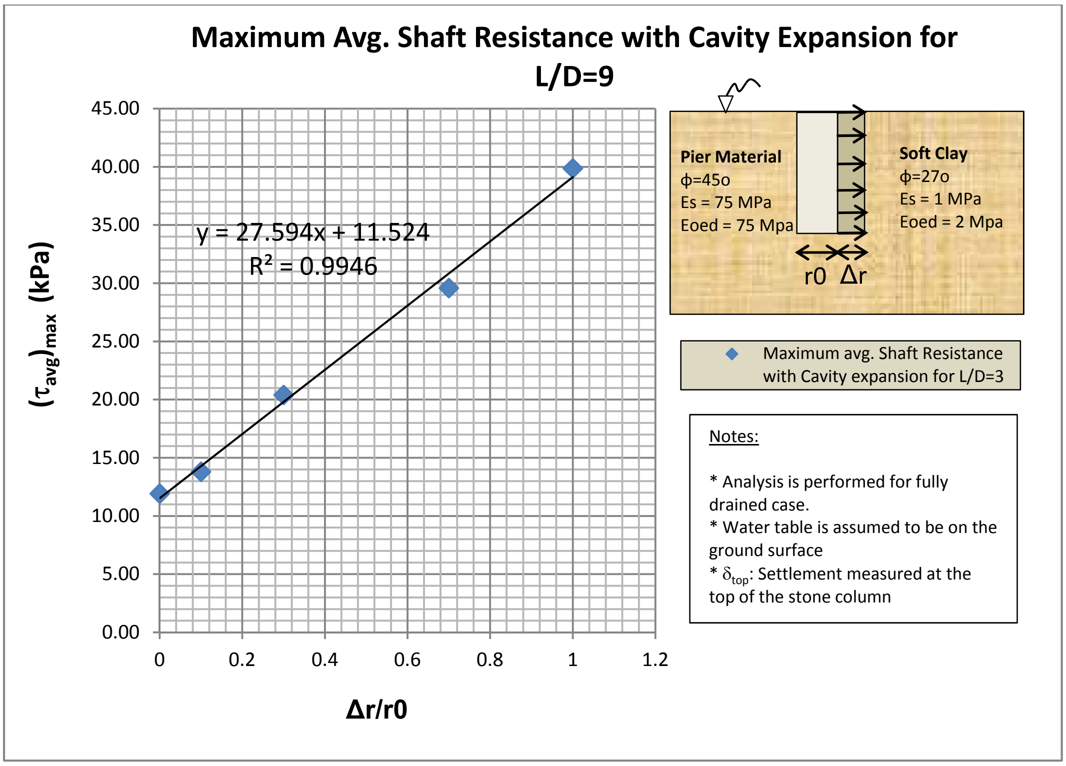

Figure a.30 Maximum average shaft resistance vs. cavity expansion ratio for L/D=9

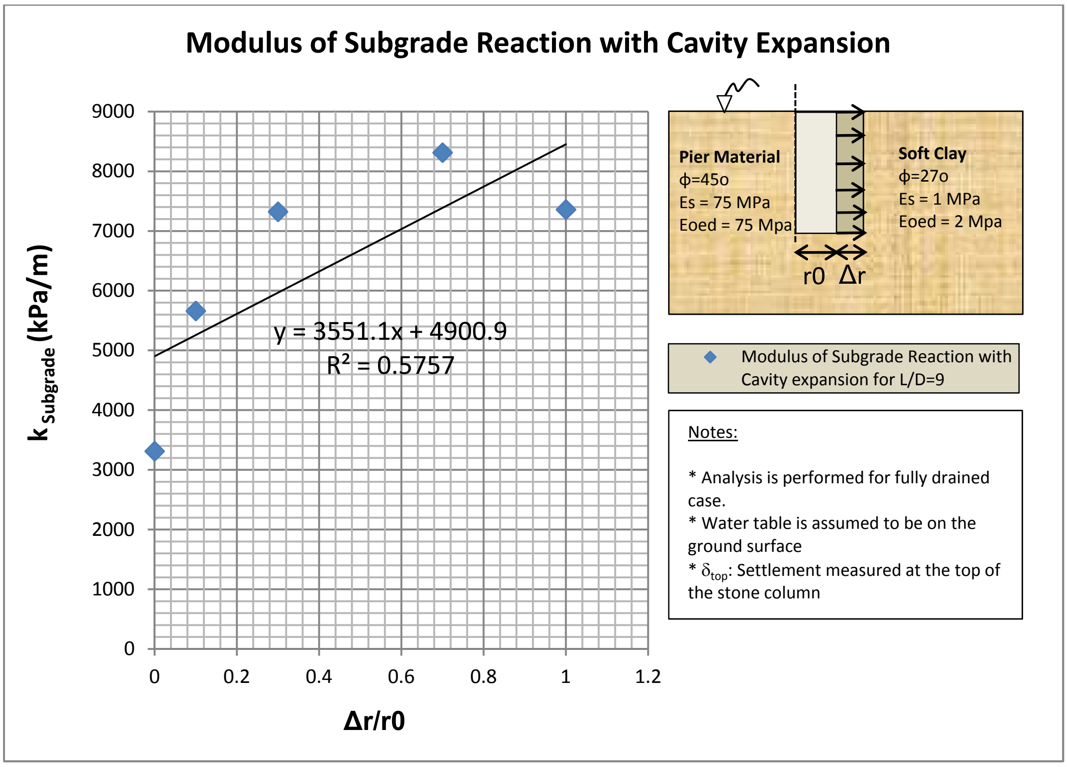

Figure a.31 Modulus of subgrade reaction vs. cavity expansion ratio for L/D=9

Aggregate Pier of L/D = 12:

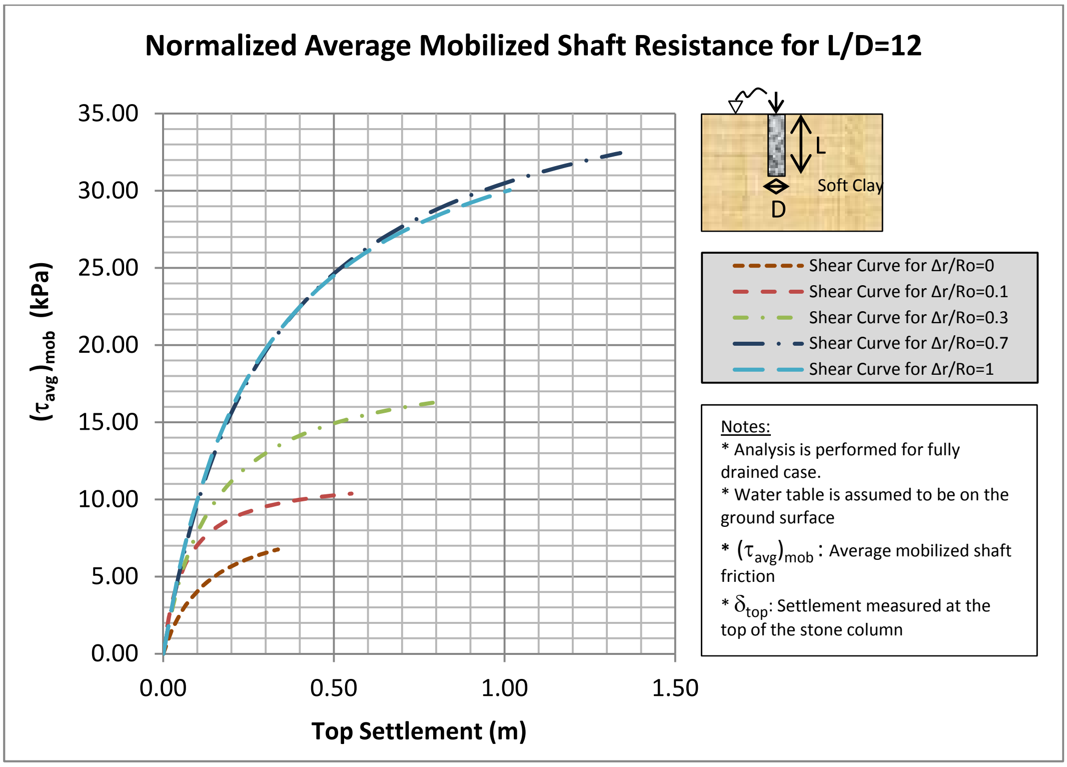

Normalized Average Mobilized Shaft Resistance for L/D=12

Notes:
* Analysis is performed for fully drained case.
* Water table is assumed to be on the ground surface
* $(\tau_{avg})_{mob}$: Average mobilized shaft friction
* δ_{top}: Settlement measured at the top of the stone column

Figure a.32 Average shaft resistance for aggregate pier for L/D=12

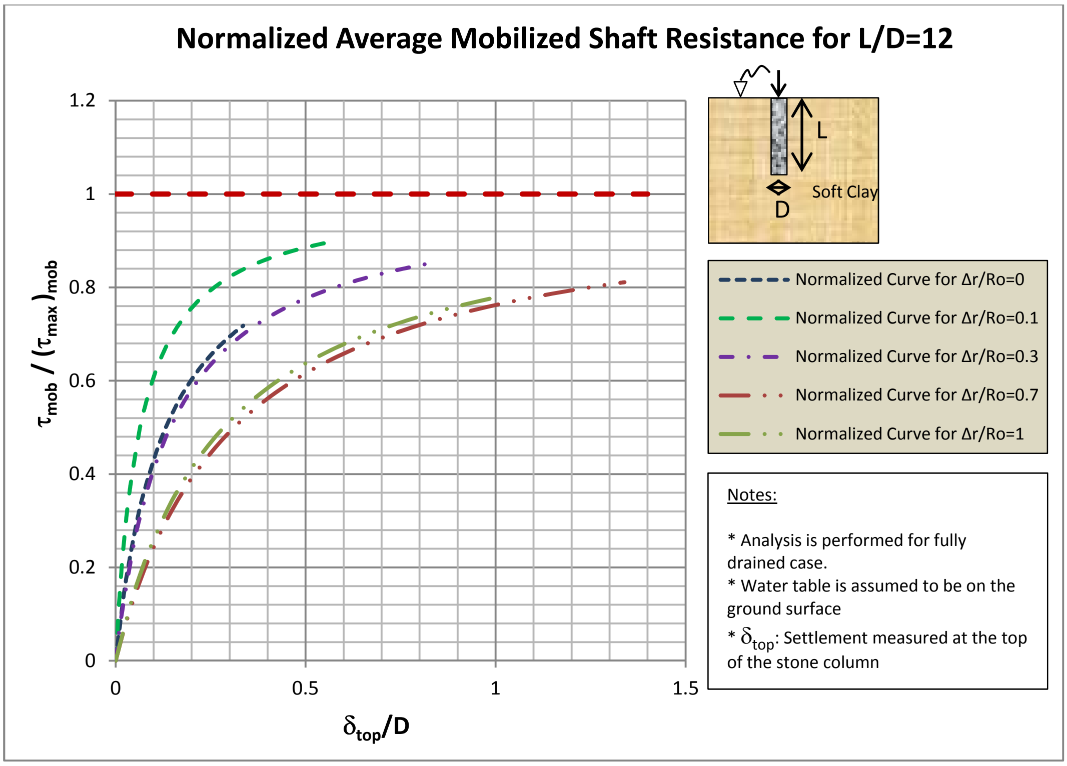

Normalized Average Mobilized Shaft Resistance for L/D=12

Notes:

* Analysis is performed for fully drained case.
* Water table is assumed to be on the ground surface
* δ_{top}: Settlement measured at the top of the stone column

Figure a.33 Normalized average shaft resistances for L/D=12

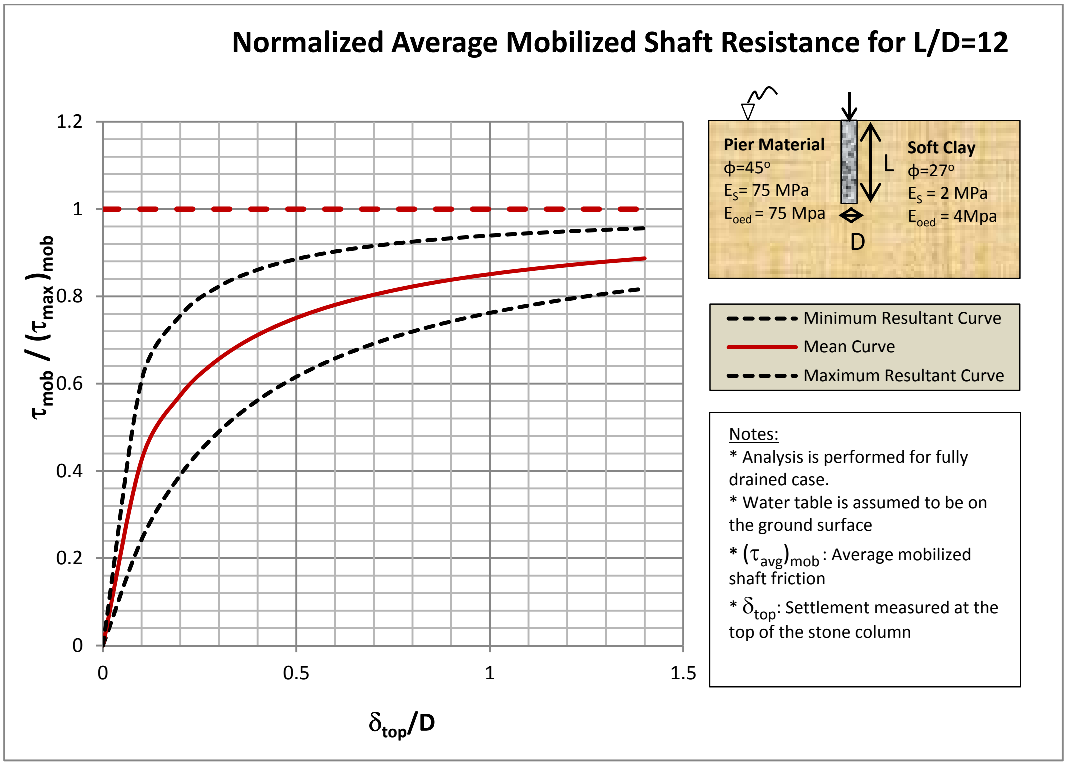

Notes:
* Analysis is performed for fully drained case.
* Water table is assumed to be on the ground surface
* $(\tau_{avg})_{mob}$: Average mobilized shaft friction
* δ_{top}: Settlement measured at the top of the stone column

Figure a.34 Average normalized curve with upper and lower threshold curves for L/D=12

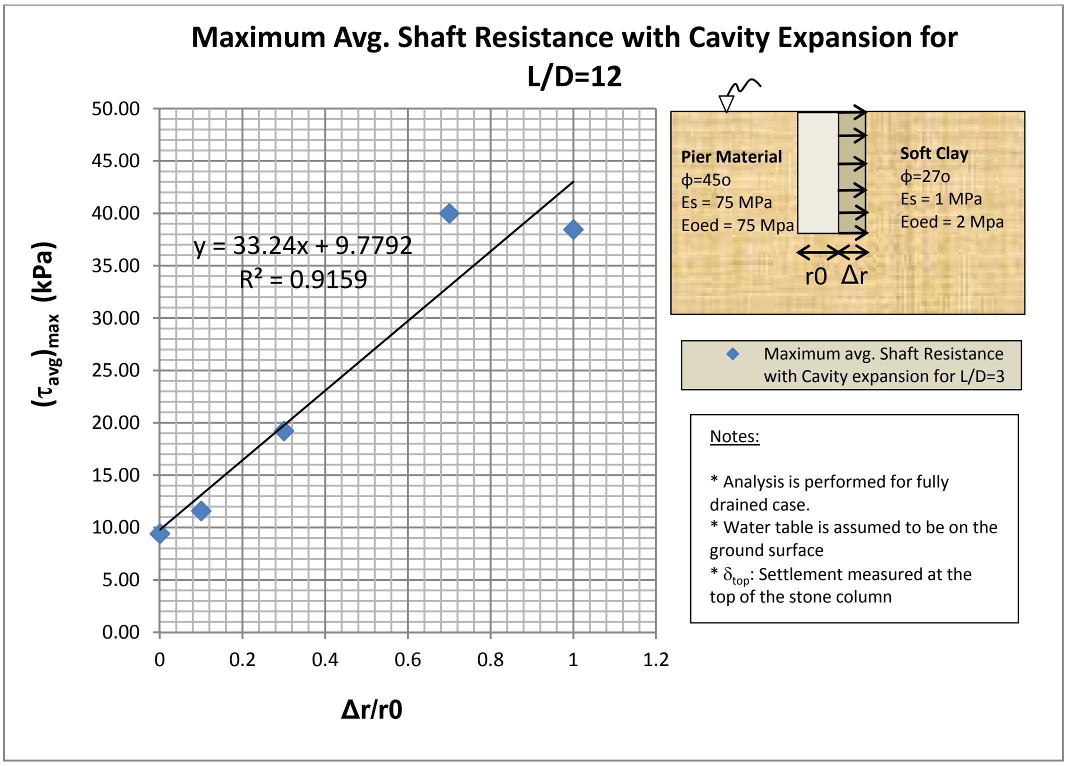

Notes:

* Analysis is performed for fully drained case.
* Water table is assumed to be on the ground surface
* δ_{top}: Settlement measured at the top of the stone column

Figure a.35 Maximum average shaft resistance vs. cavity expansion ratio for L/D=12

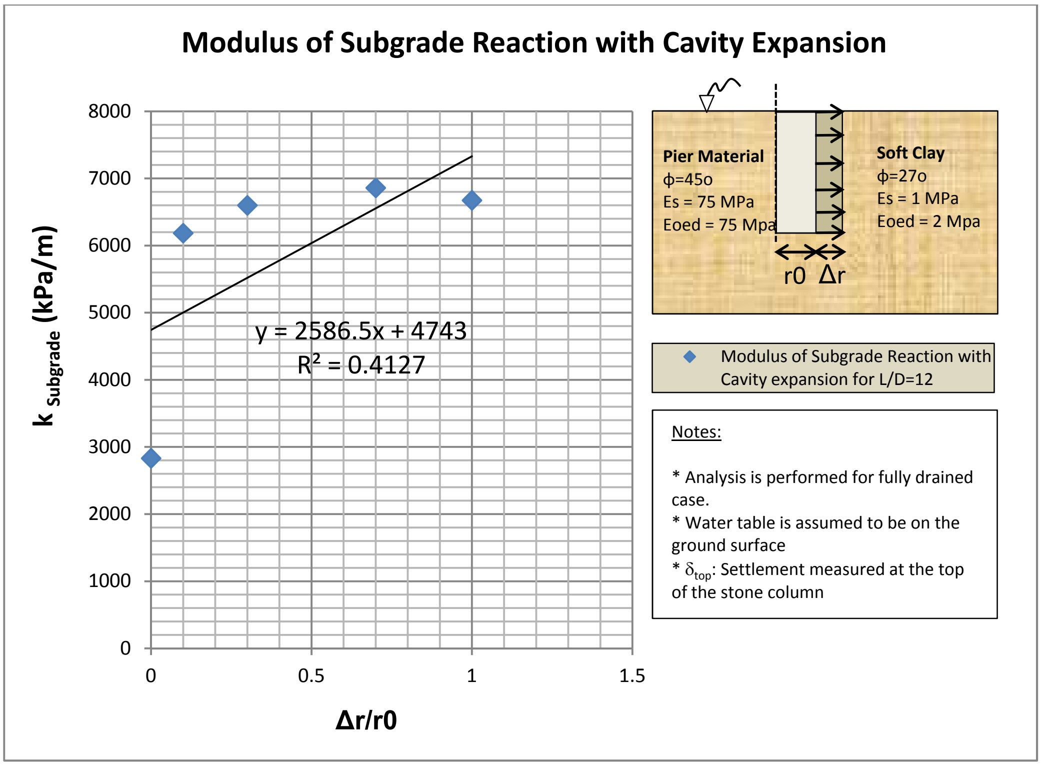

Notes:

* Analysis is performed for fully drained case.
* Water table is assumed to be on the ground surface
* δ_{top}: Settlement measured at the top of the stone column

Figure a.36 Modulus of subgrade reaction vs. cavity expansion ratio for L/D=12

Aggregate Pier of L/D=15:

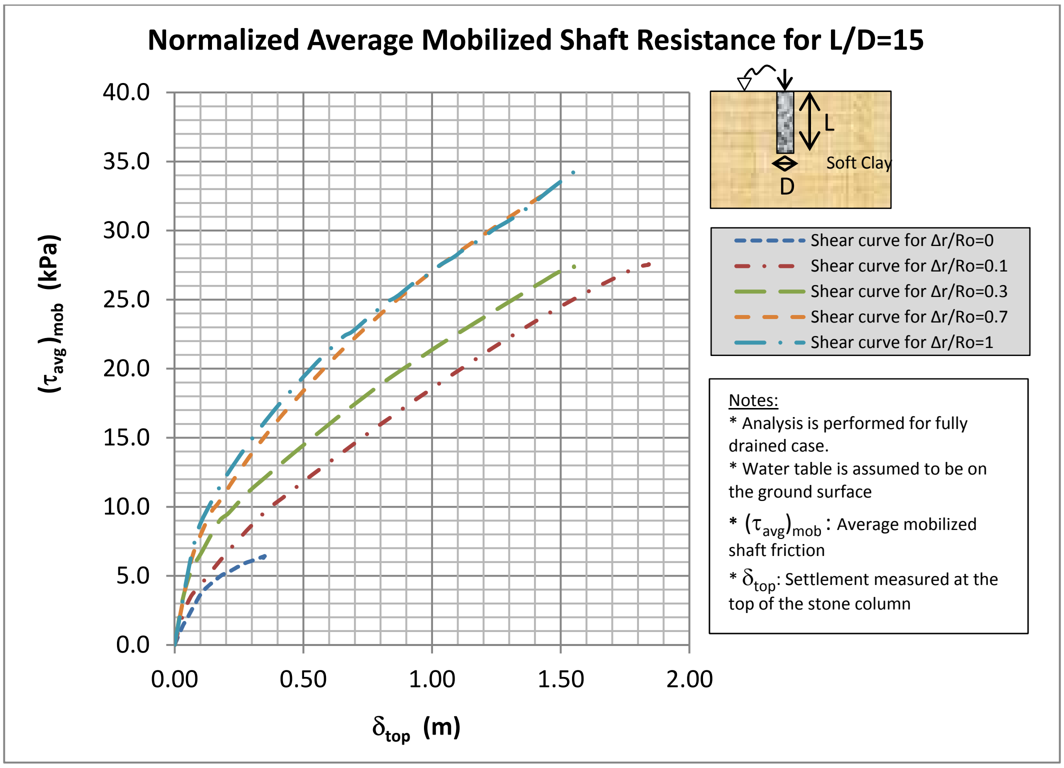

Notes:
* Analysis is performed for fully drained case.
* Water table is assumed to be on the ground surface
* $(\tau_{avg})_{mob}$: Average mobilized shaft friction
* δ_{top}: Settlement measured at the top of the stone column

Figure a.37 Average shaft resistance for aggregate pier for L/D=15

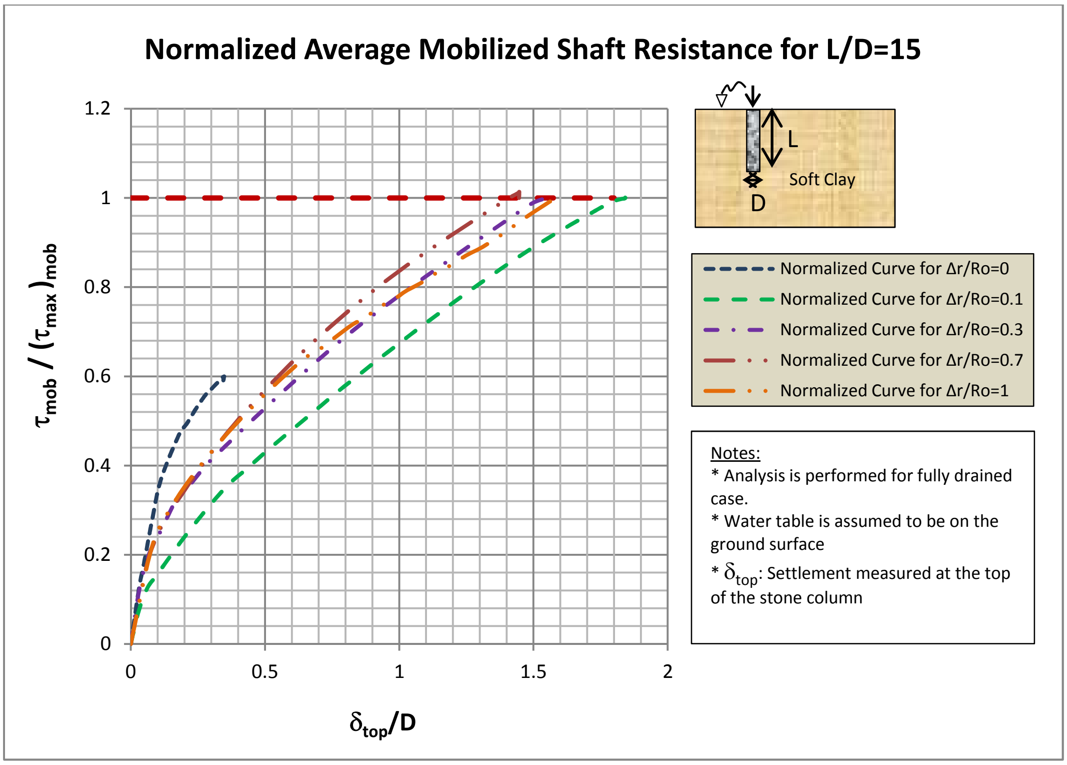

Figure a.38 Normalized average shaft resistances for L/D=15

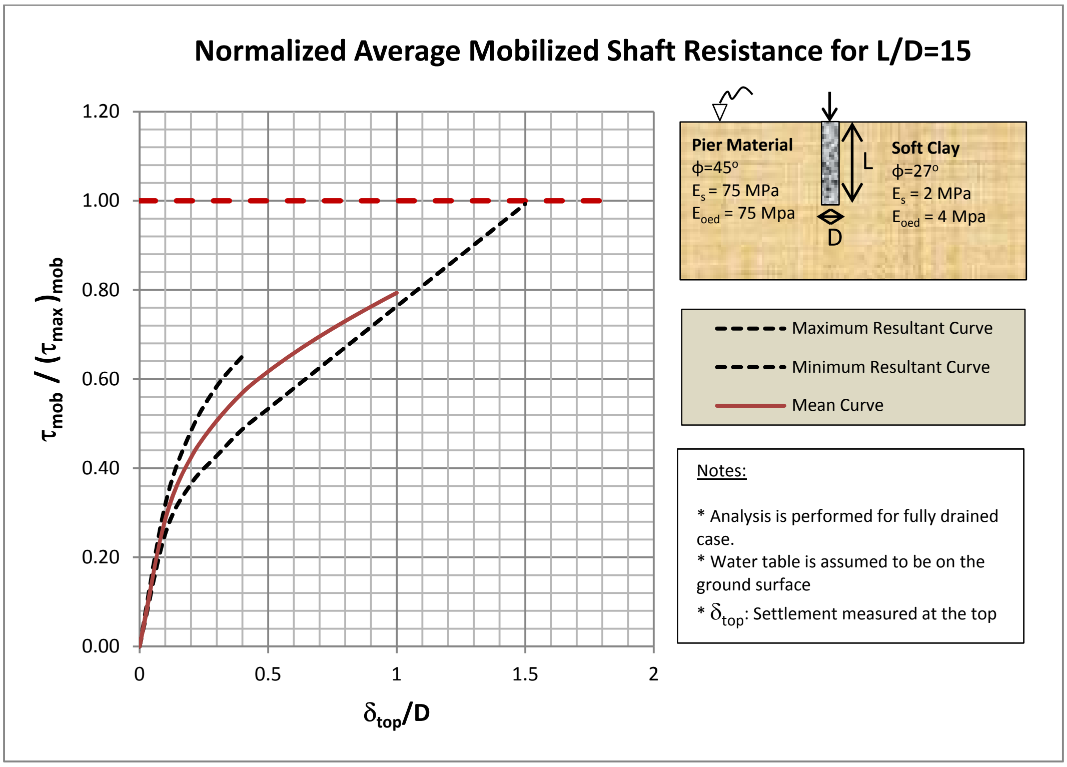

Figure a.39 Average Shear Stresses Along Pier Shaft for L/D=15

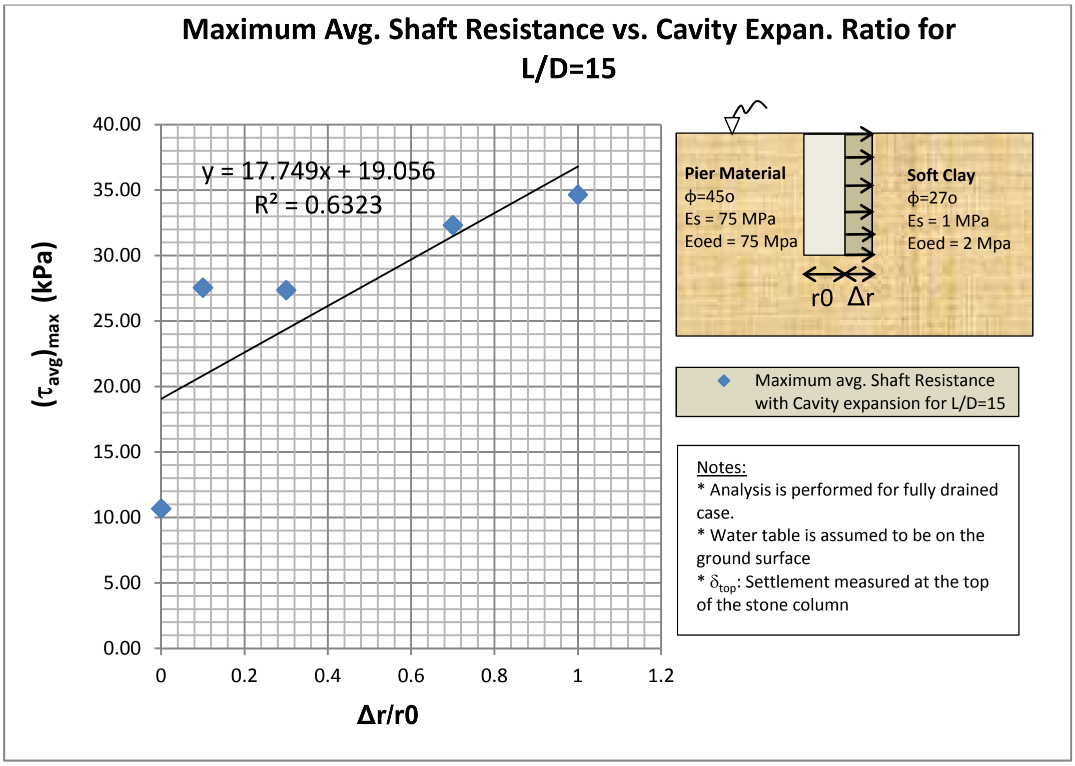

Figure a.40 Maximum average shaft resistance vs. cavity expansion ratio for L/D=15

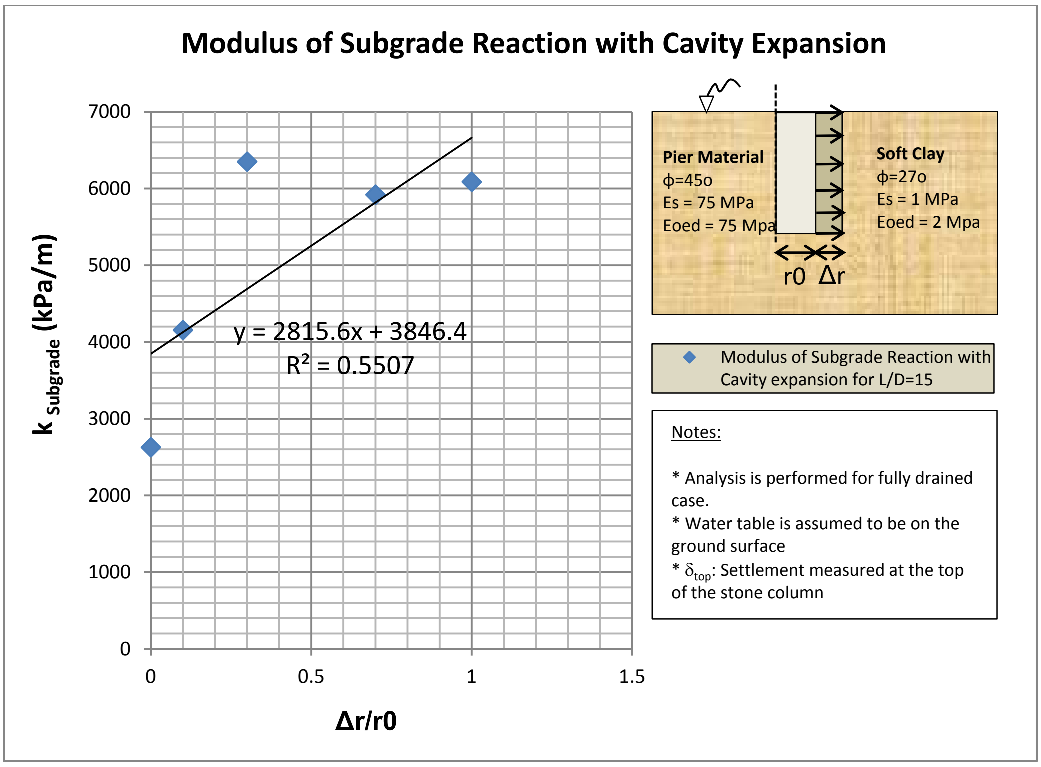

Figure a. 41 Modulus of subgrade reaction vs. cavity expansion ratio for L/D=15

TEZ FOTOKOPİSİ İZİN FORMU

ENSTİTÜ

Fen Bilimleri Enstitüsü ☒

Sosyal Bilimler Enstitüsü ☐

Uygulamalı Matematik Enstitüsü ☐

Enformatik Enstitüsü ☐

Deniz Bilimleri Enstitüsü ☐

YAZARIN

Soyadı : DOĞAN
Adı : Alparslan
Bölümü : İnşaat mühendisliği

TEZİN ADI (İngilizce) :

Assessing the Effects of Confining Stress State on the Mobilization of axial Compressive Resistance for a Single Aggregate Pier.

TEZİN TÜRÜ : Yüksek Lisans ☒ Doktora ☐

1. Tezimin tamamı dünya çapında erişime açılsın ve kaynak gösterilmek şartıyla tezimin bir kısmı veya tamamının fotokopisi alınsın. ☐

2. Tezimin tamamı yalnızca Orta Doğu Teknik Üniversitesi kullancılarının erişimine açılsın. (Bu seçenekle tezinizin fotokopisi ya da elektronik kopyası Kütüphane aracılığı ile ODTÜ dışına dağıtılmayacaktır.) ☐

3. Tezim bir (1) yıl süreyle erişime kapalı olsun. (Bu seçenekle tezinizin fotokopisi ya da elektronik kopyası Kütüphane aracılığı ile ODTÜ dışına dağıtılmayacaktır.) ☒

Yazarın imzası: Tarih: